DIAPHRAGM STIFFNESS IN WOOD-FRAME CONSTRUCTION

by

Xinlei Huang

B.A.Sc., North-eastern University, China, 2008

M.A.Sc., North-eastern University, China, 2010

A THESIS SUBMITTED IN PARTIAL FULFILLMENT OF

THE REQUIREMENTS FOR THE DEGREE OF

MASTER OF APPLIED SCIENCE

in

THE FACULTY OF GRADUATE STUDIES

(Civil Engineering)

THE UNIVERSITY OF BRITISH COLUMBIA

(Vancouver)

January 2013

Abstract

This thesis presents an investigation of the in-plane stiffness of wood-frame diaphragms. Studying the stiffness of the diaphragm is important since it affects the distribution of lateral loads to shear walls. In order to determine the force in each shear wall, it is common to classify a diaphragm as either flexible in engineering design. Wood-frame diaphragms have generally been treated as flexible, which distributes the lateral loads using the straightforward "tributary area" approach. The accuracy of this assumption is investigated in this study.

A detailed numerical model is developed for the study of the in-plane behaviour of wood-frame diaphragms. The model is validated with full-scale diaphragm tests, which has not been done so far for other diaphragm models in previous studies. As such, the model can be used as a "virtual laboratory" to predict the in-plane behaviour of wood-frame diaphragms with various configurations. A simplified model is developed based on the detailed diaphragm model to be used in the building analysis. The simplified model consists of "truss units", which can be calibrated using analytical methods. In previous studies, wood-frame diaphragms were generally simplified as beam or spring models, where individual calibration is required for diaphragms with various configurations. Compared with these models, the simplified model developed here is obtained as an assembly of truss units, thus the number of calibration times can be considerably reduced. A case study of a one-storey wood-frame building is conducted to investigate the distribution of lateral loads to shear walls under different diaphragm flexibility conditions. It is found that the wood-frame diaphragm in this work is rather rigid, but is found that the distribution of lateral loads to the shear walls is strongly dependent on the relative stiffness of the diaphragm and the shear walls.

Table of Contents

List of Tables

List of Figures

Acknowledgements

I would like to express my sincere gratitude to my supervisors Dr. Terje Haukaas and Dr. Frank Lam, for their valuable support, encouragement, and guidance throughout my thesis. Their understanding and willingness to dedicate their time so generously have been much appreciated. Without their consistent supervision, this thesis could not have reached its present form.

I gratefully acknowledge the funding for this research project, which is provided by the Strategic Network on Innovative Wood Products and Building Systems (NewBuildS). NewBuildS is a Forest Sector Research & Development Initiative funded by the Natural Sciences and Engineering Research Council of Canada (NSERC).

A special thank goes to Dr. Ricardo Foschi. His kind help and constructive advice have greatly helped me in the problem solving and provided me better understanding of my research project. I would also wish to thank Dr. Minghao Li, who was always available for discussion and helped me a lot on the modelling of the wood-frame diaphragm.

Finally, I would like to express my heartfelt gratitude to my beloved parents who have always been encouraging, supporting and caring for me all of my life. I also owe my sincere appreciation to my friends and my colleagues in the Wood Science group for their unwavering help and encouragement.

Dedication

To my dearest parents

Chapter 1: Introduction

1.1 Motivation

Floor and roof diaphragms are important components in light wood-frame buildings. In addition to carrying vertical loads, such as dead loads and live loads, a diaphragm is also an important component of the lateral force resisting system. The purpose of the lateral force resisting system is to carry the lateral loads induced by wind and earthquakes. For buildings that resist lateral loads by means of shear walls, the diaphragm serves the purpose of distributing the loads to the shear walls. To determine the force in each shear wall, it is common in current design practice to classify the diaphragm as either flexible or rigid. A diaphragm that is considered rigid distributes the lateral loads to the shear walls in proportion to the stiffness of each wall. In contrast, a diaphragm that is considered flexible distributes lateral loads based on the tributary area of each shear wall. The assumption of rigid versus flexible diaphragm can have significant impact on the predicted force in each shear wall. For example, if the force in a shear wall is underestimated, the wall may fail prematurely and cause unexpected structural damage and loss of structural integrity.

Although provisions for determining the diaphragm flexibility are found in certain design codes, the engineer usually assumes that wood-frame diaphragms are flexible. This assumption greatly simplifies the calculation of forces, but its general validity has recently been drawn into question. In fact, the problem of determining the actual flexibility of a wood-frame diaphragm is complicated by several factors, including: 1) the aspect ratio of the diaphragm; 2) the shape of the building plan; 3) the relative stiffness of shear walls compared with the diaphragm stiffness; and 4) the position and size of

openings. The uncertainty associated with the flexibility of actual light wood-frame diaphragms, combined with the importance of accurate flexibility estimates, motivates this thesis.

1.2 Objectives

The main objective of this work is to study the in-plane behaviour of light wood-frame diaphragms, and to examine the popular flexible wood-frame diaphragm assumption in engineering practice. To achieve this goal, several specific objectives are addressed in this thesis. The first objective is to develop a detailed numerical model, which can be served as a platform for further studies on wood-frame diaphragms. The input to the model involves geometrical and mechanical parameters, which can be calibrated by test data. The model can be used as a "virtual laboratory" to predict the in-plane behaviour of wood-frame diaphragms that are not actually built. As such, the stiffness of wood-frame diaphragms with various configurations can be ultimately investigated without the need to conduct expensive and time consuming full-scale diaphragm tests.

The second objective is to develop a simplified model based on the detailed wood-frame diaphragm model, which can be utilized in the study of the overall structural performance under lateral loads. An analysis of a building with the detailed diaphragm model would be complex and computationally intensive because of the high number of degrees of freedom. A simplified model is more suitable for initial studies, since it better balances the simulation accuracy with computational efficiency, while retaining the results obtained by the previously established detailed model.

The third objective of this work is to study the lateral load distribution in a light wood-frame building, which helps understand the actual flexibility of wood-frame diaphragms. Shear walls will be added to the previously generated simplified diaphragm model to formulate the building model, and the load sharing among shear walls is compared with the results obtained from the hypothetical flexible and rigid diaphragm cases. As such, the applicability of the flexible wood-frame diaphragm assumption is examined, and the provisions in the code (ICC 2003) for determining the diaphragm flexibility can be assessed.

1.3 Scope

By varying the input geometric or mechanical parameters, the proposed detailed numerical model is applicable to a wide range of wood-frame configurations. Although the model can be modified to consider the out-of-plane behaviour, e.g. the connection withdrawal effect, the potential buckling of sheathing panels, etc., this work narrows its scope to investigate the in-plane behaviour of wood-frame diaphragms.

The input hysteric parameters of the panel-frame connections are calibrated with test data for a specific type of nail to match the diaphragm configurations studied in Chapter 4. However, these parameters can also be calibrated for many other types of connections, which are not studied in this thesis. Due to the shear-only assumption, the simplified diaphragm model is applicable for diaphragms within the aspect ratio of 0.8 to 3, as discussed in Chapter 5.

This work conducts a case study on a one-storey wood-frame building to examine the popular flexible wood-frame diaphragm assumption, and to provide some general insights into the in-plane behaviour of wood-frame diaphragms. Shear walls in the

building model are modelled using linear elastic truss elements. It is known that the general behaviour of the shear wall under lateral loads would follow a nonlinear trend. However, the scope of this work is narrowed to the study of the structural performance in the early stage of loading. In other words, all structural members in the building are assumed to stay in the elastic range, i.e. the stage before the structural members undergo substantial nonlinear deformations. As introduced earlier, the in-plane behaviour of the wood-frame diaphragm is affected by the building configuration, i.e. diaphragm configurations and shear wall arrangements. However, the investigation of the in-plane behaviour of wood-frame diaphragms with various building configurations is not included in the scope of this work.

1.4 Organization of Thesis

The remainder of the thesis is organized as follows:

Chapter 2 provides a literature review that gives an overview of the research field of diaphragm stiffness. Existing diaphragm tests and numerical models in the previous research are introduced, and in-plane behaviours of various types of diaphragms, i.e. reinforced concrete diaphragms, wood-frame diaphragms, etc., are discussed. The review serves as a background for the model development and building analysis in the following chapters. In Chapter 3, a connection model, which is developed for the study of the hysteretic behaviour of general connections in light-frame wood construction, is introduced. In particular, a specific panel-frame nail connection model, which is utilized in the diaphragm model in Chapter 4, is generated and calibrated by single nail connection test data. The details of the tests and model calibration procedures are also presented in this chapter. In Chapter 4, a detailed wood-frame diaphragm model is

developed and validated with early test data. The details of the finite element modelling are presented, and discrepancies between model predictions and test results are discussed. Chapter 5 describes the analysis of a one-storey light-frame wood building. A simplified diaphragm model is developed and implemented in the building model. The building is analyzed under three different diaphragm rigidity conditions, and the corresponding lateral load distributions on shear walls are compared. Based on the comparison results, the accuracy of the code provision for determining diaphragm rigidity, and the general flexible wood-frame diaphragm assumption are examined. Finally, conclusions of the work along with recommendations for further studies are given in Chapter 6.

Chapter 2: Literature Review

Past seismic studies have shown that structures with different amount of diaphragm flexibility can behave very differently (Dolce et al. 1992). Due to the diversity of constructions, currently, there is no simple and accurate method that can be used to predict the stiffness of the diaphragm (Tena-Colunga and Abrams 1996; Pathak and Charney 2008). For simplicity, diaphragms are classified as either flexible or rigid in the design for the purpose of distributing loads to shear walls, as introduced earlier. For example, wood-frame diaphragms have been generally treated as flexible, which results in a distribution of loads based on the tributary area method. However, some researchers suggested that this assumption may not be applicable when torsional irregularities exist, e.g. asymmetric geometries or openings (Tena-Colunga and Abrams 1996). Relatively few studies have been conducted on diaphragm stiffness, and this literature review gives an overview of the currently available research performed in this field. In particular, three questions are addressed for each reviewed paper as follows: 1) what models were proposed; 2) what experimental data was employed or created; and 3) what kind of insight was gained.

Dolce et al. (1992) conducted a parametric study to investigate the effect of diaphragm flexibility on the inelastic seismic response of symmetric one-storey reinforced concrete structures. The structural model consisted of a floor system supported by seven lateral load resisting vertical elements. The floor was modelled using elastic or elasto-plastic beam elements, and the vertical members were idealized as stiffness degrading beam elements. Each vertical member was fixed at its base and connected to the floor beam by hinges. Parameters involved were the distribution of stiffness among

vertical members, distribution of the in-plane stiffness of the floor, the strength of the floor, and the flexibility of the floor. No test was conducted in the study. Analysis results showed that the diaphragm flexibility has a great influence on the response of the structural only if the vertical members have a considerably non-uniform stiffness distribution. It was found that accounting for the actual flexibility of the diaphragm in structural design may lead to an unacceptable non-linear response of the structure; the ductility demand of the more rigid and resistant vertical members may be overestimated while the strength demand may be underestimated. This conclusion was contrast to the specifications of some modern seismic codes, in which the consideration of the actual diaphragm flexibility was always suggested. In short, the study concluded that the rigid diaphragm assumption would always lead to a more conservative design for the structure.

By comparing the dynamic characteristics of structures with flexible diaphragms and rigid diaphragms, Tena-Colunga and Abrams (1996) investigated the effect of diaphragm flexibility on the seismic response of structures. Three existing buildings with masonry lateral load resisting systems and timber diaphragms were studied. Discrete, multi-degree-of-freedom dynamic models were developed for the analytical analysis, and a finite element model was developed in ABAQUS separately to examine the influence of diaphragm flexibility on torsional effects. Models with flexible and rigid diaphragm systems were computed respectively, and results were compared with the measured seismic response in earlier studies in terms of: 1) maximum lateral accelerations; 2) maximum lateral displacements; 3) torsional effects; and 4) natural periods. It was observed that both accelerations and lateral displacements of diaphragms and shear walls may increase as the flexibility of the diaphragm increases. This was attributed to the fact

that design criteria based on the rigid diaphragm assumption may not be necessarily conservative for flexible diaphragm systems. However, torsional effects can be reduced considerably as the flexibility of the diaphragm increases. It was also found that the simplified approach in current codes may underestimate the fundamental period of the structure with flexible diaphragms.

Filiatrault et al. (2002) carried out an experimental parametric study on a two-storey wood-frame house to investigate the in-plane flexibility of wood-frame diaphragms. Fourteen diaphragms with various structural configurations were tested under the 1994 Northbridge earthquake loads. Parameters involved were the nail schedule, the panel-edge blocking, the sub-floor adhesive, perpendicular walls above and below the diaphragm and wall finish materials. The results showed that panel-blocking has a considerable influence on the shear stiffness of diaphragm, and the flexural stiffness of the diaphragm was most affected by the presence of perpendicular walls. The deformation results were used to assess the accuracy of the design procedures in the Uniform Building Code (UBC) (ICBO 1997). It was found that the UBC procedures underestimated the total deformations of the diaphragm if only the first storey of the tested structure was considered. However, when considering the entire structure, the total deformations of the diaphragm were overestimated by the UBC procedures. According to the provisions of UBC, except for the configuration of no blocking and no adhesive, most tested diaphragm configurations were classified as rigid. This work provided valuable test results for wood-frame diaphragms with various structural configurations, which can be used as a database for further numerical studies.

Pathak and Charney (2008) conducted a parametric study to investigate the influence of the diaphragm flexibility on the seismic performance of light-frame wood structures. Nonlinear response history analyses were performed on one-storey light-frame wood structures with varying aspect ratios, diaphragm flexibility assumptions, and shear wall configurations. The models were built in the finite element program SAP2000. The framing members were modelled by linear isotropic 3D frame elements, and the sheathing panels were modelled using linear orthotropic shell elements. Nonlinear hysteretic springs were utilized to represent the connections. No test was conducted in this study. It was observed that for symmetric structures with flexible diaphragms, the ratio between the interior and exterior wall in-plane peak base shear (per unit length) increases as the aspect ratio of the structure increases. However, an opposite trend was observed for structures with rigid diaphragms. The analyses of structures with rigid and flexible diaphragms showed great differences when torsional irregularities existed. Thus, the consideration of the diaphragm rigidity for torsional irregular structures was suggested to minimize analysis errors. It was found that in the torsional irregular models, the presence of an interior wall helped in reducing the peak base shears in the boundary walls. Moreover, the flexibility of the diaphragm was significantly reduced by the presence of an interior wall located at the geometric center of the structure in the loading direction. In short, this study indicated that the diaphragm rigidity should be considered for torsional irregular structures, and the presence of an interior wall would help improve the performance of the structure.

Al Harash et al. (2010) investigated the effect of diaphragm openings on the inelastic seismic response of reinforced concrete structures. In particular, the rigid diaphragm

assumption for the reinforced concrete diaphragm with aspect ratio less than or equal to 3:1 (ASCE 7 2005) was assessed. A parametric study involving four locations of symmetric diaphragm openings and three types of diaphragm models, i.e. rigid, elastic and inelastic, was conducted on a 3-storey reinforced concrete building with diaphragm aspect ratio of 3:1 to investigate the inelastic behaviour of the structure under both static lateral loads (push-over) and dynamic ground motions (time-history). The analogue model was built using IDARC2, which is a computer program developed for two-dimensional analysis of 3D building systems (Panahshahi et al. 1988). In IDARC2, the reinforced concrete building was idealized as a series of plane frames linked together by floor slabs and transverse beams. The plane frames and floor slabs were modelled using tri-linear, inelastic elements with concentrated plasticity at member ends. The transverse beam was modelled using elastic springs with one vertical and one rotational degree of freedom. No test data was found in the study. The results showed that the loads resisted by the interior frames increased by the base shear redistribution due to the inelastic diaphragm deformation, particularly when diaphragm openings were located in the middle half of the building. This indicated that the actual response of the reinforced concrete building can only be captured if the inelastic diaphragm model was utilized. The rigid diaphragm assumption, which was suggested by ASCE 7 (2005), however, may result in a non-conservative estimation of diaphragm deformations and frame shears. In short, this work suggested that the inelastic behaviour of diaphragm should be considered for reinforced concrete structures with diaphragm openings.

In order to improve the global behaviour of the building, Brignola et al. (2008) proposed a framework, which can be used to protect undesired local mechanisms on

structures by controlling the in-plane stiffness of the diaphragm. Unlike other research methods, there have no numerical and experimental studies conducted in this work. Instead, the framework was proposed based on a summary of the state-of-the-art related to the influence of wood diaphragm in-plane stiffness on the seismic response of the un-reinforced masonry buildings. It was found that under seismic loads, the building collapse mechanism was affected by the diaphragm flexibility: in the case of flexible diaphragms, the resulting excessive displacements at the floor level may cause overturning of perimeter out-of-plane walls; in the case of rigid diaphragms, although the overturning mechanism can be protected, the distribution of seismic forces on shear walls increased. The increase in shear wall forces may lead to shear, sliding-shear or rocking mechanism if the quality of the masonry is poor or significant opening exists. Moreover, torsion mechanisms, which cause a concentration of outwards forces in the corners, can also be activated by rigid diaphragms. In summary, it was concluded that neither rigid nor flexible diaphragm assumptions would result in the conservative design for the un-reinforced masonry structure. The in-plane stiffness of the diaphragm should be controlled in accordance with the requirements of the displacements, accelerations and internal forces to maintain the demands of these properties within targeted levels.

In order to examine the effect of diaphragm flexibility on shear wall deflections, Pang and Rosowsky (2010) developed two types of beam-spring models to represent the diaphragm-shear wall system: a finite element based model and a simplified analogue model. In the beam-spring model, shear walls were modelled by non-linear single degree of freedom (SDOF) springs, and the diaphragm was modelled as an analogue beam, which acted as a load distribution mechanism. The finite element model can be used to

perform non-linear dynamic time history analyses on the entire structure, and the simplified analogue model was developed specifically for the seismic design. A series of full-scale shake table tests from the NEESWood project, which were conducted on a two-storey light-frame timber building, were utilized for model validations. Two diaphragm flexibility conditions were considered in the analyses of the building model, i.e. the semi-rigid diaphragm and the rigid diaphragm. By comparing with the test results, it was confirmed that the diaphragm in the building was semi-rigid. The model with the rigid diaphragm underestimated the drift responses in the second storey, which indicated that the load-sharing among shear walls were overestimated. The rigid diaphragm model deformed and rotated in a rigid body motion, which was unable to reproduce the deformed shape of the structure. Moreover, the maximum drift can only occur in the exterior walls, thus the drift demand in the interior walls was underestimated. In short, the main contribution of the study was to develop the beam-spring model, which can be used in the seismic analysis of light wood-frame constructions. It was found that the rigid diaphragm assumption may cause errors in the prediction of structural displacement response, and may overestimate the load demands for shear walls.

Li et al. (2010) studied the behaviour of a type of hybrid structure with concrete frames and wood-frame diaphragms under lateral loads. In particular, the flexibility of the diaphragm in the structure was investigated. A one-storey hybrid building was modelled in SAP2000 with four types of diaphragms models: 1) the detailed diaphragm model; 2) the simplified diaphragm model; 3) the rigid diaphragm model; and 4) the flexible diaphragm model. In the detailed model, beam elements were used to model the concrete frame and wood joists, and shell elements were used to represent the sheathing panels.

Connections between framing members and sheathing panels were modelled by nonlinear springs, and connections between joists were modelled as pin joints. The detailed model was calibrated with a test conducted on the one-storey hybrid building under both monotonic and cyclic loads. A simplified diaphragm model was developed based on the validated detailed diaphragm model, where the diaphragm was represented as linear elastic diagonal springs. The model can be used to replace the detailed diaphragm model for further studies on the behaviour of the hybrid structure. The rigid diaphragm model assumed that all components of the wood-frame diaphragm were rigid, while the flexible diaphragm model was modelled as a concrete frame without the diaphragm. By comparing the results obtained from the rigid and flexible diaphragm models with test results, it was confirmed that the diaphragm in the tested hybrid structure was closer to rigid. It was found that light wood-frame wood diaphragm has high in-plane stiffness and strength, which contributes a lot in the distribution of lateral load as well as guarantees the ductility and ultimate lateral bearing ability of the whole structure. In short, this study developed both detailed and simplified models for wood-frame diaphragms. In contrast to the popular flexible wood-frame diaphragm assumption, the diaphragm in the one-storey hybrid structure was closer to rigid.

He et al. (2011) conducted a further study on a six-storey concrete-wood hybrid building to investigate the seismic performance of multi-storey hybrid structures. The building model was built in SAP2000, and diaphragms were modelled using the simplified diaphragm models developed by Li et al. (2010). The analyses were performed under three diaphragm flexibility assumptions, i.e. the actual wood-frame diaphragm, the rigid diaphragm, and the flexible diaphragm. No test was conducted in the study. It was

observed that the load distribution results and displacement results of the structure with the wood-frame diaphragm model lay between that of the rigid and flexible diaphragm models. It was confirmed that diaphragms in the multi-storey hybrid structure were also closer to rigid. In short, this study was an application of the validated simplified diaphragm model (Li et al. 2010). The seismic analyses on the multi-storey hybrid structures confirmed that wood-frame diaphragms in the concrete frame-wood diaphragm hybrid structure were closer to rigid.

Moeini and Rafezy (2011) reviewed some modern seismic codes to find methods to classify the diaphragm flexibility. Reinforced concrete buildings with various building plane shapes, such as T-shape, L-shape, U-shape, and rectangular shape were modelled in the finite element program SAP2000 to investigate the efficiency of the code provisions. No experimental study was conducted. It was found that in general, most of the design codes accept that diaphragms should be treated as rigid. For conditions under which the flexibility of the diaphragm must be considered, some codes such as EC8 (European Committee for Standardization (CEN) 1994), NZS4203 (Standards Assiciation of New Zealand 1992) and GSC-2000 (Earthquake Planning and Protection Organization 2000) set certain qualitative criteria, which were related to the shape of the diaphragm to determine its flexibility. Other codes such as 2800 (Building and Housing Research Center 2005), UBC-97 (ICBO 1997), SEAOC-90 (Structural Engineers Association of California (SEAOC) 1990) and FEMA-273 (Federalc Emergency Management Agency 1998) set quantitative criteria, which were related to the in-plane deformation of the diaphragm and the average drift of the associated storey instead. The modelling results concluded that the quantitative and qualitative code criteria should always be used

together for the classification of diaphragm flexibility. Moreover, the effect of the aspect ratio of the diaphragm and diaphragm openings should be considered.

Sadashiva et al. (2011) carried out a series of time history analyses to quantify the effect of diaphragm flexibility on the response of symmetric structures. Numerical models with various deformation types, stories, and structural heights were built in the finite element program SAP 2000. Spring elements and beam elements were utilized to represent the walls and diaphragms, respectively. No experimental was found in this work. Analyses results showed that one-storey elastic structures were most affected by the diaphragm flexibility, and the effect reduced with increasing structural height. The fundamental natural period of the structure increased with increasing diaphragm flexibility, and the rate of the increase decreased with increasing structural height. This was attributed to the fact that a rigid diaphragm assumption may overestimate the design base shear, while underestimate the displacement demand of the structure. In short, this work suggested that the flexibility of the diaphragm should be taken into account in the structural design, especially for structures with lower structural heights.

From the above reviewed papers, it is found that whether a diaphragm in a building should be treated as flexible or rigid is very case dependent. The flexibility of the diaphragm varies with different structural configurations, and the classification method provided in the code may not always be appropriate. Two major missing aspects found in the current design practice are: 1) a robust quantitative basis that can help determine the flexibility of the diaphragm accounting for all types of structural configurations; and 2) a guidance to identify the likely change in the structural performance regarding to different levels of diaphragm flexibility (Sadashiva et al. 2011). Numerical analyses are the

commonly utilized methods in the study of the diaphragm stiffness, and insights are obtained from the comparison of the structural responses with different flexibility assumptions. It is suggested by the reviewed studies that the rigidity of the diaphragm should be considered when torsional irregularities exist, while the flexibility of the diaphragm should be considered when diaphragm openings exist.

Chapter 3: Connection Model

Panel-frame nail connections, namely, connections that are utilized to connect the sheathing panels to the framing members, are widely used in light-frame wood construction. It is well known that these connections have great influence on the behaviour of the structure. In addition to dissipating energy when subjected to seismic loads, connections between framing members and sheathing panels serve another important purpose. They are the main source of strength and stiffness for wood-frame shear walls and diaphragms (Dolan and Madsen 1992).

This chapter provides an introduction to the finite element program HYST, which simulates the hysteretic behaviour of panel-frame nail connections. Later, results from HYST will be incorporated into the wood-frame diaphragm model to represent the connections between sheathing panels and framing members, as introduced in Chapter 4. As a part of this thesis work, a series of single connection tests have been conducted to calibrate the HYST model. The comparison between the calibrated HYST model prediction and the test load-slip curve is reported in the following.

3.1 Introduction to HYST

HYST is a finite element program developed at the Civil Engineering Department of the University of British Columbia for the study of the hysteretic behaviour of general connections in light-frame wood construction. HYST was originally developed by Foschi (2000) and was later expanded and described in detail by Li et al. (2011). By using basic mechanical properties of the nail and wood, HYST captures the typical hysteretic characteristics of the connection, such as strength and stiffness degradation. Furthermore, the “pinching” effect, which is represented as a sudden loss of stiffness in the hysteresis

loop, is taken into account by tracking the formation of gaps between the nail shank and the surrounding wood medium (Li et al. 2011). The introduction to HYST is provided in this section.

In HYST, the hysteretic behaviour of a connection is influenced by two factors: the elasto-plastic characteristics of the nail and the behaviour of wood when compressed (Foschi 2000). To understand these factors, Figure 3-1 shows a lateral load, *F*, applied at the head of a nail that has been driven into the wood. Δ is the horizontal displacement of the nail head. The nonlinear behaviour of the nail connection, namely, the relationship between Δ and *F*, is typically represented by a hysteresis loop.

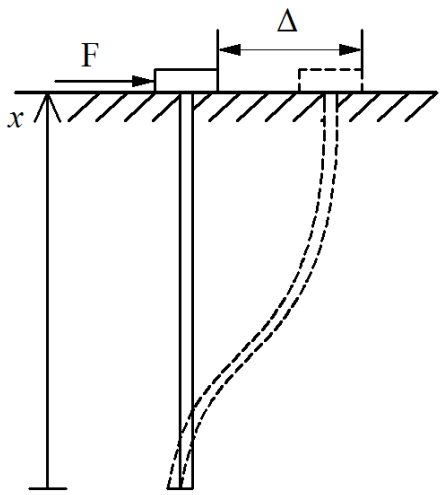

Figure 3-1 Pin connector (Foschi 2000)

Under the load *F*, the nail will deform laterally adopting a shape *w*(*x*), as shown in Figure 3-2. Because the interface between the nail and the wood medium cannot carry tensile force, the corresponding reaction from the wood medium per unit length of the nail, *p*, is a compressive force. *p* is a function of the displacement *w*, and the relationship between *p* and *w* is known as the embedment property of the wood medium (Foschi and Yao 2000).

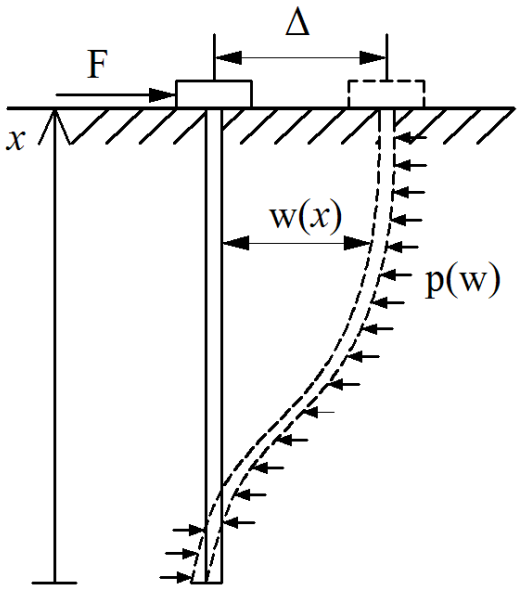

Figure 3-2 Typical mechanical connector (Foschi 2000)

An important objective in this chapter is to determine the embedment property, $p(w)$, for particular nail and wood configurations. Laboratory tests with uniform pressure along the nail would be ideal, but this is unfortunately difficult to realize in practice. In fact, because the nail undergoes bending during testing it is difficult to measure p and w along the nail. As a result, the embedment property of the wood medium cannot be obtained directly from a connection test. The remedy that is adopted in HYST is to build a detailed finite element model for the connection (Foschi 2000). As shown in Figure 3-3, the nail shank in HYST is modelled by beam elements. The compression behaviour of the wood medium is modelled by many compression-only nonlinear springs along the nail shank. Each node on the nail shank has three degrees of freedom: u, w, and w', i.e., axial displacement, lateral displacement, and rotation, respectively. The shape function for the axial displacement u is linear, while cubic polynomials are employed for the lateral displacement w. The embedment property of the wood medium is essentially the properties of the nonlinear springs.

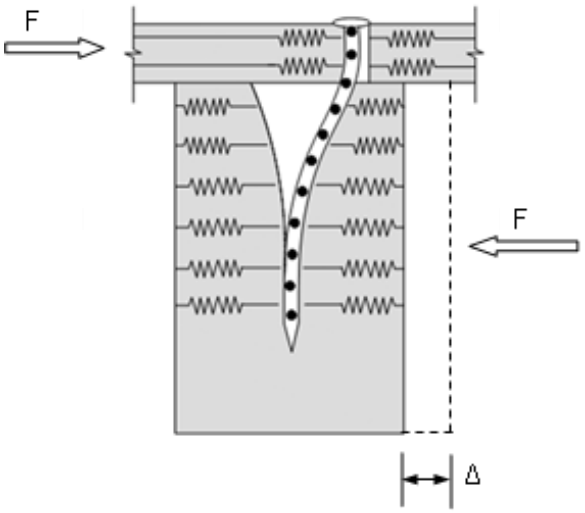

Figure 3-3 Schematics of HYST panel-frame nailed connection (Li et al. 2011)

In HYST, the beam element that is used to represent the steel nail shank is assumed to obey an elasto-plastic constitutive relation. The embedment property of the wood medium, namely, the assumed relationship between the deformation *w* and the reaction pressure *p*(*w*) under monotonic loading is represented by the following equation (Li et al. 2011):

$$\begin{cases} p(w) = (Q_0 + Q_1 w)\left(1 - e^{\frac{-K_0 w}{Q_0}}\right) \quad if \;\; w \le D_{\max} \\ p(w) = p_{\max} e^{Q_3 (w - D_{\max})^2} \qquad if \;\; w > D_{\max} \end{cases} \tag{3.1.1}$$

where

$$p_{\max} = \left(Q_0 + Q_1 D_{\max}\right)\left(1 - e^{\frac{-K_0 D_{\max}}{Q_0}}\right) \tag{3.1.2}$$

and

$$Q_3 = \frac{\log_{10}(0.8)}{\left[\left(Q_2 - 1.0\right) D_{\max}\right]^2} \tag{3.1.3}$$

The expression of $p(w)$ contains five undetermined parameters: K_0 ,Q_0 ,Q_1 ,Q_2, D_{max}, which are called embedment parameters. These embedment parameters are required for the characterization of the embedment property of the wood medium. Figure 3-4 shows the relationship expressed in Eq. (3.1.1). It is assumed that the compressive behaviour of the wood medium shows a peak p_{max} followed by a softening trend, thus $p(w)$ is represented by two exponential curves that meet at the peak load.

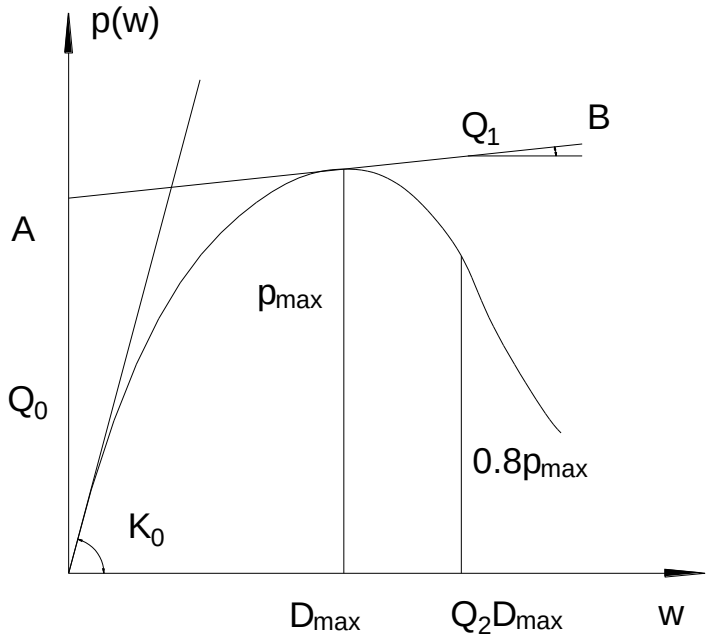

Figure 3-4 Embedment properties (Li et al. 2011)

Figure 3-4 also shows that K_0 is the initial stiffness of the embedment relationship curve. Q_0 and Q_1 are the intercept and the slope of the asymptote AB, respectively. Q_2 represents the fraction of D_{max} at which p drops to $0.8p_{max}$ during the softening stage.

The loading and re-loading rule in HYST, which represents the embedment response under cyclic load, is shown in Figure 3-5. If the wood medium is unloaded at Point A, the pressure p will decrease along the line AB with a constant unloading stiffness, K_0. After reaching Point B, the pressure p becomes zero and further unloading, i.e., further decrease

in the displacement *w*, takes place from Point *B* to Point *O*. Upon reloading, *p* remains p=0 until *w* reaches D_0. Thus, D_0 represents the magnitude of the gap between the nail shank and the wood medium. Reloading from Point *B* also follows a straight line but with a reduced stiffness K_{RL}. The relationship between K_{RL} and K_0 is expressed as follows (Li et al. 2011):

$$\begin{cases} K_{RL} = \left(\dfrac{D_y}{D_0} \right)^{\alpha} K_0 & if \;\; D_0 \geq D_y \\ K_{RL} = K_0 & if \;\; D_0 < D_y \end{cases} \tag{3.1.4}$$

where $D_y=Q_0/(K_0-Q_1)$ represents a yielding deformation that is given by the intersection of the initial slope and the asymptote, as shown in Figure 3-5. It is observed in Eq. (3.1.4) that the adjustment from K_0 to K_{RL} depends on D_0, and a stiffness degradation exponent α. The reloading will proceed until Point *C*. Subsequent unloading from Point *C* will follow the line *CD*, which has the same slope as K_0, until the second p=0 Point *D* is reached. After the reloading, the magnitude of the gap changes from D_0 to D_0'.In summary, the reloading rules in HYST permit the modelling of strength and stiffness degradation during cyclic loading, which affects the energy dissipation of the connection.

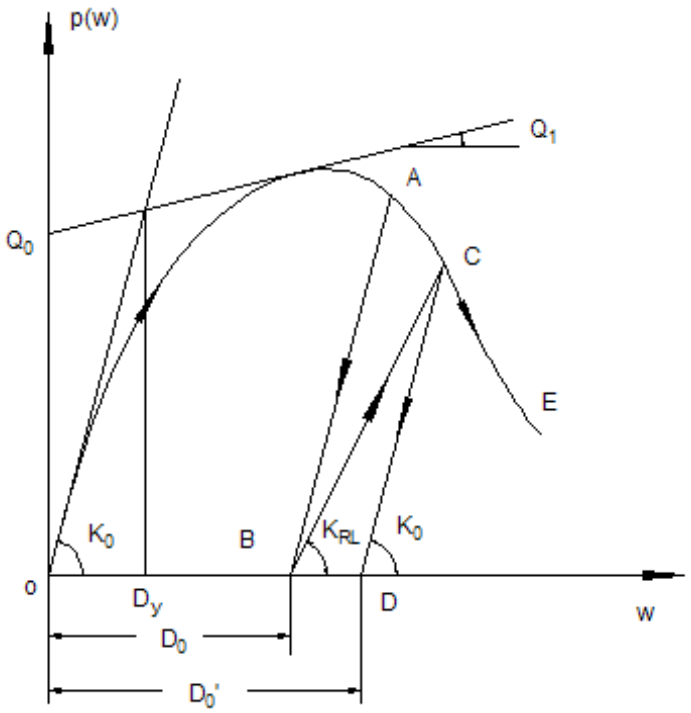

Figure 3-5 Loading and unloading paths (Li et al. 2011)

The input to HYST involves mechanical properties for the steel nail shank and embedment parameters for the wood medium. In the program, the principle of virtual work is utilized as the basis of the finite element analysis. Specially, the total work of all forces acting on the connection in any virtual displacement is zero, as expressed in the following:

$$\delta W = \delta W_I + \delta W_E = 0 \tag{3.1.5}$$

where δW is the total virtual work, δW_I is the total internal work, and δW_E is the total external work. In HYST, the total internal work is computed as:

$$\delta W_I = \int_0^L p(|w|)(\frac{w}{|w|})\delta w dx + \int_V \sigma(\varepsilon)\delta\varepsilon dv \tag{3.1.6}$$

and the total external work is computed as:

$$\delta W_E = -F\delta w_{x=L} \tag{3.1.7}$$

By substituting Eq. (3.1.6) and Eq. (3.1.7) into Eq. (3.1.5) , the following relationship is obtained:

$$\int_0^L p(|w|)(\frac{w}{|w|})\delta w dx + \int_V \sigma(\varepsilon)\delta\varepsilon dv = F\delta w_{x=L} \qquad (3.1.8)$$

In these equations, w and $p(w)$ are the displacement of the nail and the corresponding reaction pressure force of the wood medium, as shown earlier in Figure 3-2. $(w/|w|)$ indicates the direction of the displacement, and δw represents the virtual displacement. V is the total volume of the nail shank. ε and $\sigma(\varepsilon)$ are the strain and stress in the nail, and $\delta\varepsilon$ is the virtual strain corresponded to w. F is the external lateral load applied at $x=L$, namely, the position of the nail head, as shown earlier in Figure 3-1. $\delta w_{x=L}$ represents the virtual displacement of the nail head. For simplicity, the HYST model ignores frictional forces between the nail and the wood medium (Foschi 2000).

In Eq. (3.1.6), the internal work of the connection consists of two integral terms, which account for the compression of the wood medium and the bending of the nail respectively. In Eq. (3.1.7), the relationship between the applied lateral load and the displacement of the nail head, which is represented as the load-slip response of the connection, can be obtained from connection tests. By using an optimization algorithm, $p(w)$ in Eq. (3.1.8) is calibrated with either the load-slip curve from monotonic loading connection tests or the backbone curve from cyclic loading connection tests, as explained shortly. After obtaining the calibrated $p(w)$, the HYST model can be used to predict the hysteric behaviour of the connection under various load conditions.

In this study, the HYST model is calibrated using a search-based optimization program (Li et al. 2011). The calibration of the model is essentially the calibration of wood embedment properties. Specifically, the embedment parameters of the wood

medium are adjusted in the optimization program to minimize the error ε_e between the model prediction and the test result, as expressed in the following:

$$\varepsilon_e = \sum_{i=1}^{n} (F_{i,HYST} - F_{i,test})^2 \tag{3.1.9}$$

where $F_{i,test}$ is the load at point i of the load-slip curve from connection tests, and $F_{i,HYST}$ is the predicted load at the same point i, from the HYST model. n is the total number of points along the load-slip curve, which are considered in the comparison.

The starting point of the optimization is to specify initial values and upper and lower bounds of the embedment parameters. Then, the total number of trials is selected, which in turn determines the step size of the optimization. In the program, trial solutions within the upper and lower bounds are generated following the specified step size, and errors corresponding to these trial solutions are calculated. If a trial solution results in a smaller error, the program updates the best solution. The optimization continues until the error reaches a stop criterion, i.e., the predetermined total number of trials, and the optimal embedment parameters are those that yield the minimum error. The optimization is considered effective if the coefficient of determination, R^2, which indicates how well the model prediction line fits the connection test load-slip curve, is close to 1; otherwise, the above optimization procedures should be repeated with an increased total number of trials, until the error between the model prediction and the test result reaches the requirement.

3.2 Connection Test

The nail connections that connect the sheathing panels to the framing members represent a crucial part of the diaphragm models that are presented in later chapters. As introduced in Section 3.1, this type of nail connection is modelled using HYST. In order to establish a good connection model, it was decided to carry out laboratory tests of the nail connection as part of this thesis work. Every effort was made to replicate the details of the connection that appear later in this thesis. The results of connections tests, as well as the calibrated embedment parameters for the connection model, are reported in this section.

To match the diaphragm configurations that are studied in Chapter 4, the connection test specimen is constructed using 4×4 in (102×102 mm) Douglas-fir framing and 23/32 in (18 mm) thick plywood sheathing panel. 10d common nails (76 mm in length and 3.69 mm in diameter) are utilized to connect the sheathing panels to the framing members. A total of 20 specimens are divided into four groups according to the combination of grain orientations for both sheathing panels and framing members, as listed in Table 3-1. Each group contains 5 replications. The average load-slip curve of all 20 tests will be used for the calibration of the connection model. As such, the wood-frame diaphragm is assumed to experience the average nail behaviour when subjected to loads.

Table 3-1 Group configurations

Group Number	Direction of Grain in Framing Lumber	Direction of Face Grain in Plywood Sheathing Panel
1	Parallel	Perpendicular
2	Perpendicular	Perpendicular
3	Perpendicular	Parallel
4	Parallel	Parallel

The test setup is shown in Figure 3-6 and Figure 3-7. The top of the plywood panel is rigidly connected with the loading head of the actuator, and the bottom of the framing lumber is fixed on the test table by a steel bar. A transducer is utilized to measure the relative movement between the sheathing panel and the bottom of the framing member. Schematic drawings for sizing specifications are shown in Figure 3-8.

In the test, the load is applied vertically to the top of the plywood sheathing panel. The test specimen is loaded in tension, until the load decreased to at least 80% of the peak load. The test is displacement controlled, with the actuator displacement rate of 0.3 mm per second. The loading is monotonic, and load and displacement data are continuously recorded.

(a) **(b)**

Figure 3-6 Single nail test setup: (a) front view (b) back view

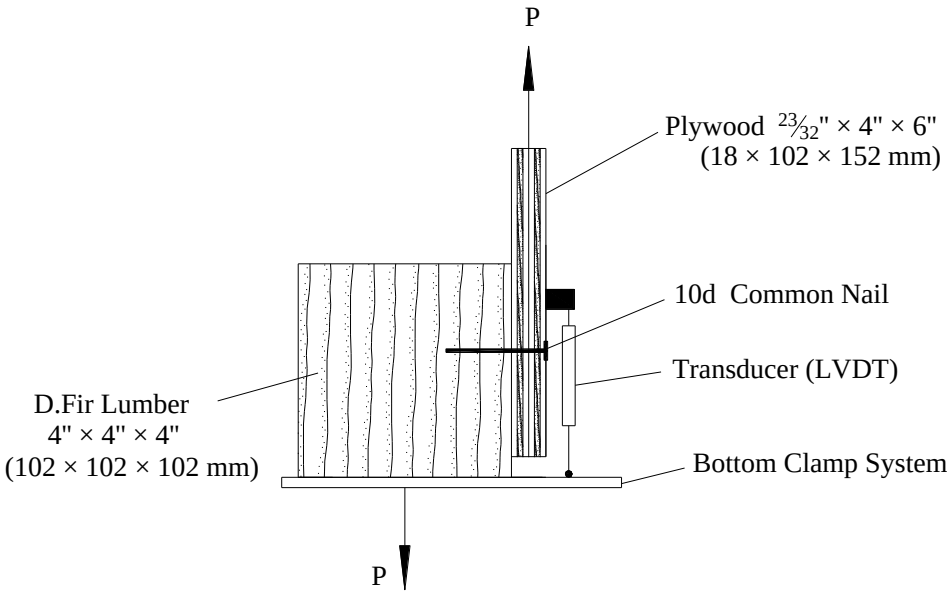

Figure 3-7 Specific test apparatus

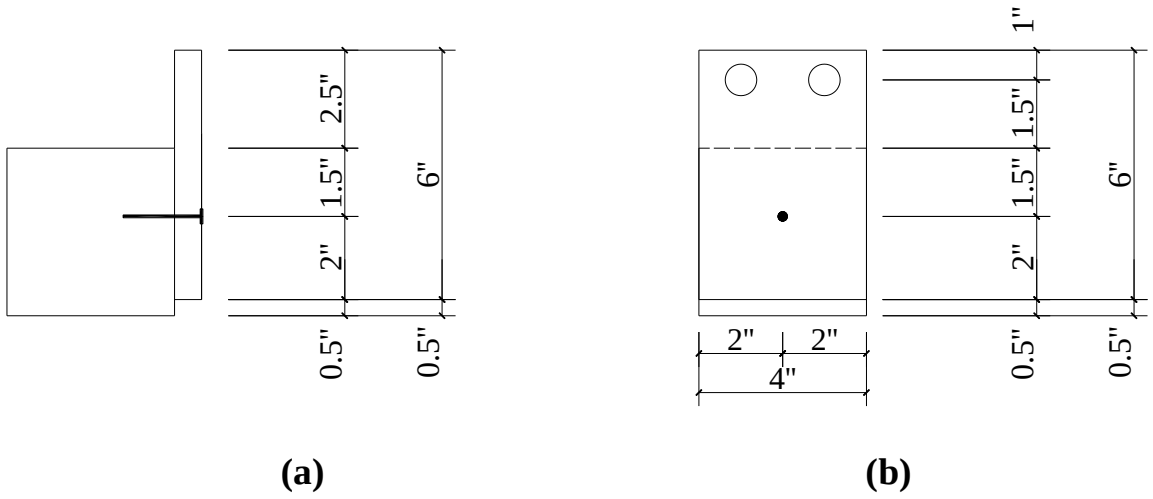

Figure 3-8 Sizing specifications (1 in=25.4 mm): (a) side view (b) front view

As shown in Figure 3-9, under the applied load, the nail bends laterally and the shank of the nail experiences a partial withdrawal. The observed major failure mode for the connection is the nail pull-through, namely, the head of the nail pulls through the plywood panel.

(a) **(b)**

Figure 3-9 Failure of single nail connection: (a) front view (b) side view

To expose the variability in the test results, eight parameters (EEEP parameters) are selected to reflect the characteristic of the load-slip curve for each specimen: peak load, peak displacement, elastic stiffness, yield load, yield displacement, failure load, ultimate displacement, and ductility. This is done in accordance with ASTM (ASTM 2011). These parameters are determined based on an equivalent energy elastic plastic (EEEP) curve, which is a perfectly elastic plastic idealization of the load-slip response of the specimen. The EEEP curve is illustrated in Figure 3-10. The envelope curve is either the backbone curve from cyclic tests or the load-slip curve from monotonic tests. The EEEP curve is constructed to provide the same amount of energy dissipated in a test. In other words, the area beneath the EEEP curve is equal to the area enclosed by the envelope curve from the origin to the ultimate displacement.

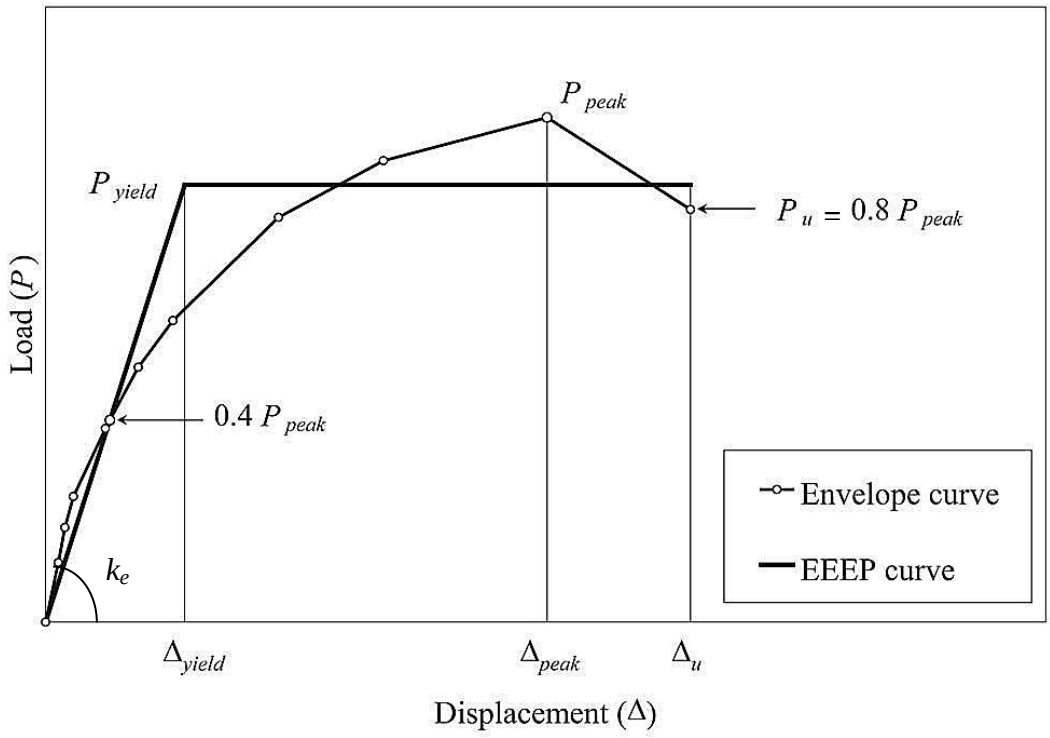

Figure 3-10 Performance parameters of specimen (ASTM 2011)

In Figure 3-10, the peak load, P_{peak}, is the maximum load resisted by the connection on the envelope curve. The peak displacement, Δ_{peak}, is the displacement at P_{peak}. The elastic stiffness, k_e, is the slope of the secant, which passes through the origin and the point on the envelope curve where the load is equal to $0.4P_{peak}$. The failure load P_u is found on the post-peak stage of the envelope curve, where the resistance dropped to $0.8P_{peak}$. The corresponding displacement, Δ_u, is defined as the ultimate displacement. The elastic line of the EEEP curve begins at the origin, and has the slope that is equal to k_e. The plastic line of the EEEP curve is a horizontal line, which extends until the ultimate displacement. The yield load, P_{yield}, and the displacement at yield, Δ_{yield}, is defined as the intersection of the elastic and plastic lines of the EEEP curve. P_{yield} must be greater than or equal to P_u, and is determined by the following equation (ASTM 2011):

$$P_{yield} = \left(\Delta_u - \sqrt{\Delta_u^{\,2} - \frac{2A}{k_e}} \right) k_e \qquad (3.2.1)$$

where A is the area under the envelop curve from the origin to the ultimate displacement. If $\Delta_u^{\,2} < 2A/k_e$, it is permitted to assume $P_{yield} = 0.85P_{peak}$. The yield displacement is calculated based on P_{yield} using the relationship:

$$\Delta_{yield} = \frac{P_{yield}}{k_e} \qquad (3.2.2)$$

The ductility is calculated as the ratio of the ultimate displacement and the yield displacement, as expressed in the following:

$$D = \frac{\Delta_u}{\Delta_{yield}} \qquad (3.2.3)$$

The test load-slip curves for the four groups of specimens are shown in Figure 3-11 to Figure 3-14. It is observed that even within the same group, the behaviour of the connection varies between specimens. The aforementioned eight EEEP parameters are utilized as performance indicators for the specimens. For each group, variations among responses of specimens are discussed in terms of these parameters, as listed in Table 3-2 to Table 3-5. The coefficient of variation (COV) of each parameter is given in the tables as well.

Test results for Group 1 specimens are shown in Figure 3-11, and the corresponding EEEP parameters are summarized in Table 3-2. It is observed that all the specimens perform similarly at the beginning. However, there is a wide variation in the elastic stiffness, which has a COV of 21.03%. The peak load values are in close agreement. The strongest Specimen 2 can resist a maximum load of 3.78 kN, while the weakest Specimen 3 resists 3.42 kN. The difference between the two is only 10%. The failure load is

determined bead on the peak load, thus it follows the same pattern as the peak load. The variation in the yield load is also very small, with a COV of 5.22%. Although all the specimens yield similar peak loads as well as yield loads, displacements at the peak load and yield load are varied, with the COV of 21.09% and 22.72% respectively. Compared with other specimens, specimen 4 has a much larger ultimate displacement, which allows it to deform without failing thus dissipate a greater amount of energy. The ductility of Specimen 4 is smaller than Specimen 2 and Specimen 3, which suggests that the specimen with the largest displacement capacity is not necessarily the most ductile specimen. The ductility is a function of the elastic stiffness, the yield load and the ultimate displacement. Given the variation that exists when calculating these three parameters, scattered results are expected for the ductility, with a COV of 19.89%.

Figure 3-12 shows test results for Group 2 specimens, and the EEEP parameters for each load-slip curve are summarized in Table 3-3. It is observed that specimens in this group also behave similarly at the beginning part of the load-slip curve. All specimens yield similar peak loads, failure loads, yield loads, as well as displacements at the peak load and failure load. Specimen 4 is the most ductile specimen and also fails at the largest displacement. Wide variations are still observed in the elastic stiffness, the yield displacement and the ductility, with the COV of 23.74%, 32.4% and 32.18% respectively.

The test load-slip curves for Group 3 specimens are shown in Figure 3-13, and the corresponding EEEP parameters are listed in Table 3-4. Compared with Group 1 and Group 2, specimens in this group also have similar behaviour at the beginning. Variations in the peak load, the failure load, the yield load and the yield displacement are small, while large discrepancies are observed in other parameters. Specimen 5 is the strongest

specimen, while has a low ductility factor of 5.71. Specimen 2 is the most ductile specimen, while can only resist a maximum load of 3.4 kN. It is found that Specimen 5 fails rapidly after reaching the peak load; on the contrary, Specimen 3 can maintain the smaller load through a large displacement thus has a larger ductility ratio. Specimen 3 has the lowest elastic stiffness and also fails at the lowest displacement.

Test results for Group 4 specimens are shown in Figure 3-14, and the EEEP parameters are given in Table 3-5. It is observed that unlike other groups, variations exist from the beginning of the load-slip curves for this group of specimens. This results in a large COV of 39.67% in the elastic stiffness. All specimens have similar peak loads, yield loads, failure loads, but other EEEP parameters are inconsistent. Compared with other specimens, Specimen 3 and Specimen 5 fail much more rapidly, which reduce their abilities to dissipate energy. Specimen 2 is the strongest specimen while has the lowest elastic stiffness. Although Specimen 2 has the largest displacement capacity, the ductility ratio is very low. The most ductile specimen is Specimen 4, which is, however, the weakest specimen.

The observed variations among the responses of the specimens in the same group are believed to stem from the inherent variation of the wood material. In particular, the moisture content, the density, and the position of defects or knots will all have influence on the behaviour of the connection. For example, previous studies (Winistorfer and Soltis 1994; Rammer and Winistorfer 2001) found that the lateral stiffness and strength of the connection increase with increasing wood density and decrease as the moisture content increases.

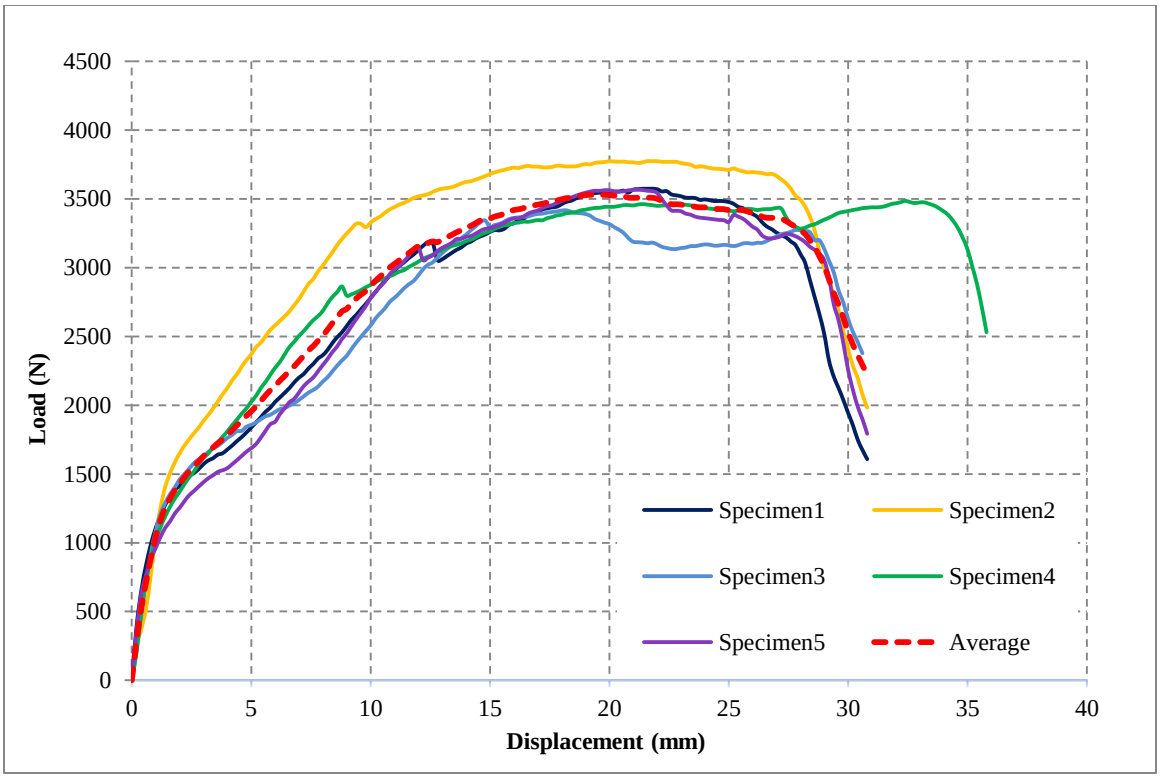

Figure 3-11 Load-slip curves for Group 1 specimens

Table 3-2 EEEP parameters for Group 1 specimens

Parameters	Specimen Number					COV
	1	2	3	4	5	
k_e (kN/mm)	0.69	0.94	0.83	0.67	0.49	21.03%
P_{peak} (kN)	3.57	3.78	3.42	3.49	3.57	3.37%
Δ_{peak} (mm)	21.80	21.60	18.20	32.40	21.20	21.09%
P_{yield} (kN)	3.04	3.38	2.88	3.16	3.11	5.22%
Δ_{yield} (mm)	4.44	3.60	3.49	4.73	6.34	22.72%
P_u (kN)	2.86	3.02	2.73	2.79	2.85	3.37%
Δ_u (mm)	28.48	28.96	29.82	35.51	29.28	8.51%
D	6.41	8.04	8.55	7.51	4.62	19.89%

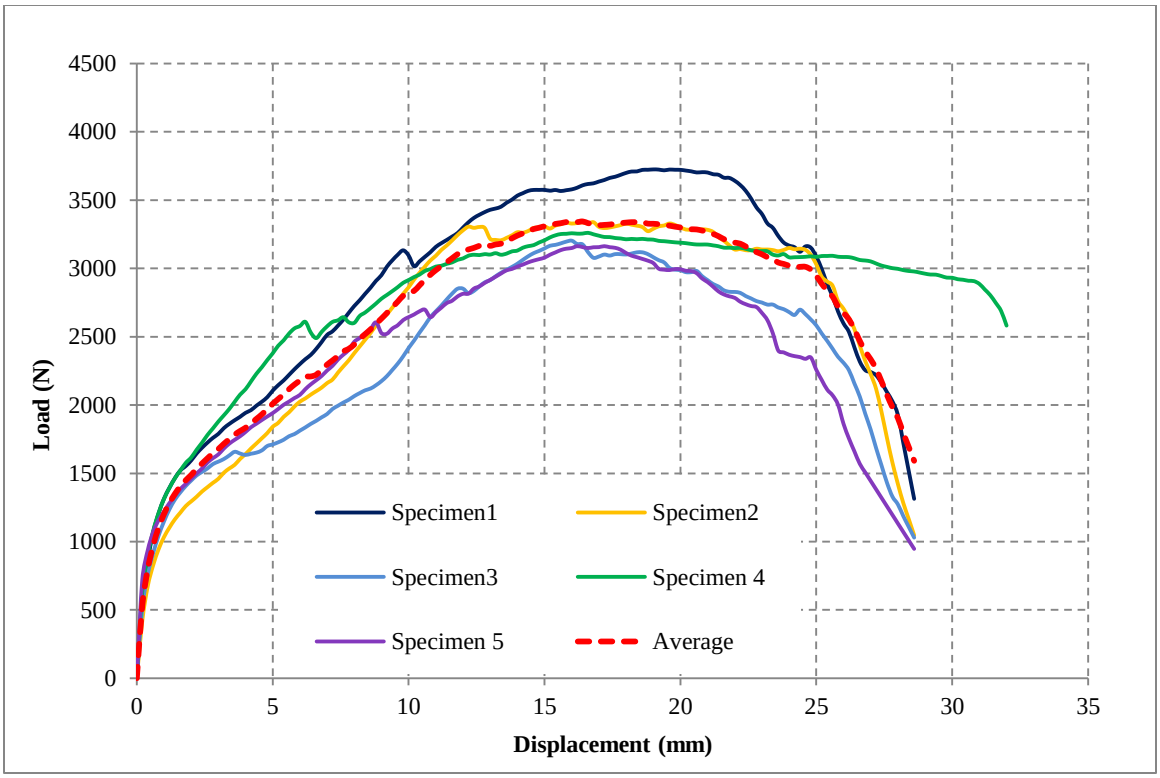

Figure 3-12 Load-slip curves for Group 2 specimens

Table 3-3 EEEP parameters for Group 2 specimens

Parameters	Specimen Number					COV
	1	2	3	4	5	
k_e (kN/mm)	1.00	0.60	0.97	1.33	1.11	23.74%
P_{peak} (kN)	3.73	3.34	3.20	3.26	3.16	6.06%
Δ_{peak} (mm)	19.00	16.80	16.00	16.60	16.20	6.37%
P_{yield} (kN)	3.13	2.95	2.57	2.90	2.63	7.35%
Δ_{yield} (mm)	3.13	4.93	2.66	2.18	2.38	32.40%
P_u (kN)	2.98	2.67	2.56	2.61	2.53	6.06%
Δ_u (mm)	25.23	26.10	25.07	31.95	23.39	11.14%
D	8.06	5.30	9.44	14.65	9.85	32.18%

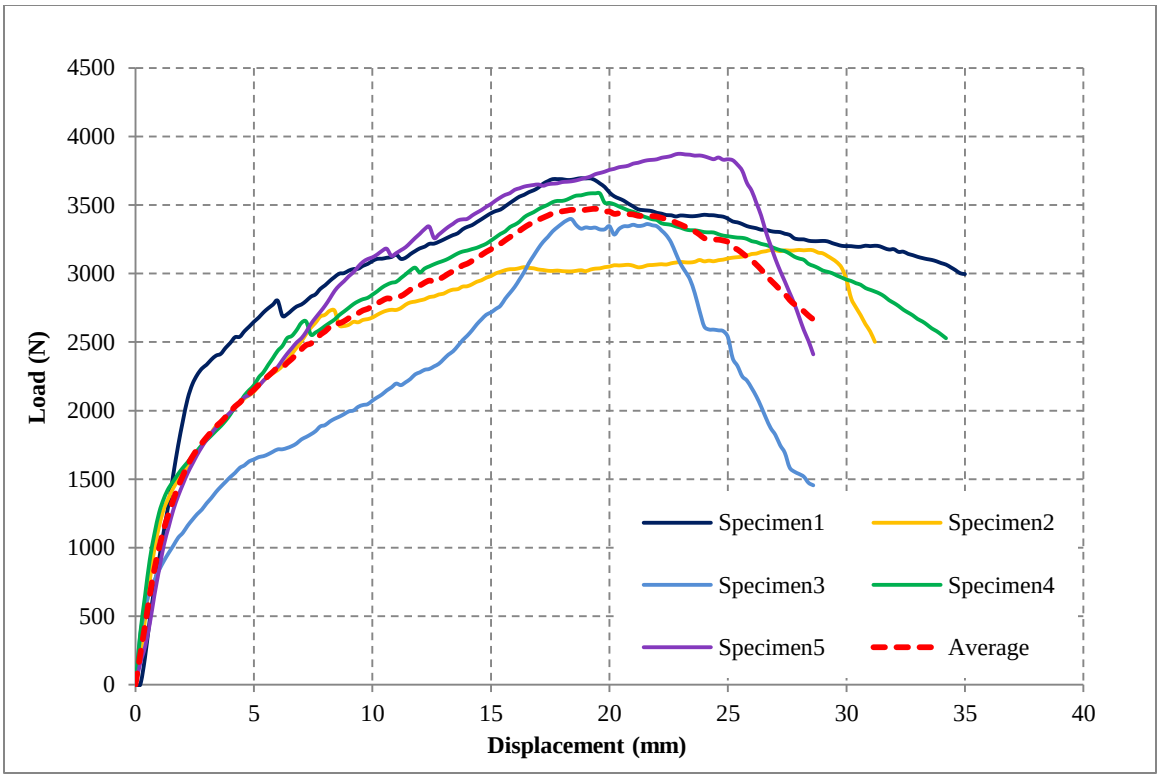

Figure 3-13 Load-slip curves for Group 3 specimens

Table 3-4 EEEP parameters for Group 3 specimens

Parameters	Specimen Number					COV
	1	2	3	4	5	
k_e (kN/mm)	0.96	1.08	0.43	1.03	0.70	29.05%
P_{peak} (kN)	3.70	3.17	3.40	3.59	3.87	6.83%
Δ_{peak} (mm)	18.80	28.00	18.40	19.40	23.00	16.86%
P_{yield} (kN)	3.21	2.80	2.65	3.01	3.31	8.14%
Δ_{yield} (mm)	3.35	2.60	6.21	2.93	4.73	33.73%
P_u (kN)	2.96	2.54	2.72	2.87	3.10	6.83%
Δ_u (mm)	35.00	31.11	23.82	31.21	27.02	12.99%
D	10.44	11.99	3.84	10.64	5.71	37.12%

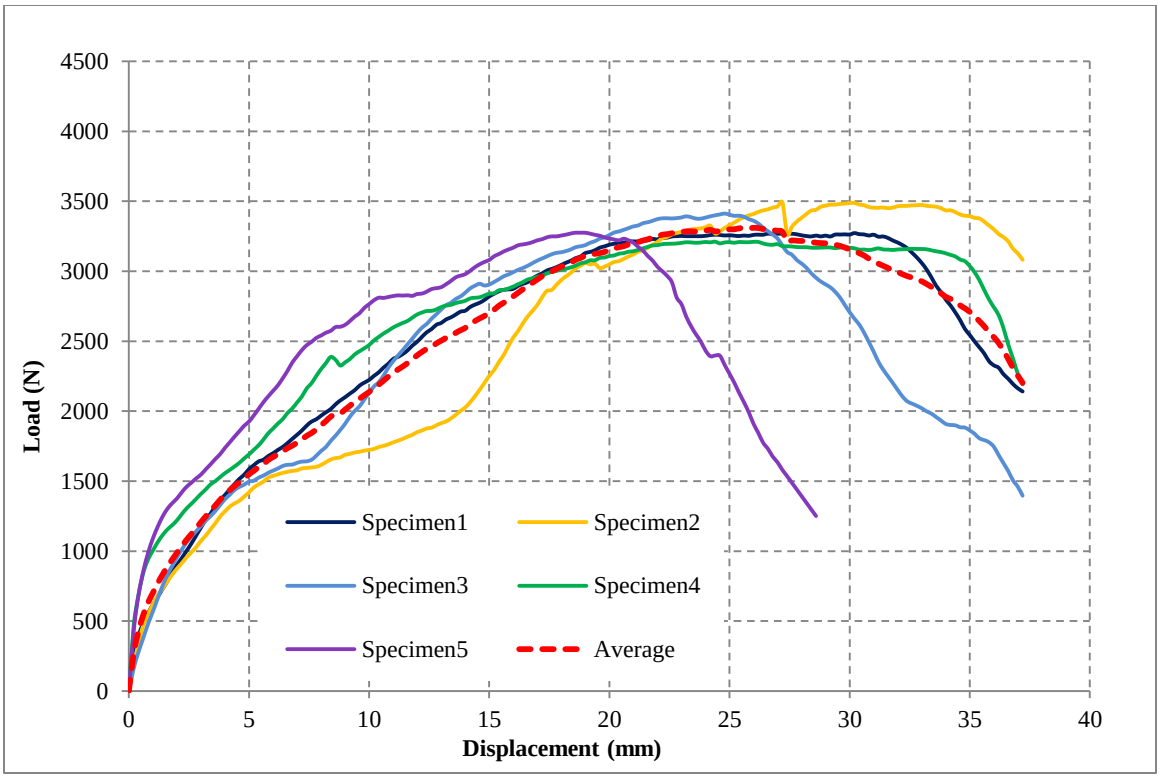

Figure 3-14 Load-slip curves for Group 4 specimens

Table 3-5 EEEP parameters for Group 4 specimens

Parameters	Specimen Number					COV
	1	2	3	4	5	
k_e (kN/mm)	0.37	0.29	0.34	0.56	0.80	39.67%
P_{peak} (kN)	3.27	3.49	3.41	3.21	3.28	3.11%
Δ_{peak} (mm)	30.20	27.20	24.80	24.40	18.60	15.28%
P_{yield} (kN)	2.90	2.92	2.89	2.86	2.76	1.90%
Δ_{yield} (mm)	7.87	10.12	8.39	5.12	3.46	34.12%
P_u (kN)	2.62	2.79	2.73	2.57	2.62	3.11%
Δ_u (mm)	34.70	37.20	29.91	36.45	23.36	15.93%
D	4.41	3.68	3.57	7.12	6.75	29.89%

The average load-slip curve from for each group is shown in Figure 3-15. The total average load-slip curve over the four groups is represented by the dashed line. The EEEP parameters for each curve are summarized in Table 3-6. On average, it is observed that Group 1 is the strongest among the four groups, which has a load capacity of 3.53 kN. Group 2 is the most ductile group, and has the largest elastic stiffness as well. Except for Group 4, behaviours of connections of the other three groups are in close agreement. Specimens in Group 4 are the weakest with lower stiffness at the beginning. However, the displacement capacity of this group is much larger than other groups. The ductility ratio of Group 4 is also the lowest because of the significantly larger yield displacement.

The variations of the load-slip curves indicate the variability of the connection behaviour when changing the grain direction for the framing and the sheathing panel. The total average load-slip curve of the four groups of specimens, which is considered as the average connection behaviour in all directions of the wood grain, is utilized to calibrate the HYST model. Specifically, a total of ten wood embedment parameters, namely, five for the framing lumber layer and five for the sheathing panel layer, are estimated based on the total average test load-slip curve in the calibration. In HYST, a modulus of elasticity of 200GPa is used for the steel, and a steel yield strength f_y of 690 MPa is used for 10d common nails based on previous research (Chui et al. 1998).

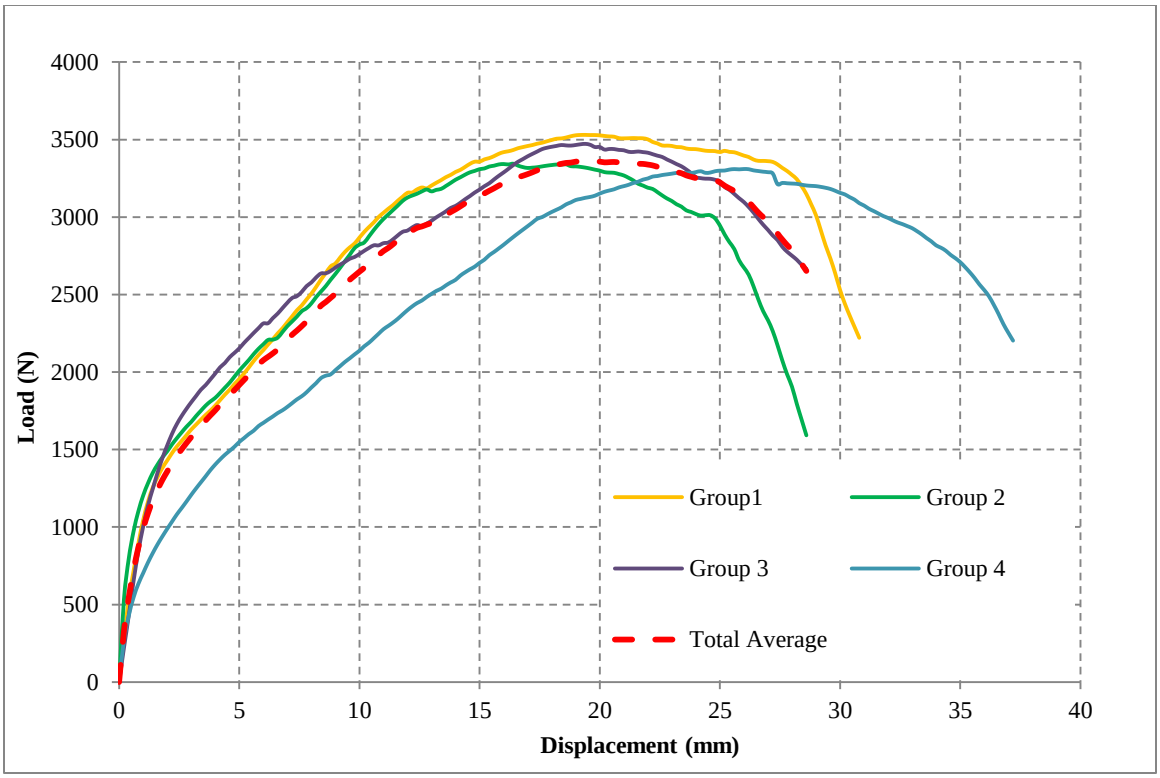

Figure 3-15 Load-slip curve of single nail connection test

Table 3-6 EEEP parameters for averages of groups

Parameters	Group Number				COV of Group 1, 2 and 3	COV of All Groups
	1	2	3	4		
k_e (kN/mm)	0.73	0.98	0.83	0.37	12.13%	30.88%
P_{peak} (kN)	3.53	3.34	3.47	3.31	2.25%	2.64%
Δ_{peak} (mm)	19.40	16.40	19.40	26.00	7.69%	17.30%
P_{yield} (kN)	1.93	1.75	2.03	2.01	6.07%	5.68%
Δ_{yield} (mm)	4.82	3.41	4.20	8.96	13.94%	40.08%
P_u (kN)	2.82	2.68	2.78	2.65	2.26%	2.65%
Δ_u (mm)	29.39	26.00	27.79	35.38	5.00%	11.89%
D	6.10	7.63	6.61	3.95	9.38%	22.12%

In the optimization program, which is introduced in Section 3.1, for simplicity, the same Q_2 and D_{max} are assigned to the framing layer and the sheathing layer. The other three embedment parameters for the two wood layers are adjusted separately to fit the average load-slip curve in Figure 3-15. The calibrated wood embedment parameters are listed in Table 3-7. These parameters are considered effective since the coefficient of determination between the model and the test result is 0.995, which is very close to 1. The comparison between the model load-slip curve and the average test load-slip curve is shown in Figure 3-16, and the corresponding EEEP parameters for the two curves are listed in Table 3-8. It is observed that the model predicted load-slip curve fits well with the test curve, and all the EEEP parameters are in close agreement. This demonstrates that the five embedment parameters provide enough flexibility for the HYST model, which is capable of fitting the average test load-slip response of the connection.

Table 3-7 Calibrated embedment parameters for HYST model

Embedment Parameters	Douglas-fir Lumber	Plywood Panel	Total Error	Coefficient of Determination
Q_0 (kN/mm)	0.219	0.095	ε= 0.4026 (kN^2)	R^2=0.995
Q_1 (kN/mm^2)	0.072	0.097		
Q_2	1.200	1.200		
K_0 (kN/mm^2)	0.597	0.613		
D_{max} (mm)	8.000	8.000		

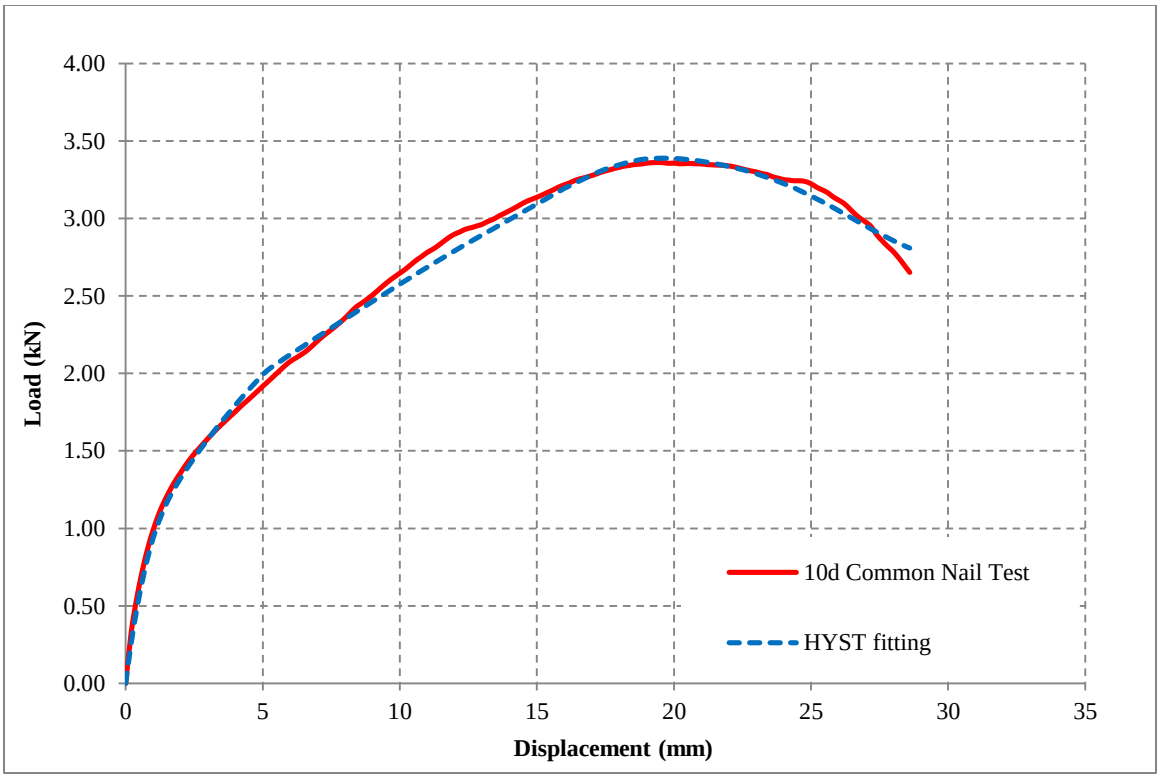

Figure 3-16 HYST fitting verse test curve

Table 3-8 Comparison of EEEP parameters between the test and the model fitting

Parameters	Test	Model Fitting	Difference
k_e (kN/mm)	0.69	0.65	5.79%
P_{peak} (kN)	3.36	3.39	0.83%
Δ_{peak} (mm)	19.40	19.60	1.03%
P_{yield} (kN)	1.90	1.99	4.85%
Δ_{yield} (mm)	4.88	5.11	4.65%
P_u (kN)	2.69	2.81	4.46%
Δ_u (mm)	28.44	28.60	0.56%
D	5.83	5.60	3.92%

Chapter 4: Wood-frame Diaphragm Model

After studying the connections between framing members and sheathing panels in the previous chapter, attention is devoted here to the entire floor diaphragm. This chapter introduces a detailed model for the structural analysis of wood-frame diaphragms. The model is built using the finite element program FLOOR2D (Li and Foschi 2004) and a simple introduction for the program is provided. Existing full-scale diaphragm tests carried out at Virginia Polytechnic Institute and State University (Bott 2005) are utilized to verify the model. Detailed descriptions about the test and the model are listed in the following sections.

The diversity of modern constructions enhances the uncertainties of the performance of wood-frame diaphragms. Although full-scale testing is a good way to investigate diaphragm behaviour, this method has serious limitations due to the high requirements of cost and time. Available test data is limited. Thus the actual performance of wood-frame diaphragm with different combinations of geometry, materials and construction parameters still remains unclear for engineers. As a result, utilizing numerical approach is highlighted to better understand the structural behaviour of wood-frame diaphragm. With an effective model, the performance of diaphragm under various construction situations can be conveniently studied. One use of the validated FLOOR2D model is to create a "virtual laboratory" that yields accurate results for wood-frame diaphragms that are not actually built. Moreover, the detailed FLOOR2D model can be utilized to create simplified models for wood-frame diaphragms. The simplified model will then be incorporated into the whole building model to study the overall performance of the structure.

4.1 Introduction to FLOOR2D

This section gives an introduction to FLOOR2D, which is a finite element program developed at University of British Columbia (Li and Foschi 2004) for the structural analysis of light wood-frame diaphragms. In FLOOR2D, three types of elements are utilized to model the typical members in wood-frame diaphragms: sheathing elements, frame elements, and connection elements. All three types of elements are isoparametric elements. Thus, by selecting appropriate shape functions, the sides of the elements can be curved to closely model the real deformation of the structure (He 2002).

Sheathing elements are represented by three dimensional thin plate elements. The plate element is assumed to be orthotropic with a linear elastic stress-strain relationship. The axial deformation of the plate element is linear while cubic polynomials are utilized to represent the deformation shape of the plate element under bending. Frame elements are approximated as three dimensional beam elements. The beam element is assumed to be isotropic with a linear elastic stress-strain relationship. The axial deformation of the beam element is also linear and the bending deformation shape is defined by cubic polynomials. In order to obtain continuity of displacement between sheathing and frame elements, the beam element uses the same set of shape functions as that of sheathing elements. As such, the relationship between element displacements at any point and the element nodal displacements can be directly calculated (He 2002).

Connections between framing members are modeled by asymmetric spring elements, which consist of three rotational and three translational linear springs. The rigidity of the connection can be adjusted by changing the stiffness of the springs. For example, the pin connection can be realized by assigning relatively large stiffness to translational springs,

and relatively small stiffness to rotational springs. In this study, connections between framing members are assumed to be strong in compression, while relatively weaker in tension and shear. Thus, relatively large stiffness values, e.g. 1000 times larger than the typical stiffness of connections, are assigned to compression springs. Stiffness values for the other two translational springs are employed based on previous connection test results (Chui et al. 1998). Because framing members are assumed to be able to rotate freely, relatively small stiffness values are assigned to rotational springs.

As introduced in Chapter 3, connections between framing members and sheathing panels are modeled by HYST. Although connections are generally located discretely along framing members, the model in FLOOR2D considers "equivalent smeared" properties (Li and Foschi 2004). Specifically, connections are assumed to be uniformly smeared along the connection lines between framing members and sheathing panels. All connections are assumed to behave nonlinearly, which takes into account the shear slip between the framing and sheathing components. For a given connection slip, HYST automatically calculates the corresponding hysteretic force. The effect of nail withdrawal is not considered in this work because previous research (Li et al. 2011) has found that withdrawal would only become significant for short nails.

The analysis in FLOOR2D is static, which allows the structure to undergo an imposed monotonic or cyclic load, or an arbitrary displacement history. In addition, P-Delta effects, namely, the amplification of the bending deformation due to axial effects are also considered for all the members of the wood-frame diaphragm in the program. The basic element unit used for the finite element approximation of the diaphragm is shown in Figure 4-1. All three types of elements introduced above are included in the

element unit in a sandwich pattern: each sheathing panel is modeled as a single sheathing element, which is connected to the underneath frame elements by smeared connection elements.

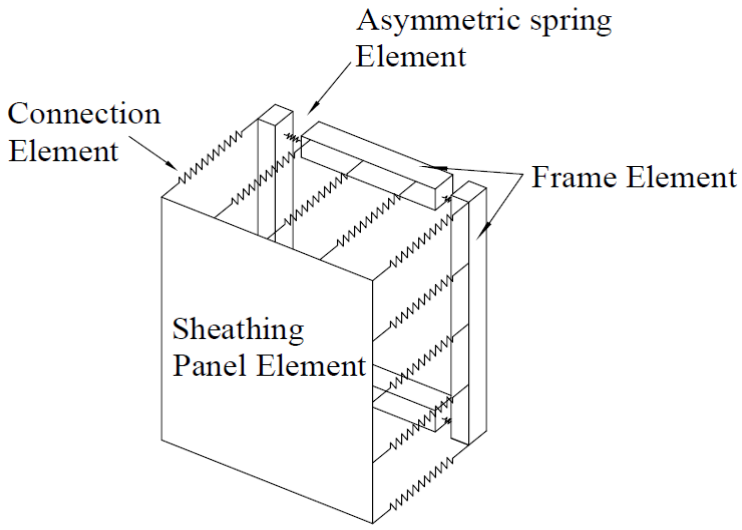

Figure 4-1 Basic element unit in FLOOR2D

The principle of virtual work is utilized as the basis of the nonlinear finite element analysis. According to Eq. (3.1.5), for a diaphragm subjected to static loads, the total internal virtual work must be equal to the total external virtual work, as expressed in the following (Li et al. 2011):

$$\sum(\delta W_I)_P + \sum(\delta W_I)_F + \sum(\delta W_I)_S + \sum(\delta W_I)_C = \mathbf{R_C}^{\mathrm{T}}\boldsymbol{\delta a} \qquad (4.1.1)$$

where $(\delta W_I)_P$, $(\delta W_I)_F$, $(\delta W_I)_S$, $(\delta W_I)_C$ are the internal virtual work in plate elements, frame elements, asymmetric spring elements, and connection elements between framing members and sheathing panels, respectively. $\mathbf{R_C}$ represents the external load vector, and $\boldsymbol{\delta a}$ represents the nodal displacement vector. $\mathbf{R_C}^{\mathrm{T}}\boldsymbol{\delta a}$ accounts for the external virtual work of the diaphragm.

As mentioned earlier, in FLOOR2D model, connections between framing members and sheathing panels are assumed to be smeared along the connection lines. The virtual work in these connections is integrated over the length of the connection lines. In this study, Guass quadrature is employed as the numerical integration method, which is carried out at each Gauss point on the connection lines. The global solution vector $\mathbf{a}_{i+1}$ of Eq. (4.1.1) is solved using New-Raphson iteration schemes with appropriate boundary conditions imposed (Li et al. 2011). The output data in FLOOR2D includes both the deformation of the specific node, e.g. the node where the load is applied, and the reaction forces from the supports, at each step of the demand history. Deformations of connections, which located at the positions of the Gauss integration points, are also stored in the output file.

4.2 Description of Diaphragm Tests

In order to investigate the in-plane stiffness of light wood-frame diaphragms, (Bott 2005) conducted non-destructive tests on six full-scale diaphragms. A description of these tests is given in this section. The test results will be used for the validation of numerical models, as introduced in Section 4.5. In the tests, all specimens were framed with Douglas-fir 2×12 (38×286 mm) joists that were spaced at 16 in (406.4 mm), and were sheathed with 4×8 ft (1.2×2.4 m) sheets of 23/32 in (18.3 mm) tongue-and-groove plywood panels. Connections between framing members and sheathing panels were 10d common nails. The nails were spaced in a 6/12 nail pattern, specifically, 6 in (152.4 mm) around the perimeter and 12 in (304.8 mm) on the interior supports of each sheathing panel.

The diaphragm configurations in the test were divided into three groups according to their aspect ratios and orientations, as shown in Figure 4-2, Figure 4-3, and Figure 4-4 respectively. Each group contained 2 specimens. Construction parameters considered for these groups included blocking and location and size of openings. The first group of specimens were 16×20 ft (4.8×6.0 m) in dimension and were loaded parallel to the direction of the joists on the 20 ft (6.0 m) side. The second group of specimens were 20×16 ft (6.0×4.8 m) in dimension and were loaded perpendicular to the direction of the joists on the 16 ft (4.8 m) side. The third group of specimens were 10×40 ft (3.0×12.0 m) in dimension and were loaded parallel to the direction of the joists on the 40 ft (12.0 m) side. Table 4-1 lists the construction parameters considered in this study for the three groups of specimens.

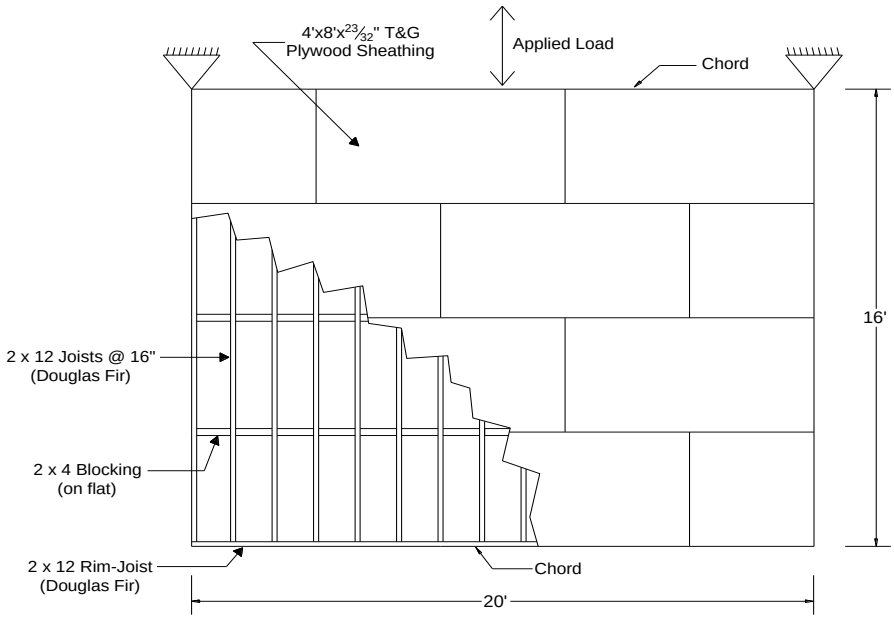

Figure 4-2 Group 1: 16×20 ft (4.8×6.0 m) specimen (Bott 2005)

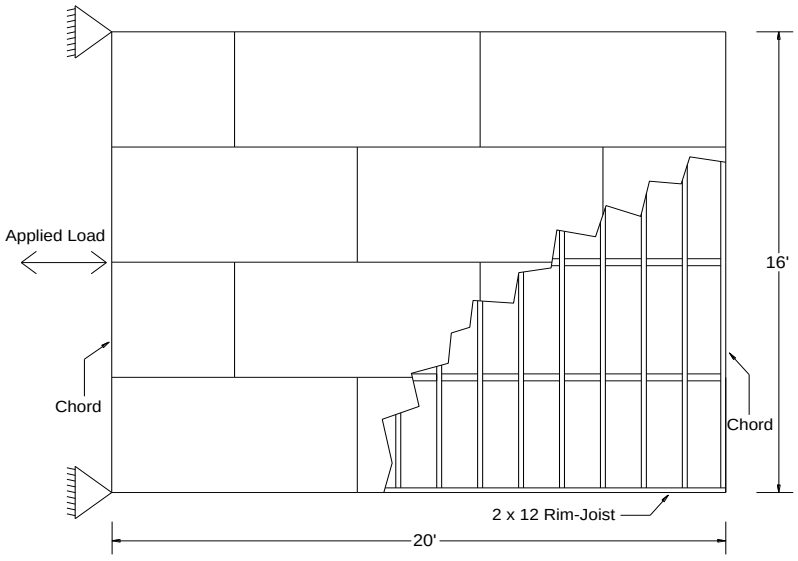

Figure 4-3 Group 2: 20×16 ft (6.0×4.8 m) specimen (Bott 2005)

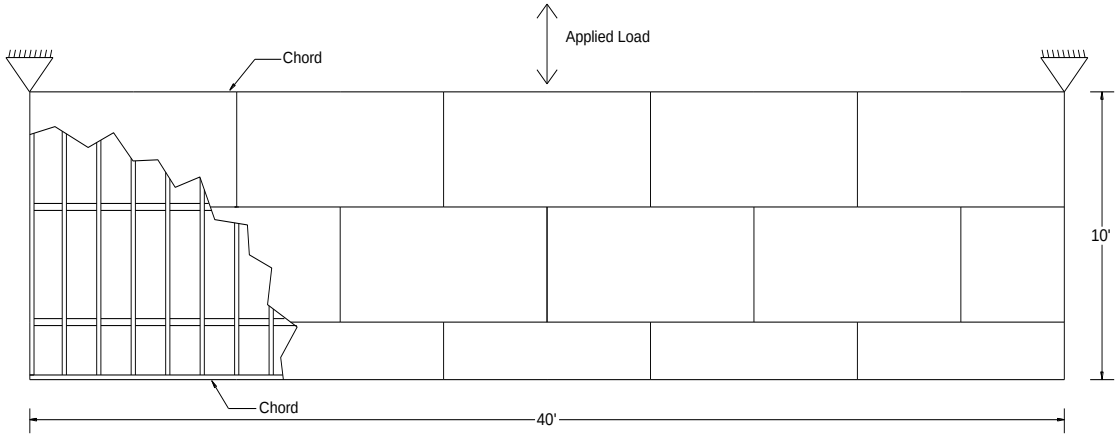

Figure 4-4 Group 3: 10×40 ft (3.0×12.0 m) specimen (Bott 2005)

Table 4-1 Construction parameters for diaphragm specimens

Group of Specimen	Construction Parameters
1	With blocking Without blocking 4 × 8 ft (1.2 × 2.4 m) Corner sheathing opening 8 × 12 ft (2.4 × 3.6 m) Center sheathing opening
2	With blocking 4 × 8 ft (1.2 × 2.4 m) Corner sheathing opening 8 × 12 ft (2.4 × 3.6 m) Center sheathing opening
3	With blocking 4 × 8 ft (1.2 × 2.4 m) Corner sheathing opening

The specimens in the test were subjected to five equal displacement-based sinusoidal load cycles, and the magnitudes were ±0.25 in (6.35 mm), ±0.20 in (5.08 mm) and ±0.80 in (20.3 mm) for specimens Group 1, 2, and 3, respectively. As an example, Figure 4-5 shows all the elements of the test apparatus for Group 1specimens. The load was applied at the midspan of the diaphragm through a 20 ft (6.0 m) long C6×10.5 steel load distribution channel. The channel was fastened to the sheathing panel using 5/8 in (16 mm) diameter lag screws. For Group 1 specimens, since there was no joist at the center of the diaphragm, 4×4 (89×89 mm) blocks were placed under the sheathing to provide the backing for the lag screws. With the steel load distribution channel, loads can be uniformly transferred to the diaphragm. The test load-slip curves were obtained from the actuator located at the end of the load distribution channel. Detailed information of the test boundary condition is illustrated in Figure 4-6. It is shown that the specimen was supported on the steel frame, which consists of steel tubes. Each end of the steel tube was pin-connected to the triangular reaction frame, which allows the diaphragm to be rotated in-plane. Several PVC pipes were placed under the joists of the specimen to act as frictionless rollers. The end of the diaphragm was attached to the side of the steel tube using a steel angle. Lag screws were utilized to fix the steel angle on the diaphragm.

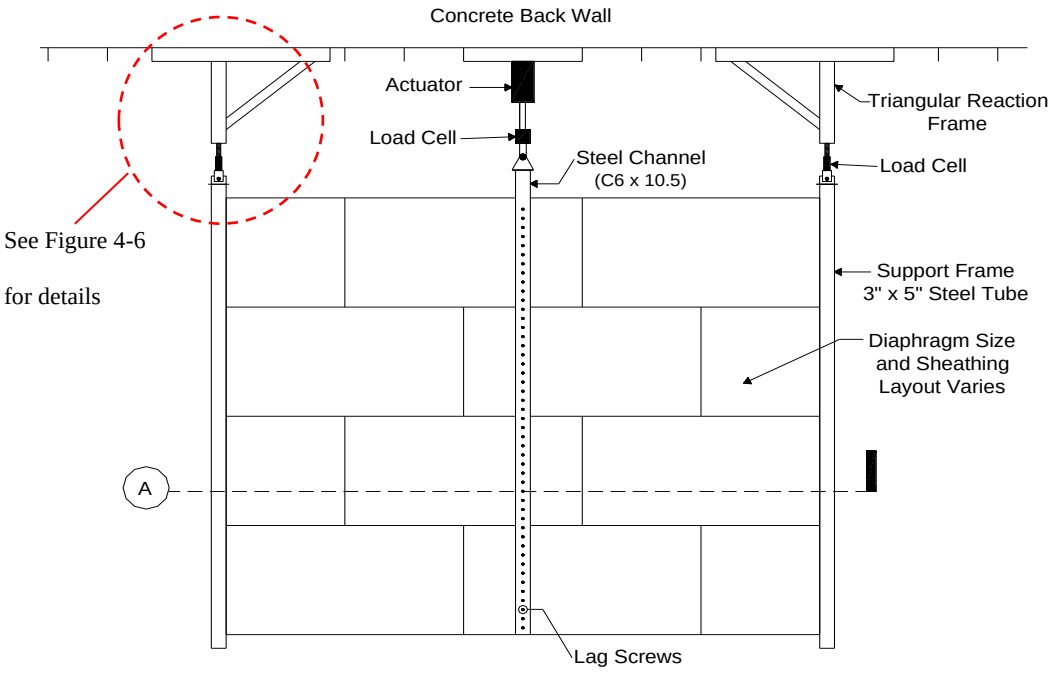

Figure 4-5 Test apparatus and configuration (Bott 2005)

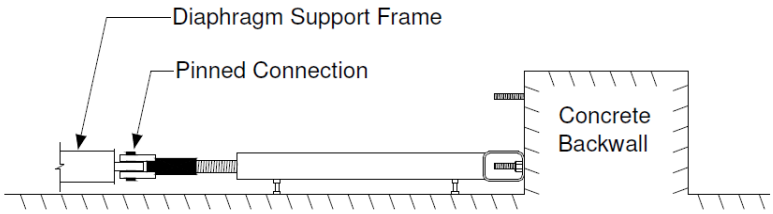

(a)

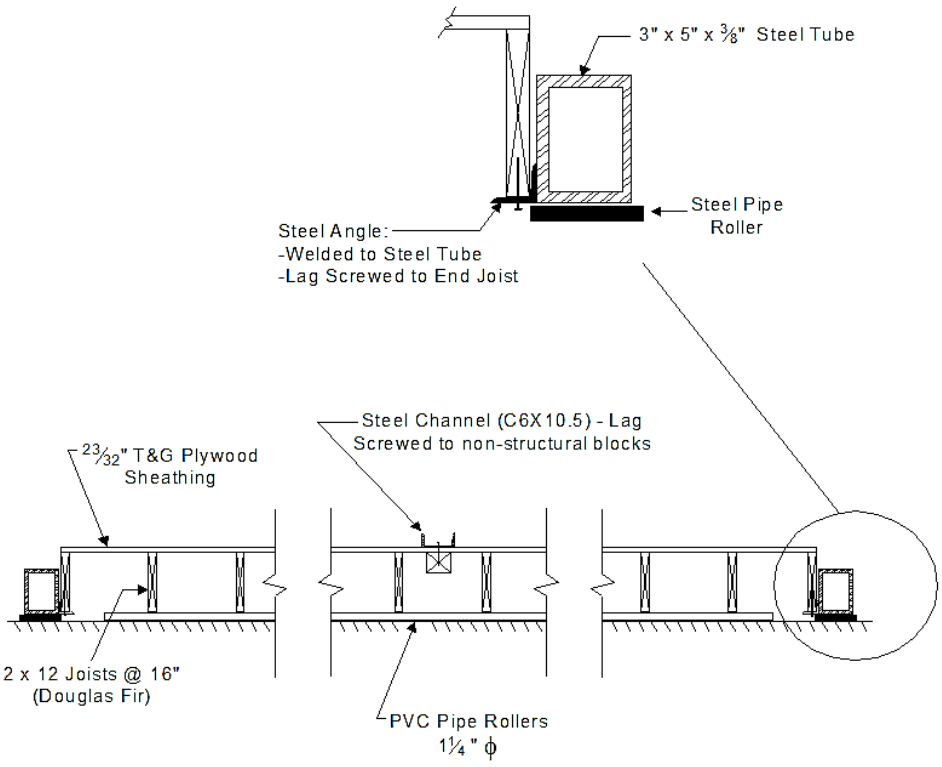

(b)

Figure 4-6 Test boundary condition (Bott 2005):

(a) elevation view of triangular reaction frame (b) partial section A of the test apparatus

4.3 Stiffness Definitions

Bott (2005) considered three types of stiffness in his thesis as the results of the diaphragm tests: cyclic stiffness, shear stiffness, and flexural stiffness. This aims to evaluate the benefit of changing construction parameters since it is found that the overall stiffness of the diaphragm, namely, the cyclic stiffness is mostly influenced by the shear stiffness. In other words, the construction parameter that causes more increases in the shear stiffness will be more effective in the stiffening of the diaphragm. The following sections provide definitions for these three types of stiffness.

4.3.1 Cyclic Stiffness

Stiffness is a measure of the resistance of a structure to deformation, which is defined as the amount of force required to cause a unit deformation. For a linear-elastic structure, the stiffness is calculated as the slope of the force-displacement curve. However, when subjected to cyclic loads, the shape of the force-displacement curve changes from a straight line to an elliptical loop. This requires a different approach to calculate the stiffness, and a so called "peak-to-peak" method is utilized by Bott (2005). The method is illustrated in Figure 4-7. The cyclic stiffness of the diaphragm is approximated as the slope of the imaginary line between the maximum positive deflection point and the maximum negative deflection point, as computed using the following equation:

$$k = \frac{\left|F_{\max}^{+}\right| + \left|F_{\max}^{-}\right|}{\left|\Delta_{g,\max}^{+}\right| + \left|\Delta_{g,\max}^{-}\right|} \tag{4.3.1}$$

where $F_{\max}^{+}$ and $F_{\max}^{-}$ represent the respective maximum positive and negative forces applied to the diaphragm, and $\Delta_{g,\max}^{+}$ and $\Delta_{g,\max}^{-}$ are the maximum positive and negative global deformations, respectively.

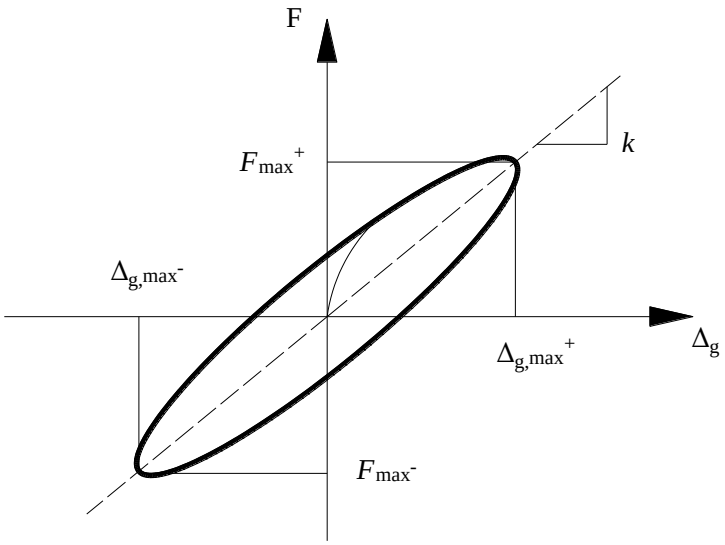

Figure 4-7 Peak-to-peak method (Bott, 2005)

4.3.2 Shear Stiffness

In the test, a concentred load is applied at the midspan of the diaphragm. The center of the diaphragm deforms relatively to the ends, and the global deformation of the diaphragm is the sum of the shear deformation and the flexural deformation. Figure 4-8 shows the shape of the diaphragm due to the shear deformation. It is observed that the diaphragm deforms as a separate straight line on each side of the load. The shear deformation, Δ_S, is computed using small angle assumptions as:

$$\Delta_S = \frac{L}{2} \cdot \gamma \tag{4.3.2}$$

where L is the span of the diaphragm, and γ is the shear strain, which is determined from the deflection measured by diagonal string potentiometers using the geometric manipulation, as expressed in the following:

$$\gamma = \Delta_L \cdot \frac{\sqrt{b^2 + d^2}}{bd} \tag{4.3.3}$$

where Δ_L is the average diagonal deformation from a pair of diagonal string potentiometers, and b and d are the width and depth of the pair of diagonal string potentiometers, respectively. For a torsionally irregular diaphragm, e.g. a diaphragm with a corner opening, Δ_L for the left and right halves are not equal. In other words, shear deformations for each half of the diaphragm are different, thus should be calculated separately.

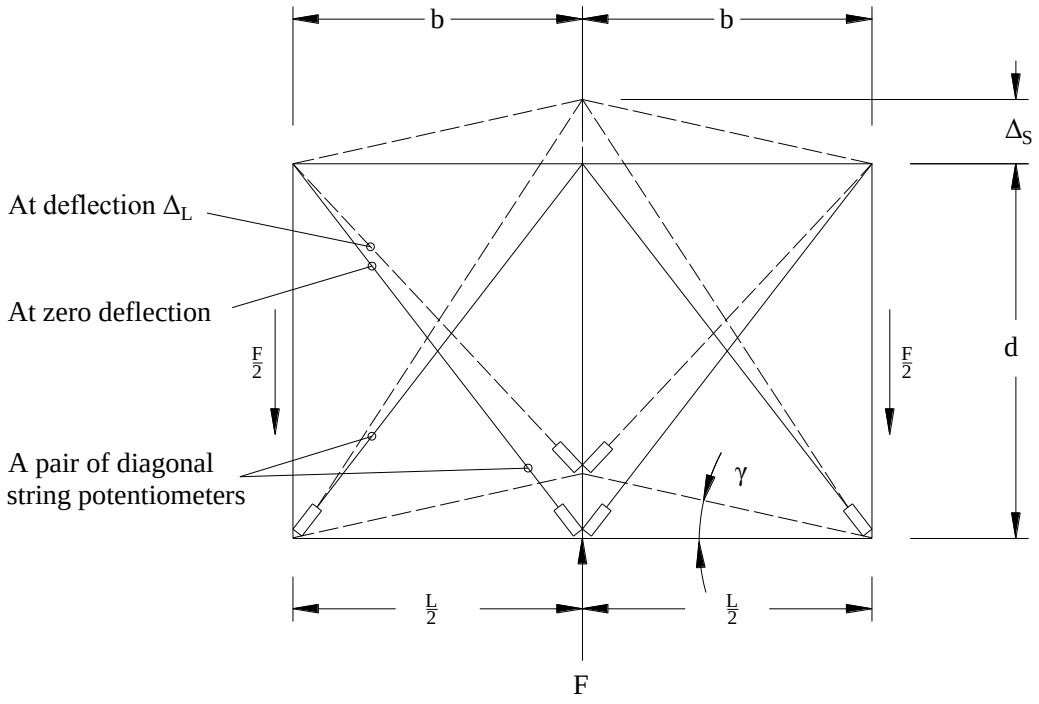

Figure 4-8 Diaphragm shear deformation (Bott, 2005)

After obtaining the shear deformation, the experimental shear stiffness k_{shear} is calculated as:

$$k_{shear} = \frac{\left|V_{\max}{}^{+}\right| + \left|V_{\max}{}^{-}\right|}{\left|\Delta_{S,\max}{}^{+}\right| + \left|\Delta_{S,\max}{}^{-}\right|} \tag{4.3.4}$$

where $V_{\max}{}^{+}$ and $V_{\max}{}^{-}$ are the respective maximum positive and negative shear forces applied to the diaphragm, and $\Delta_{S,\max}{}^{+}$ and $\Delta_{S,\max}{}^{-}$ are the corresponding maximum positive and negative shear deformations, respectively. For a symmetric diaphragm, the shear force for each half of the diaphragm is equal to half of the applied load, i.e., $V=F/2$. However, asymmetric configurations such as a corner opening may cause the diaphragm to resist more shear force on the "stiff" side and less on the "soft" side. As such, V should be determined independently for the two halves of the diaphragm and the corresponding k_{shear} should be kept separate as well (Bott 2005).

Instead of using k_{shear}, Bott (2005) considered a more commonly accepted form of shear stiffness, GA_s, to represent the shear rigidity of the diaphragm. For a diaphragm with a concentred load applied at the midspan, using elastic beam theory, the theoretical shear deformation of the diaphragm is computed as:

$$\Delta_S = \frac{V \cdot \frac{L}{2}}{GA_S} \tag{4.3.5}$$

According to Eq. (4.3.4), since $k_{shear}=V/\Delta_S$, GA_s can be expressed in terms of k_{shear} by rearranging Eq. (4.3.5) as:

$$GA_S = k_{shear} \cdot \frac{L}{2} \tag{4.3.6}$$

4.3.3 Flexural Stiffness

The flexural deformation of the diaphragm, Δ_f, is determined by subtracting the shear deformation from the global deformation. For simplicity, Bott (2005) considered the average shear deformation of the two halves of the diaphragm, $\Delta_{S,avg}$, in the calculation of the flexural deformation, as expressed in the following:

$$\Delta_f = \Delta_g - \Delta_{S,avg} \tag{4.3.7}$$

After obtaining the flexural deformation, the experimental flexural stiffness, k_f, is calculated as:

$$k_f = \frac{\left|F_{\max}^{+}\right| + \left|F_{\max}^{-}\right|}{\left|\Delta_{f,\max}^{+}\right| + \left|\Delta_{f,\max}^{-}\right|} \tag{4.3.8}$$

where $\Delta_{f,\max}^{+}$ and $\Delta_{f,\max}^{-}$ are the maximum positive and negative flexural deformations, respectively. Similar to the shear stiffness, Bott (2005) also considered a more common form of flexural stiffness, EI, to substitute for k_f. According to the elastic beam theory, the

theoretical flexural deformation of a diaphragm with a concentrated load applied at the center is computed as:

$$\Delta_f = \frac{FL^3}{48EI} \tag{4.3.9}$$

By combining Eq. (4.3.8) with Eq. (4.3.9), the sought quantity, *EI*, can be expressed in terms of k_f as:

$$EI = k_f \cdot \frac{L^3}{48} \tag{4.3.10}$$

It is noted that under cyclic loads, the behaviour of the diaphragm is represented as a hysteresis loop. In order to verify that the numerical model is capable of predicting the actual behaviour of the diaphragm, the model predicted hysteresis loop should be compared with the test hysteresis loop. The stiffness values provided by Bott (2005) are insufficient for model validations, thus the raw test data is still required.

4.4 Diaphragm Models

The modelling of the wood-frame diaphragm is introduced in this section. The detailed wood-frame diaphragm models that are built in FLOOR2D are intended to replicate the tests introduced in Section 4.2. Because the main focus of this study is the in-plane behaviour of wood-frame diaphragms, all the out-of-plane degrees of freedom of the model are constrained. In the numerical modelling, in order to simulate the steel load distribution channel, blocking or joists at the position of the channel are changed to rigid members. The rigid member is defined as a member that has the same modulus of elasticity and shear modulus as steel. In the case that no framing members are placed at the center of the diaphragm, i.e. Group 1 specimens, the 4×4 (89×89 mm) blocks, which are used to support the lag screws, are changed to rigid members. Connections between

the rigid members and sheathing panels are still 10d nails, except the spacing of the nails on the rigid member connection line becomes much denser, i.e. 2 in (51 mm). As such, loads can be uniformly transferred along the rigid connection line, which proves that the rigid member is capable of modelling the steel load distribution channel in the test.

Figure 4-9 shows an example of the boundary condition for a diaphragm model of specimens Group 1. Rigid members are placed at the two edges of the diaphragm to simulate the supporting steel frames. As mentioned earlier, because the end of the diaphragm is fixed on the side of the supporting steel frames, it is assumed that there is no relative displacement between the two in the longitudinal direction (Y direction). Both the transverse direction (X direction) and the longitudinal direction displacements for the bottom end points of the model are fixed, while rotations in the XY plane are free.

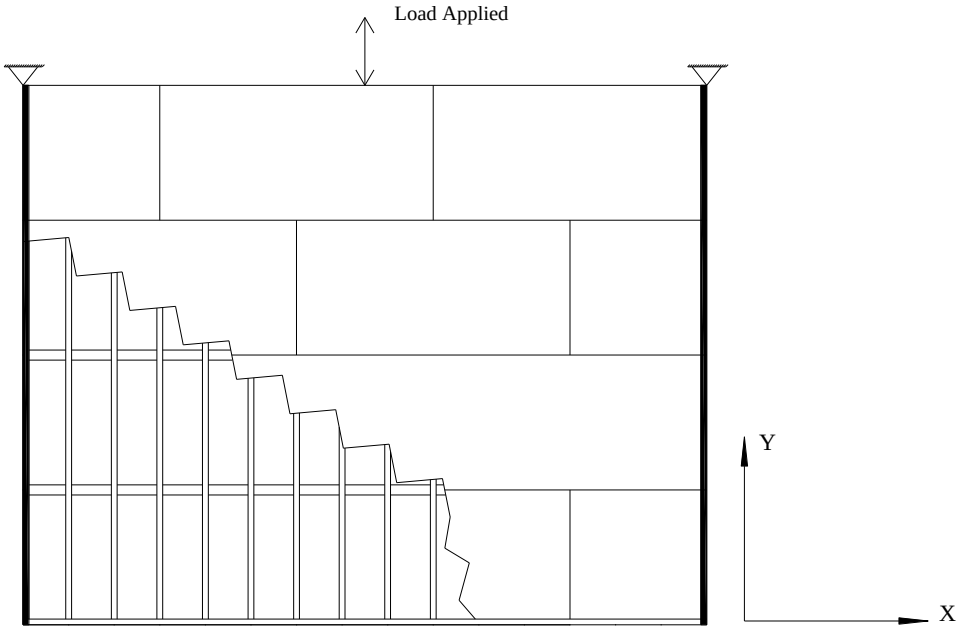

Figure 4-9 Boundary conditions for the numerical model

4.5 Model Validation and Discussion

By comparing with the diaphragm tests introduced in Section 4.2, the FLOOR2D diaphragm models are validated in this section. Results obtained from the models are represented as load-displacement curves for the node where the load is applied. The comparisons between model and test hysteresis loops for the three groups of specimens are shown in Figure 4-10 to Figure 4-18, respectively. Table 4-2 to Table 4-4 summarize the comparisons between the model and test results in terms of the cyclic stiffness and peak load. The peak load is calculated as the average of maximum loads in both positive and negative load directions.

Comparisons between test and model hysteresis loops for specimens Group 1 are shown in Figure 4-10 to Figure 4-13. The corresponding cyclic stiffness and peak loads are compared in Table 4-2. It is observed that for this group of specimens, in general, the model prediction agrees well with the test result. For the fully sheathed and blocked specimen, the model behaves softer than the actual specimen. Specially, the cyclic stiffness of the model is 12.8% lower than that of the test specimen. Similar phenomenon is also observed for the unblocked specimen and the center opening specimen, with 8.3% and 6.0% lower cyclic stiffness, respectively. The model of the corner opening specimen behaves stiffer than the test diaphragm. However, the difference between the two is only 1.8%. For the blocked, corner opening and center opening specimens, the areas of model hysteresis loops are similar as that of test hysteresis loops. This indicates that the energy dissipation predicted by the model agrees well with the test result. However, the test hysteresis loop of the unblocked specimen is much fatter than the model hysteresis loop, which indicates that in this case the model underestimates the energy dissipation.

Comparisons between test and model hysteresis loops for specimens Group 2 are shown in Figure 4-14 to Figure 4-16, and the cyclic stiffness and peak loads are compared in Table 4-3. It is observed that for this group of specimens, although the energy dissipation of the model agrees well with the test result, the model behaves much stiffer than the test specimen. For the blocked specimen, the model is 31.2% stiffer than the test diaphragm, and the discrepancy increases to 38.2% for the corner opening specimen. The model stiffness of the center opening specimen is closer to the test result, however, the discrepancy is still around 17.9%. The peak load follows the same pattern as the cyclic stiffness. For the blocked, corner opening and center opening specimens, peak loads obtained from models are 32.2%, 38.1% and 17.8% higher than test results, respectively.

Comparison results for specimens Group 3 are shown in Figure 4-17 and Figure 4-18, and the corresponding cyclic stiffness and peak loads are compared in Table 4-4. It is observed that models for this group of specimens also behave stiffer than the test diaphragms. For the fully sheathed specimen, the energy dissipation of the model is similar as that of the test specimen, while the stiffness and the peak load of the model are 19.6% and 19.9% higher than the test results, respectively. On the contrary, the model of the corner opening specimen underestimates the energy dissipation, while predictions of the stiffness and peak load are closer to the test results.

The discussion of the discrepancy between the model and test results is addressed later in this chapter.

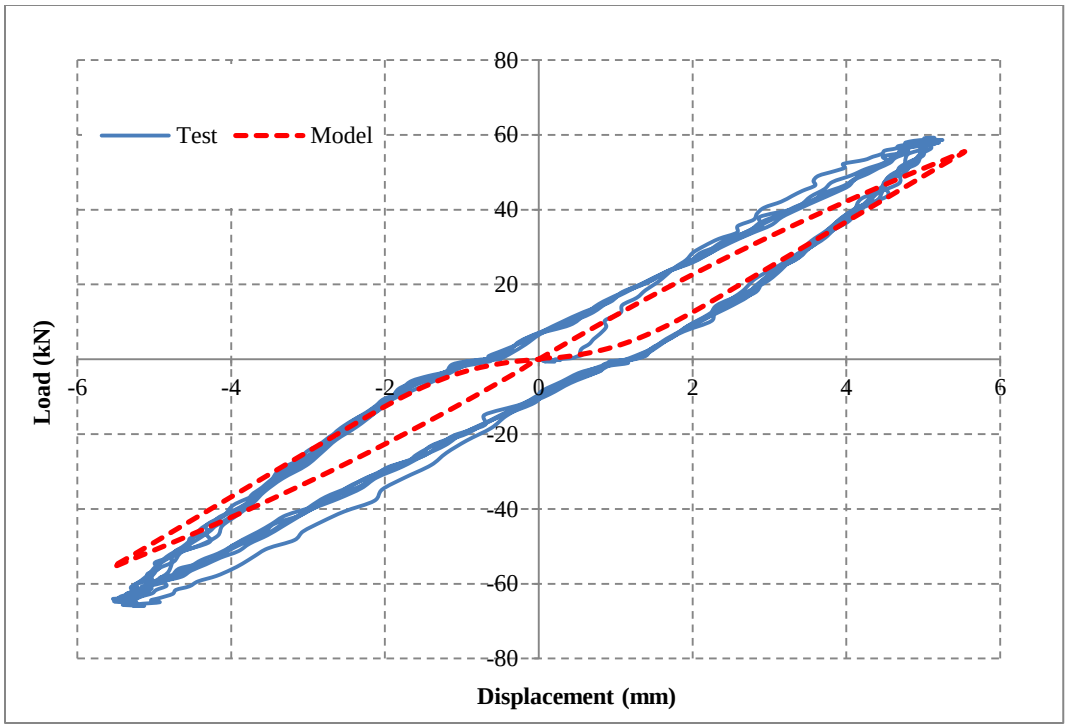

Figure 4-10 Comparison for specimens Group 1: with blocking, fully sheathed

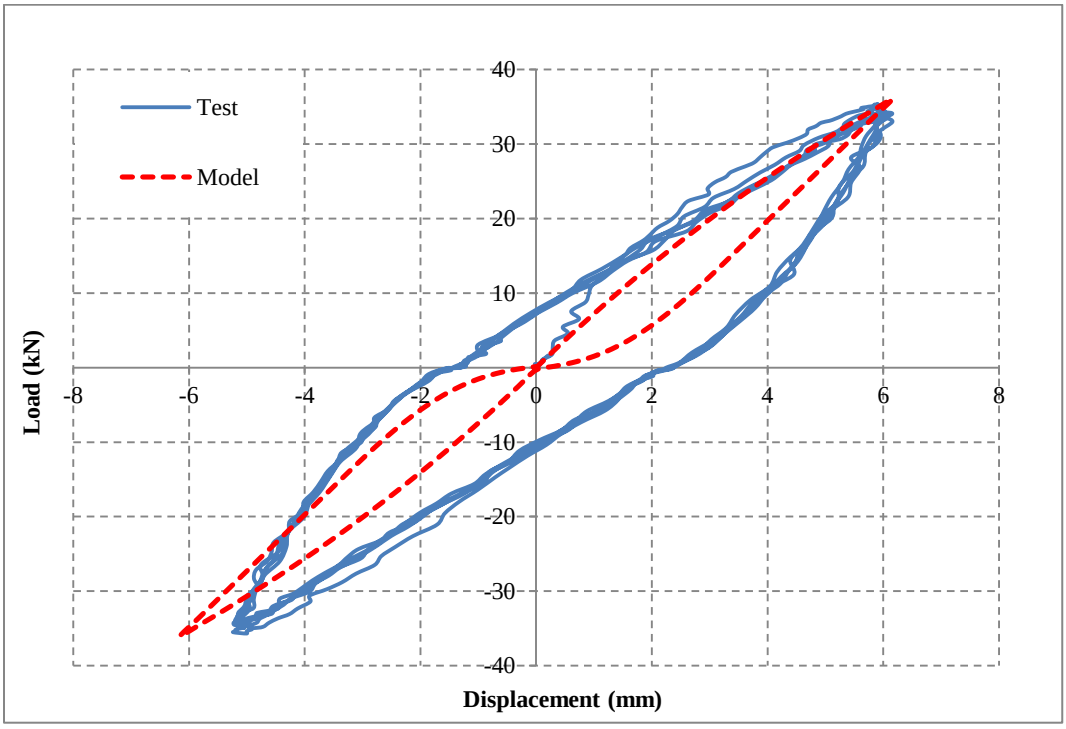

Figure 4-11 Comparison for specimens Group 1: without blocking, fully sheathed

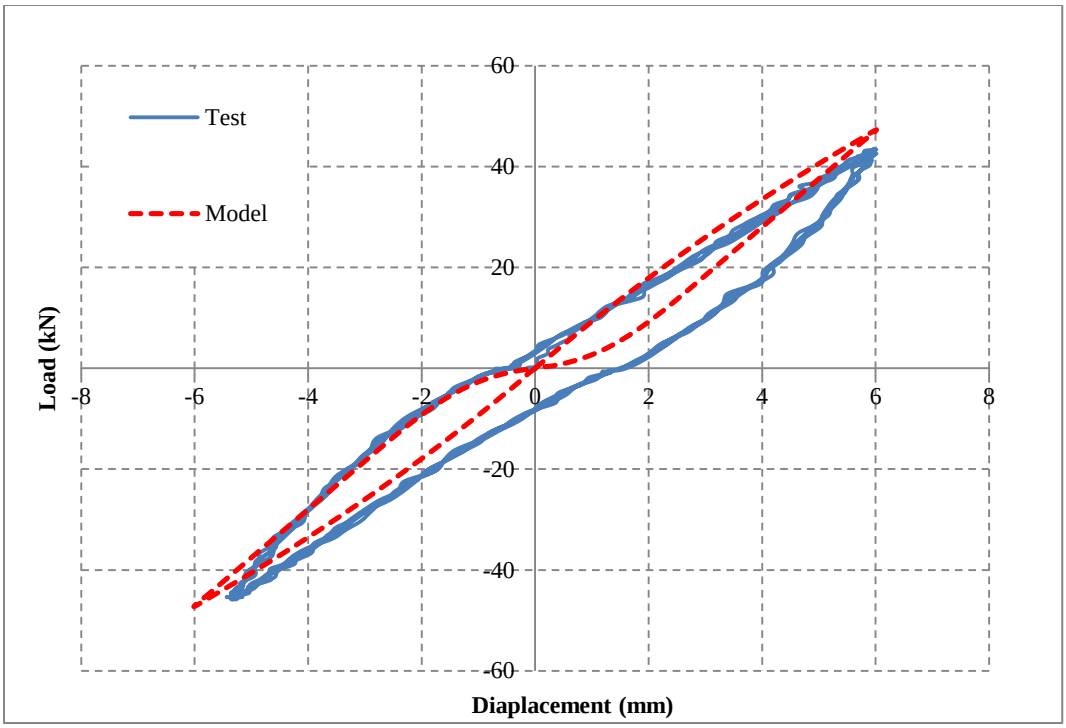

Figure 4-12 Comparison for specimens Group 1: with blocking, 4×8 ft corner opening

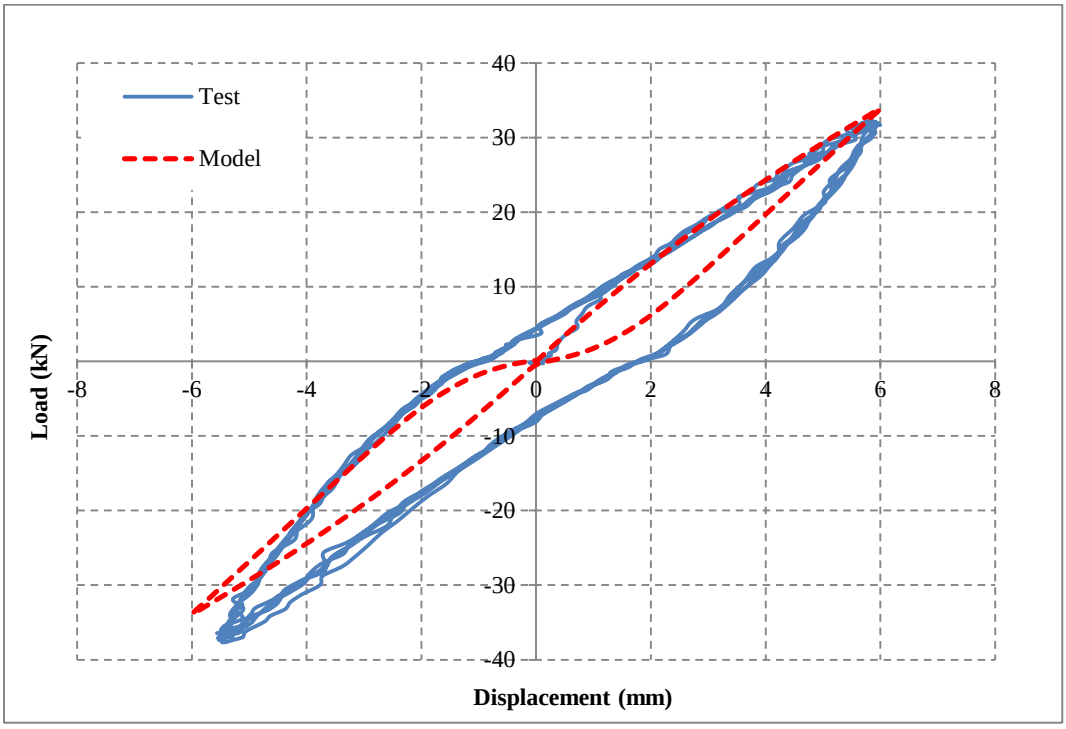

Figure 4-13 Comparison for specimens Group 1: with blocking, 8×12 ft center opening

Table 4-2 Comparisons of model predictions and test results: Group 1

Diaphragm Property	Group 1	Construction Parameter			
		With Blocking	Without Blocking	Corner Opening	Center Opening
Cyclic Stiffness (kN/mm)	Model	10.12	5.72	7.93	5.68
	Test	11.59	6.23	7.79	6.04
	Difference	-12.8%	-8.3%	1.8%	-6.0%
Peak Load (kN)	Model	53.22	32.55	45.32	33.17
	Test	55.51	35.50	44.66	34.95
	Difference	-4.1%	-8.3%	1.5%	-5.1%

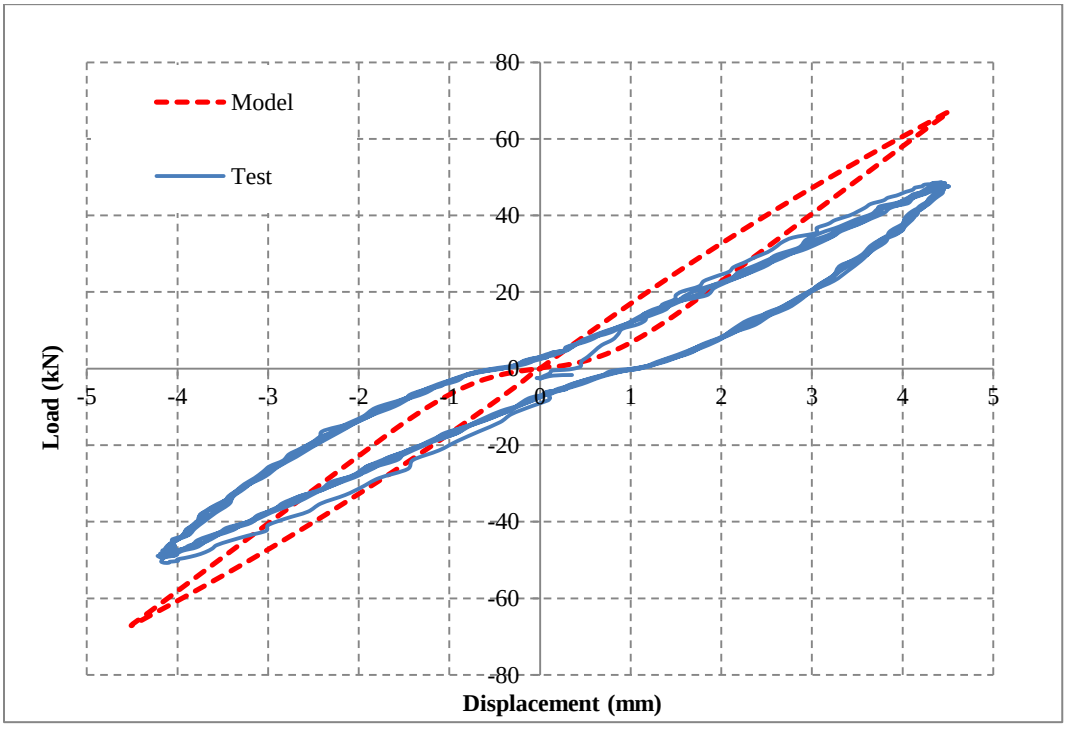

Figure 4-14 Comparison for specimens Group 2: with blocking, fully sheathed

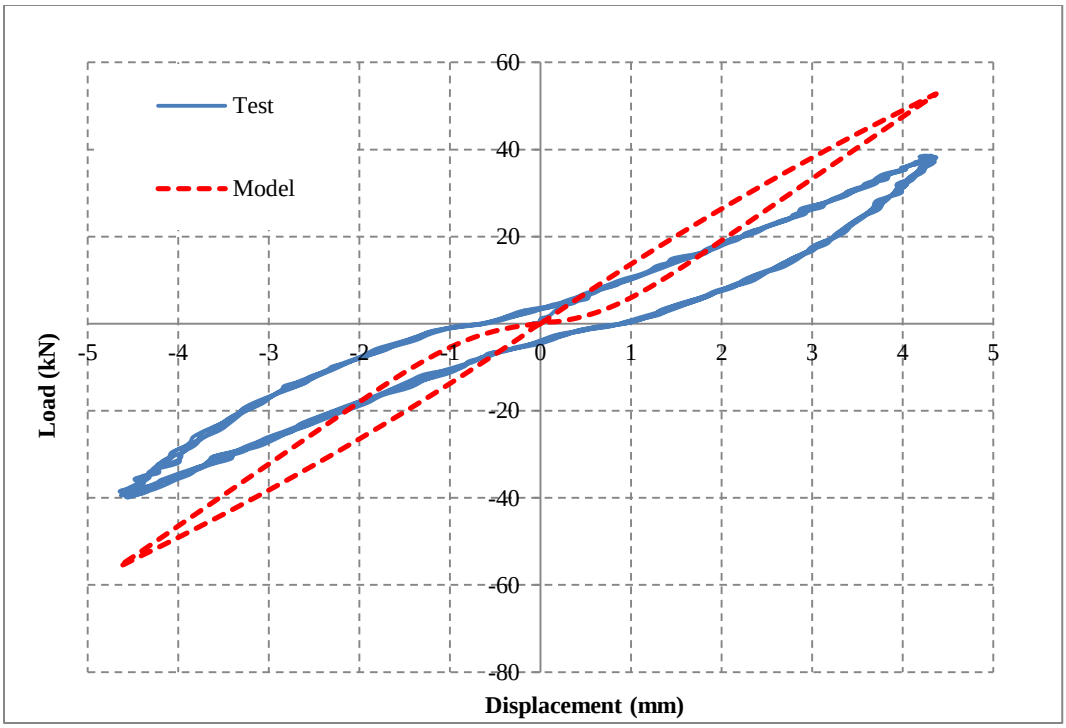

Figure 4-15 Comparison for specimens Group 2: with blocking, 4×8 ft corner opening

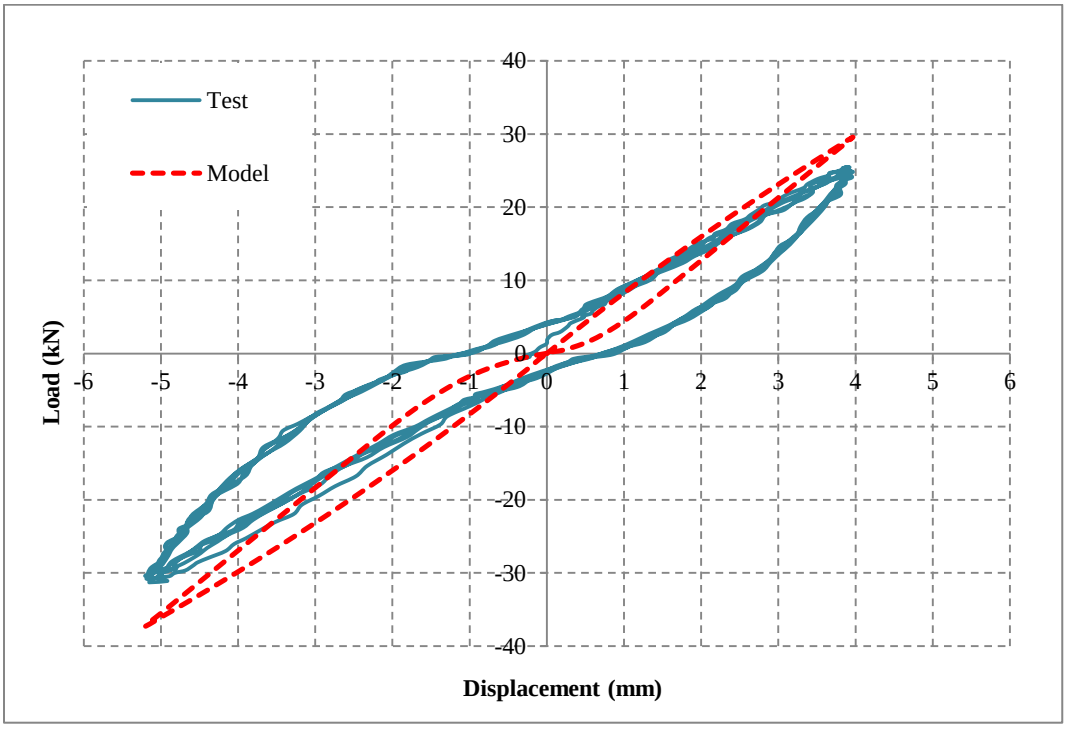

Figure 4-16 Comparison for specimens Group 2: with blocking, 8×12 ft center opening

Table 4-3 comparisons of model predictions and test results: Group 2

Diaphragm Property	Group 2	Construction Parameter		
		With Blocking	Corner Opening	Center Opening
Cyclic Stiffness (kN/mm)	Model	14.93	12.03	7.29
	Test	11.38	8.70	6.18
	Difference	31.2%	38.2%	17.9%
Peak Load (kN)	Model	65.68	54.24	33.43
	Test	49.68	39.27	28.38
	Difference	32.2%	38.1%	17.8%

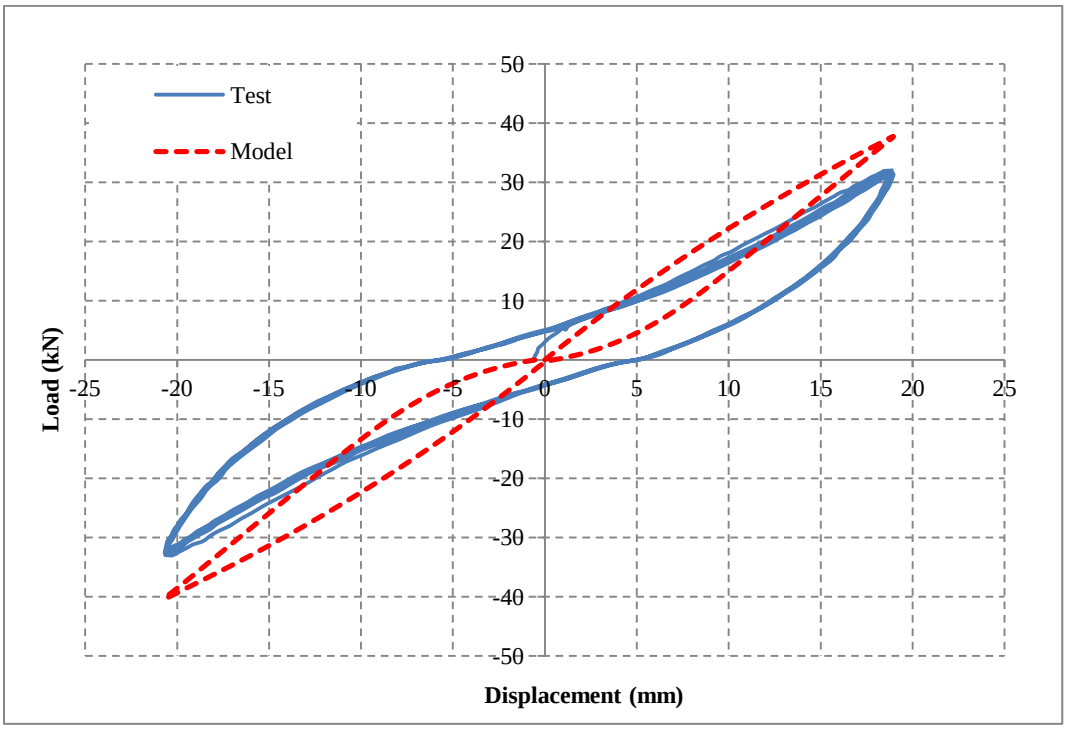

Figure 4-17 Comparison for specimens Group 3: with blocking, fully sheathed

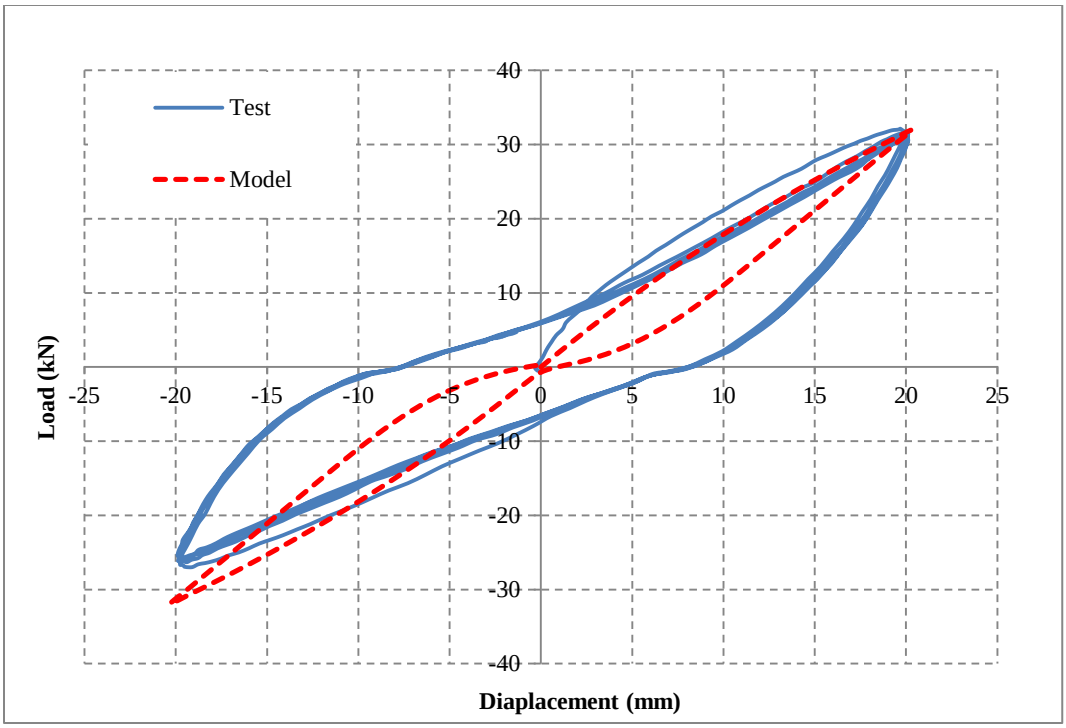

Figure 4-18 Comparison for specimens Group 3: with Blocking, 4×8 ft corner opening

Table 4-4 Comparisons of model predictions and test result: Group 3

Diaphragm Property	Group 3	Construction Parameter	
		With Blocking	Corner Opening
Cyclic Stiffness (kN/mm)	Model	1.97	1.57
	Test	1.65	1.47
	Difference	19.6%	6.9%
Peak Load (kN)	Model	39.03	31.95
	Test	32.54	29.57
	Difference	19.9%	8.0%

The possible reasons for the discrepancies between model predictions and test results are explained as follows: in FLOOR2D, the properties of connections between framing members and sheathing panels have a considerable influence on the behaviour of the diaphragm model. The property of the connection is determined through connection tests, as introduced in Chapter 3. However, no connection test data is provided in the diaphragm tests (Bott 2005). As a result, connection test results introduced in Section 3.2 are utilized as the input connection properties for the diaphragm model instead. Because of the differences between the tests, e.g. the density and moisture content of wood, nail properties, etc., connections in the diaphragm tests and the connection tests may behave differently. This in turn results in the discrepancies between the diaphragm model and test results.

As introduced in Section 4.2, specimens in Group 2 have the same dimension as that of Group 1, only the load direction changes to be perpendicular to the joists. The test stiffness values for the two groups are very similar, as shown in Table 4-2 and Table 4-3. As mentioned earlier, the stiffness of the model in Group 1 agrees well with that of the test result. However, models in Group 2 show much higher stiffness than the actual test specimens. In other words, models in Group 2 behave much stiffer than the models in Group 1. Compared with Group 1, the span of the diaphragm in Group 2 decreased and the depth of the diaphragm increased. Moreover, the number of bending resisting members increased. Theoretically, specimens in Group 2 should behave stiffer than specimens in Group 1. The similar results obtained from the tests might due to the slip of the lag screws, which are used to attach the steel load distribution channel to the sheathing panels. Specially, in the test, loads are applied through the steel load

distribution channel. The slip of the lag screw may cause uneven loading between the far and the near ends of the diaphragm. As such, the behaviour of the diaphragm might be controlled by local damage mechanism, which leads to the underestimate of the diaphragm stiffness.

The difference between the energy dissipation of the model and the test result is explained as follows: in Section 4.1, it is introduced that frame elements, sheathing elements and connections between framing members in FLOOR2D are all assumed to be linear elastic. When subjected to lateral loads, the energy dissipation of the diaphragm model only depends on the nonlinear behaviour of the connections between framing members and sheathing panels. Other types of energy dissipation mechanisms, e.g. frictions between members, squeeze between adjacent sheathing panels etc., are not considered. In short, assumptions made for the FLOOR2D model result in the underestimation of the energy dissipation.

Another difference between model and test results is that the model hysteretic loop has the so-called “kink” behaviour. In Figure 4-10 to Figure 4-18, it is observed that for test hysteresis loops, the displacement and load have different zero points. On the contrary, for the model hysteresis loops, the displacement always goes back to zero when the load drops to zero. The reason is illustrated as follows: in FLOOR2D, because all the other elements are assumed to be linear elastic, the hysteretic behaviour of the diaphragm is governed by the behaviour of connections between framing members and sheathing panels. As introduced in Chapter 3, the hysteretic behaviour of the connection model depends on both properties of the nail and the wood medium. According to Figure 3-5, the embedment response of the wood medium under reverse cyclic loading, i.e. cyclic

loading in both positive and negative directions, is shown in Figure 4-19. Along the unloading path 2, the reaction force from the wood medium becomes zero after reaching Point A. Path 3 represents the formation of the gap, thus from Point A to O, the force remains zero. Even though the force reaches the zero point earlier than the displacement, they have the same zero point positions. This indicates that the variability of zero point positions between the load and displacement for the model only comes from the elasto-plastic characteristic of the nail. However, when the deformation of the diaphragm is small, most of the connections may remain in the elastic range. The force drops to zero as the displacement becomes zero, which results in the kink behaviour of the model hysteresis loop.

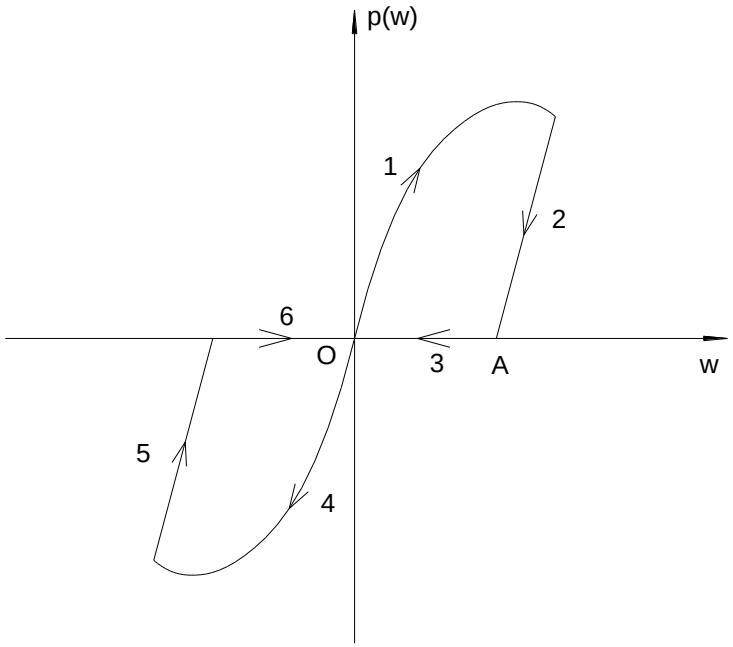

Figure 4-19 Embedment response under reverse cyclic loading

It is found that FLOOR2D has the limitation to separate the shear stiffness from the flexural stiffness for a wood-frame diaphragm. For example, for a fully sheathed and blocked specimen in Group 1, the global deflection of the diaphragm is 6.35 mm. In the model, the average deformation of the intersected diagonal lines is 5.3 mm. The shear deformation and the flexural deformation of the diaphragm model are calculated using Eq. (4.3.2) and Eq. (4.3.7), which are equal to 6.25 mm and 0.1 mm, respectively. Based on the deformation results, the corresponding shear stiffness and flexural stiffness of the diaphragm are determined using Eq. (4.3.6) and Eq. (4.3.10), and the comparison between model and test results are shown in Table 4-5. It is observed that compared with test results, the model underestimates the shear stiffness while seriously overestimates the flexural stiffness of the diaphragm. When subjected to loads, the model can be used to predict the "global behaviour", i.e. the global deformation and the cyclic stiffness, for the diaphragm. However, the model is not applicable for the prediction of the "separate behaviour", i.e. the shear stiffness and flexural stiffness and the corresponding shear and flexural deformations of the diaphragm.

Table 4-5 Comparison of stiffness

Stiffness Type	FLOOR2D Model	Test	Difference
Shear Stiffness GA (kN)	1.51E+04	2.75E+04	-45.09%
Flexural Stiffness EI (kN·m)	2.92E+12	1.52E+11	1828.98%

Chapter 5: Building Model

In the previous chapter, a detailed numerical model of wood-frame diaphragms is established and validated with test data. The next step of the study is to add shear walls to investigate the overall structural response of light wood-frame buildings under lateral loads. This chapter gives a case study on a one-storey building. An analysis of this building with detailed FLOOR2D diaphragm models would be computational costly due to the high number of degrees of freedom. A simplified linear elastic model would be a better choice, at least for initial studies, because it better balances simulation accuracy with computational efficiency. Specially, in the building, diaphragms are modelled by truss elements. The axial stiffness of these truss elements is calibrated by means of the detailed numerical model from the previous chapter. This approach makes it possible to analyze entire buildings at a reasonable computational cost, while retaining the results obtained by the previously established FLOOR2D model. This enables the study of the distribution of forces to each shear wall under different diaphragm flexibility assumptions. Such results are presented and discussed in this chapter, and ultimately the accuracy of the popular assumption of flexible wood-frame diaphragms is examined.

5.1 Simplified Diaphragm Model

For illustration purposes, a diaphragm modelled by truss elements is shown in Figure 5-1. In this approach, the diaphragm is discretized into a set of “truss units”. A truss unit consists of truss elements around a rectangular perimeter, with two diagonally bracing truss elements inside the rectangle. In the truss unit considered in this thesis, the perimeter truss elements are assumed to be axially rigid. Thus, the entire in-plane

stiffness of the diaphragm is represented by the axial stiffness of the diagonally bracing truss elements.

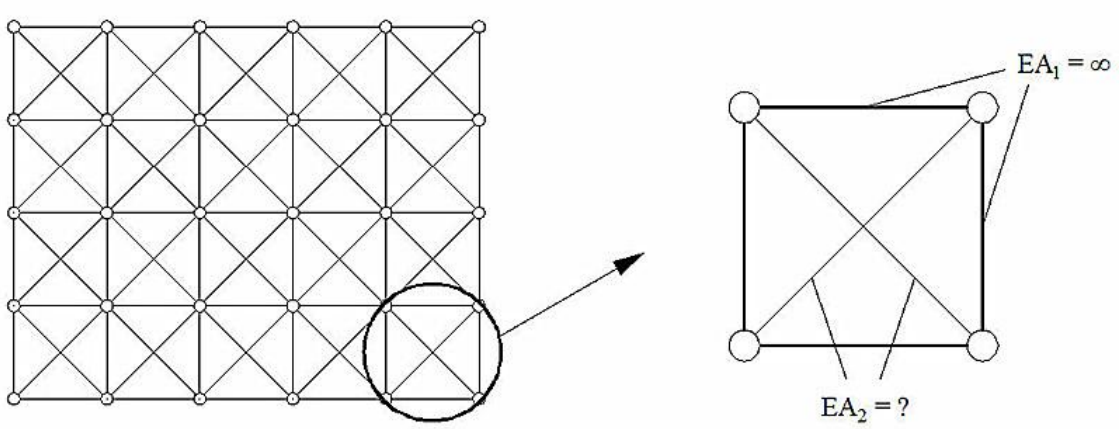

Figure 5-1 Simplified diaphragm model

5.1.1 Shear Modulus of the Diaphragm

In order to obtain the simplified diaphragm model, i.e. calibrating the axial stiffness of the truss elements, a special plane element is introduced in this thesis to represent the wood-frame diaphragm, as shown in Figure 5-2. The plane element is assumed to be isotropic with a linear stress-strain relationship. When subjected to in-plane loads, only the shear deformation is considered. The flexural deformation and the potential out-of-plane deformation due to buckling are neglected. The in-plane stiffness of a linear elastic plane member is here measured by the shear modulus, *G*, which is considered as a homogeneous material property. The equivalent *G* for diaphragms without openings can be calculated based on the results from FLOOR2D analyses, as explained in the following.

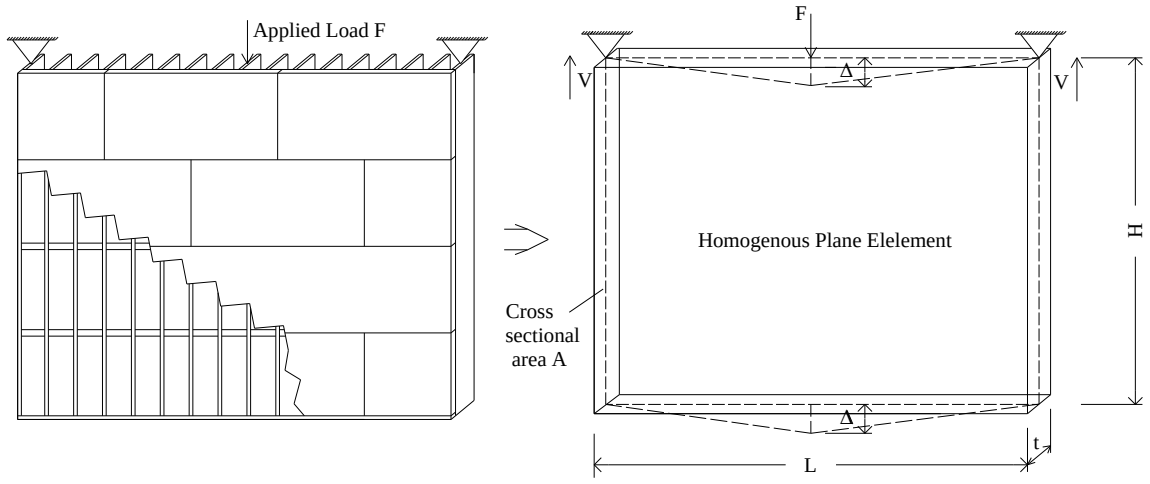

Figure 5-2 Plane element

In Figure 5-2, under the in-plane load *F*, since only the shear deformation is considered, the equation of the unit virtual load method is expressed as:

$$1 \cdot \Delta = \int_0^L \frac{\bar{V}(x) \cdot V(x)}{GA_v} dx \tag{5.1.1}$$

where Δ is the displacement at the midspan of the plane element, L is the length of the diaphragm that is perpendicular to the direction of the applied load. $\bar{V}(x)$ is the shear force due to a unit virtual load at midspsan, and $V(x)$ is the shear force due to the load F. For reference, the shear force diagrams $\bar{V}(x)$ and $V(x)$ are shown in Figure 5-3. A_v=5/6A is the "shear area" of the cross section (Hibbeler 2005), and A is the cross-sectional area of the plane element, as expressed in the following:

$$A = H \cdot t \tag{5.1.2}$$

where H is the depth of the diaphragm that is parallel to the loading direction, and t is the thickness of the diaphragm, which is equal to the depth of the joist member.

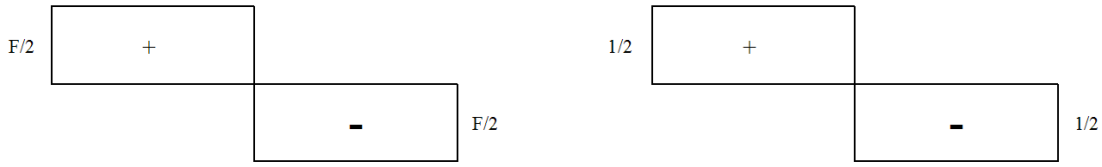

Figure 5-3 Shear force diagrams under the load F and unit load

By substituting those shear force values, and the expression for A_v into Eq. (5.1.1), the following expression is obtained:

$$\Delta = \int_0^L \frac{\frac{1}{2} \cdot \frac{F}{2}}{GA_v} dx = \frac{FL}{4GA_v} = \frac{3FL}{10GA} \tag{5.1.3}$$

Finally, the shear modulus G is obtained by rearranging Eq. (5.1.3) in the following manner:

$$G = \frac{3FL}{10A\Delta} \tag{5.1.4}$$

where F and Δ are determined based on the load-displacement results obtained from FLOOR2D models.

In previous studies, it has been observed that within a certain range of diaphragm aspect ratios, shear dominates the structural behaviour of the diaphragm (Countryman 1952; Bott 2005; Earl 2009). For example, Countryman (Countryman 1952) suggested a range from 2.0 to 3.3. The aspect ratio is the ratio between the length of the diaphragm that is perpendicular to the direction of the joists and the length of the diaphragm that is parallel to the direction of the joists, as shown in Figure 5-4. It is emphasized that the computation of G described in Eq. (5.1.4) is valid within a limited range of aspect ratios. Within that range, shear dominates the in-plane behaviour of the diaphragm and the effect of bending can be neglected. To determine this range, for diaphragms introduced in

Section 4.2, G is calculated within the aspect ratio range of 0.8 to 4, as listed in Table 5-1 and Table 5-2. In the tables, Δ, F, L, H, and A are the same as those illustrated in Figure 5-2. The results listed in the tables are shown in Figure 5-5 to indicate the variation in G within the aspect ratio range of 0.8 to 4.

Table 5-1 lists the calculated G values for diaphragms that are loaded parallel to the direction of the joists, and the variation of G is shown in Figure 5-5 by a solid line. It is observed that within the aspect ratio range of 0.8 to 3, there is no significant difference between the calculated G values. However, when the aspect ratio increases beyond 3, since the influence of bending increases, G decreases as the aspect ratio increases. Compared with the average G value that is calculated within the aspect ratio range of 0.8 to 3, G drops by 13% when the aspect ratio increases to 4.

The calculated G values for diaphragms that are loaded perpendicular to the direction of the joists are listed in Table 5-2, and the variation of G is also shown in Figure 5-5 by a dashed line. For most of the diaphragms in this loading direction, since the span is smaller than the depth, the behaviour of the diaphragm is governed by shear. It is observed that G increases slightly as the aspect ratio increases. When the aspect ratio increases beyond 2.5, G remains around the same value, i.e. 13.1 MPa.

In Figure 5-5, it is observed that within the aspect ratio range of 0.8 to 3, the calculated G values of the two loading directions are in close agreement, with a maximum discrepancy of 7%. However, when the aspect ratio goes beyond 3, for diaphragms that are loaded parallel to the direction of the joists, G decreases as the aspect ratio increases; on the contrary, the value of G remains steady for diaphragms that are loaded perpendicular to the direction of the joists, as mentioned above. The between the

G values of the two loading directions keeps increasing, and when the aspect ratio reaches 4, the discrepancy increases to 15%. As a result, the aspect ratio range within which the calculation of *G* is appropriate is from 0.8 to 3, and the value of *G* for diaphragms introduced in Section 4.2 is taken as the average of *G* in this range, i.e. 12.7 MPa, for both loading directions.

Table 5-1 *G* Values for loading direction parallel to the joists

Dimension (ft)	Aspect Ratio (L/H)	Δ=L/1500 (mm)	F (kN)	L (mm)	H (mm)	A (mm^2)	G (MPa)
16 × 20	0.80	3.3	53.3	4876.8	6096.0	1855012.8	12.9
16 × 16	1.00	3.3	43.5	4876.8	4876.8	1484010.2	13.2
20 × 16	1.25	4.1	42.8	6096.0	4876.8	1484010.2	13.0
24 × 16	1.50	4.9	41.8	7315.2	4876.8	1484010.2	12.7
24 × 12	2.00	4.9	31.9	7315.2	3657.6	1113007.7	12.9
20 × 8	2.50	4.1	21.3	6096.0	2438.4	742005.1	12.9
24 × 8	3.00	4.9	20.5	7315.2	2438.4	742005.1	12.4
28 × 8	3.50	5.7	19.8	8534.4	2438.4	742005.1	12.0
32× 8	4.00	6.5	19.0	9753.6	2438.4	742005.1	11.4

Table 5-2 *G* values for loading direction perpendicular to the joists

Dimension (ft)	Aspect Ratio (H/L)	Δ=L/1500 (mm)	F (kN)	L (mm)	H (mm)	A (mm^2)	G (MPa)
16 × 20	0.80	4.1	39.8	6096.0	4876.8	1484010.2	12.1
16 × 16	1.00	3.3	40.6	4876.8	4876.8	1484010.2	12.3
20 × 16	1.25	3.3	51.2	4876.8	6096.0	1855012.8	12.4
24 × 16	1.50	3.3	61.7	4876.8	7315.2	2226015.4	12.5
24 × 12	2.00	2.4	62.5	3657.6	7315.2	2226015.4	12.6
20 × 8	2.50	1.6	54.1	2438.4	6096.0	1855012.8	13.1
24 × 8	3.00	1.6	64.8	2438.4	7315.2	2226015.4	13.1
28 × 8	3.50	1.6	74.9	2438.4	8534.4	2597017.9	13.0
32× 8	4.00	1.6	86.6	2438.4	9753.6	2968020.48	13.1

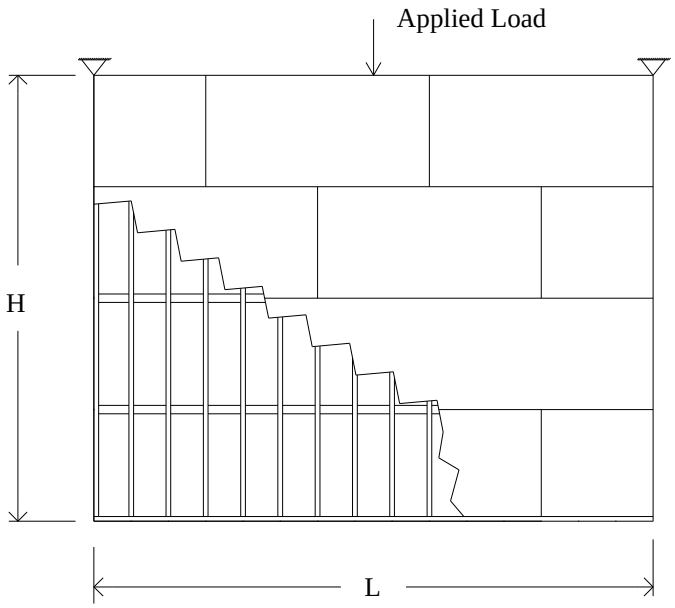

Aspect Ratio = L/H

(a)

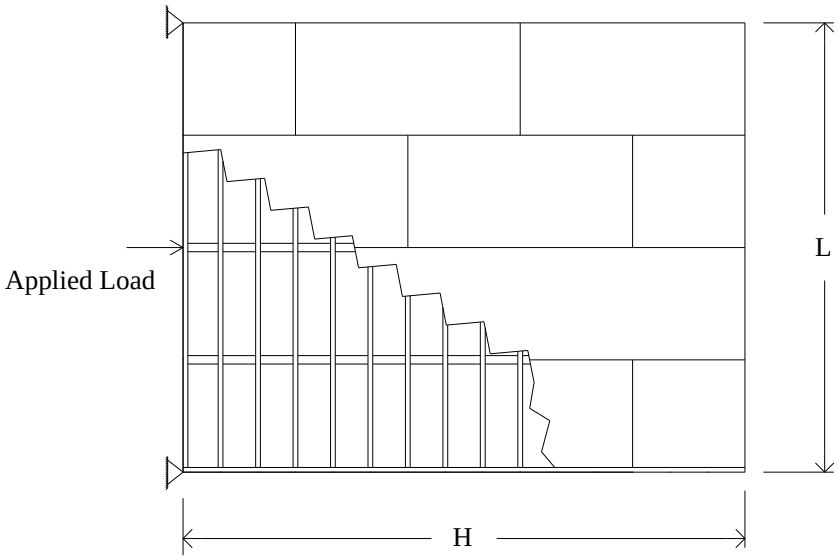

Aspect Ratio = H/L

(b)

Figure 5-4 Illustration of the diaphragm aspect ratio:

(a) loading direction parallel to the joists (b) loading direction perpendicular to the joists

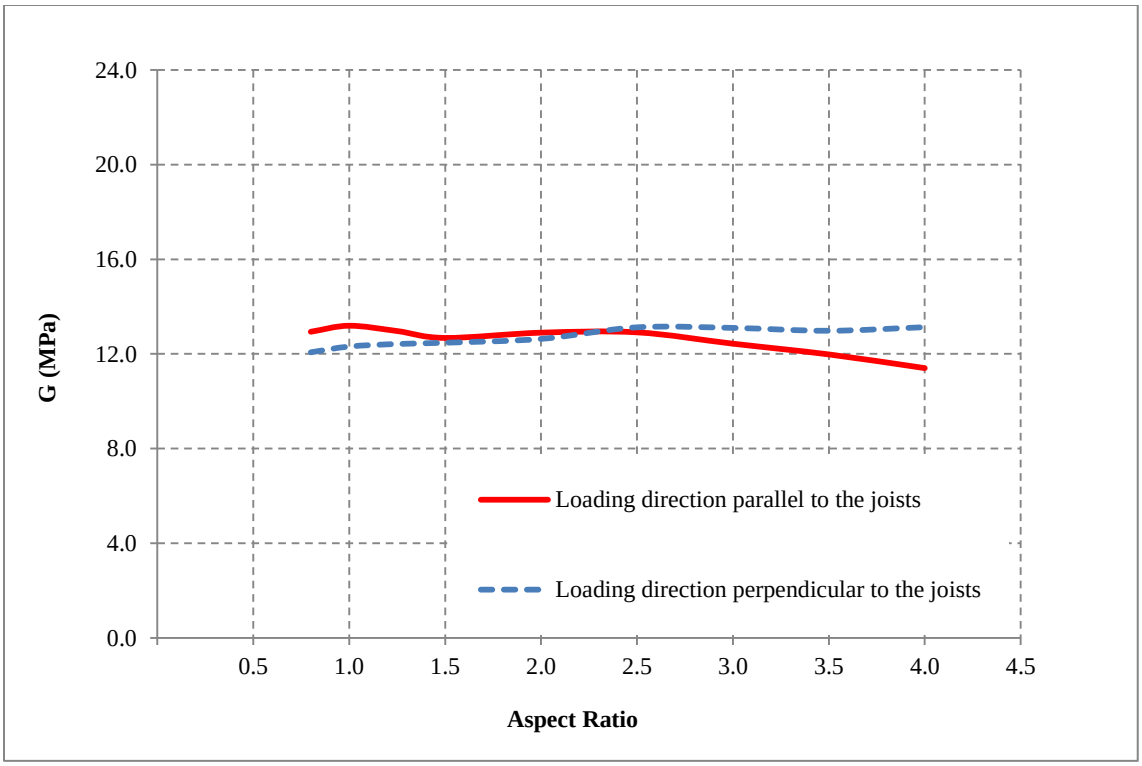

Figure 5-5 Comparison of *G* between the two loading directions

5.1.2 Calibration of the Truss Unit

This section illustrates how to use the value of G determined in the previous section to calibrate the truss unit of the simplified diaphragm model. Consider the two truss units in Figure 5-6. When subjected to a point load, F, by assuming infinite axial rigidity, EA_t, for the perimeter truss elements and equal axial rigidity for the diagonal truss elements, the deformation at the midspan of the diaphragm, Δ, can be calculated using the unit virtual load method as:

$$1 \cdot \Delta = \sum_{n=1}^{4} \frac{\overline{N}_n N_n L_t}{EA_t} \tag{5.1.5}$$

where E, A_t, L_t are the modulus of elasticity, cross-sectional area, and the length of the truss element, respectively; n represents the number of the diagonal truss element, as shown in Figure 5-6. $\overline{N}$ is the axial force in the truss element due to the unit virtual load,

and N is the axial force due to the load F. For reference, Table 5-3 listed the axial forces for the four diagonal truss elements in Figure 5-6.

Table 5-3 Axial forces for diagonal truss elements

Truss Element Number	$\bar{F}_N$	F_{NP}
1	1/4cosθ	F/4cosθ
2	-1/4cosθ	-F/4cosθ
3	-1/4cosθ	-F/4cosθ
4	1/4cosθ	F/4cosθ

where θ is the angle between the diagonal and vertical truss elements, and

$$\cos\theta = \frac{d}{\sqrt{a^2 + d^2}} \tag{5.1.6}$$

By substituting the calculated axial forces in Table 5-3 and L_t=d/cosθ into Eq. (5.1.5), Δ is expressed as:

$$\Delta = \frac{F\left(a^2 + d^2\right)^{\frac{3}{2}}}{4d^2 EA_t} \tag{5.1.7}$$

As introduced in Section 5.1.1, the deformation at the midspan of the diaphragm can also be calculated according to Eq. (5.1.3). The two calculated Δ are equal, thus by combining Eq. (5.1.7) with Eq. (5.1.3), the following relationship is obtained:

$$\frac{3F\left(2a\right)}{10GA} = \frac{F\left(a^2 + d^2\right)^{\frac{3}{2}}}{4d^2 EA_t} \tag{5.1.8}$$

As a result, the axial rigidity of the truss element can be expressed in terms of G by arranging Eq. (5.1.8) as:

$$EA_t = \frac{5GA(a^2 + d^2)^{\frac{3}{2}}}{12ad^2} \tag{5.1.9}$$

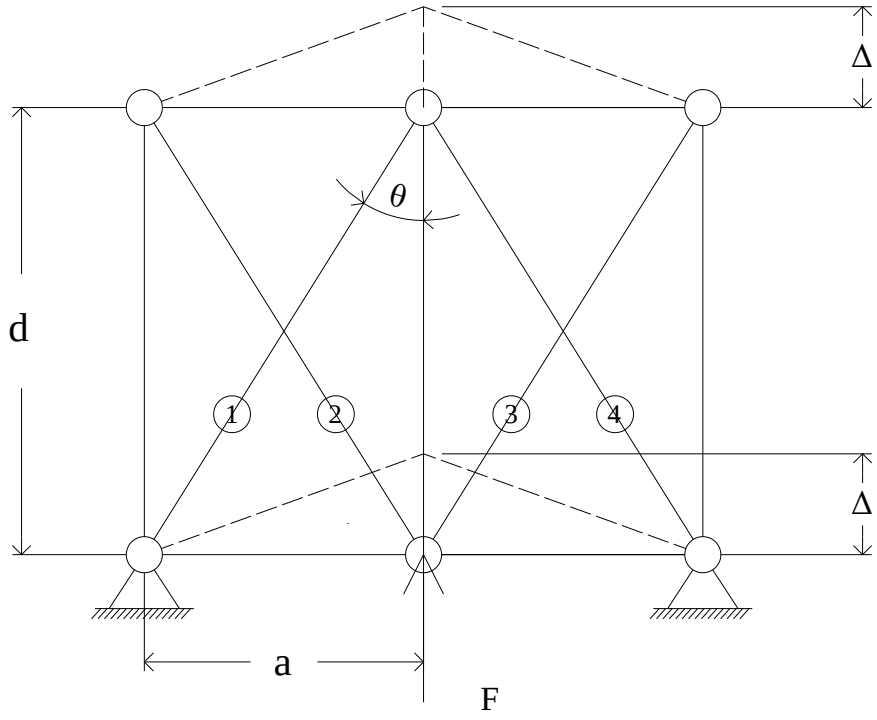

Figure 5-6 Diaphragm truss units

The steps to obtain the simplified diaphragm model are summarized in the following:

1. The first step is to discretize the diaphragm into a suitable number of truss units according to its configuration; for example, as shown in Figure 5-7, a diaphragm with a corner opening is discretized into 18 truss units with three different dimensions.
2. In the second step, for each type of the truss unit, the axial stiffness of the diagonally bracing truss elements is calibrated by substituting the dimension of the truss unit and the value of *G* into Eq. (5.1.9).
3. Finally, the simplified diaphragm model is represented as an assembly of all the truss units.

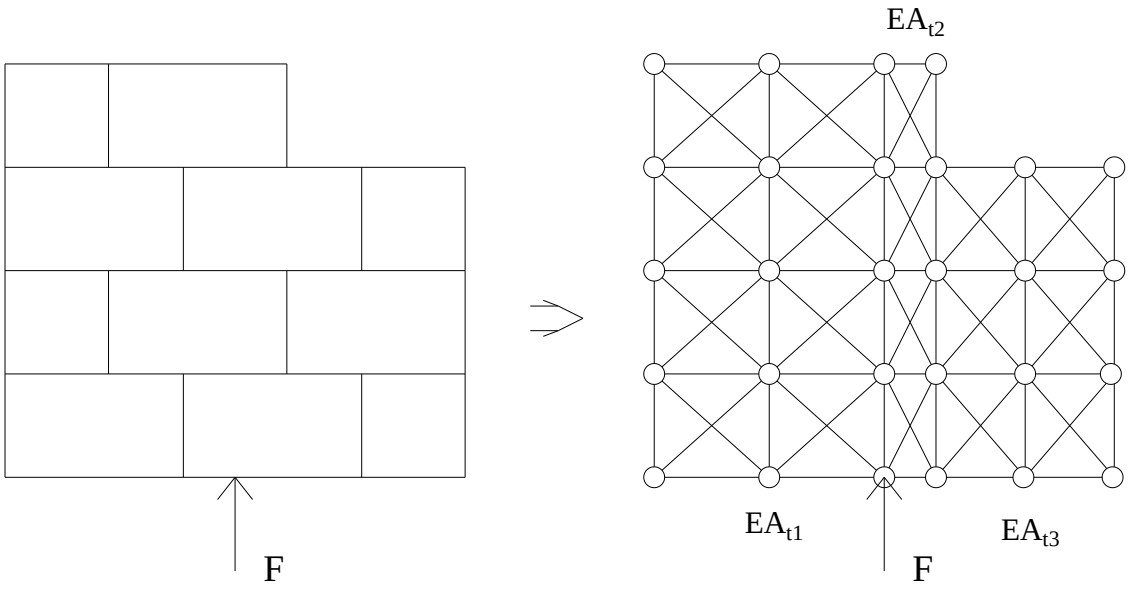

Figure 5-7 Simplified model for the diaphragm with a corner opening

For a diaphragm with a point load at midspan, such as the diaphragm shown in Figure 5-2, the shape of the diaphragm due to shear deformation is straight. In particular, such a diaphragm deforms as a separate straight line on each side of the point load. This indicates that the in-plane deformation of the diaphragm is not affected by discretization into smaller truss units. Therefore, regardless of how many truss units are utilized to model the diaphragm, the deformation will remain the same.

When subjected to distributed loads, the deformed shape of the diaphragm becomes more precise with an increase in the number of truss units. However, for models consisted of truss elements, since the finite element solution is always nodally exact for any loading (Boeraeve 2010), the predicted nodal displacement will remain the same regardless of the discretization. For example, in Figure 5-8, the diaphragm is discretized into 4 truss units and 16 truss units, respectively. It is observed the model with more truss units yields a more precise deformed shape. However, both the two models have nodes located at the midspan, thus yield the same maximum deformations.

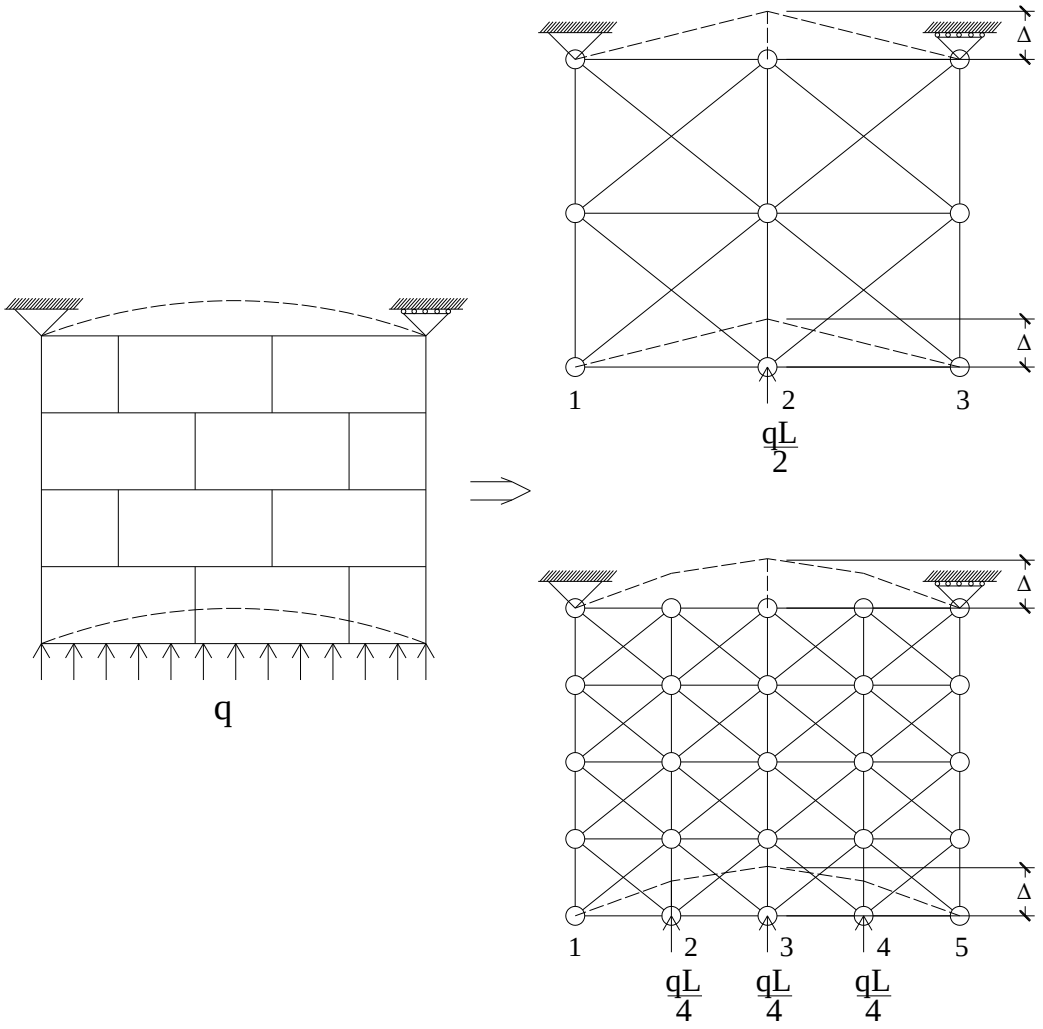

Figure 5-8 Discretization of the diaphragm

5.2 Case Study: One-Storey Building Model

In this section, the simplified diaphragm model obtained in the previous section is incorporated into to a one-storey light wood-frame building to study the distribution of lateral loads to shear walls. In particular, the load sharing results among shear walls are investigated under three diaphragm flexibility assumptions: the flexible diaphragm, the rigid diaphragm, and the semi-rigid diaphragm, i.e. the diaphragm with the stiffness falls somewhere in between the two extremes.

5.2.1 Building Model

Figure 5-9 shows the plan view of the building and the layout of shear walls (denoted by W), which are determined by reference to that of the first-storey of the NEESWood benchmark structure (Pang and Rosowsky 2010)**.** The height of the building is 2.74m. In the building, the type of the diaphragm is the same as that introduced in Section 4.2, and all joists are assumed to be in the longitudinal direction (Y direction in Figure 5-9). The force-displacement curve of the shear wall is shown in Figure 5-10, and the initial stiffness, K_0, is taken as the stiffness of the shear wall in this work, values are listed in Table 5-4. The building is modelled in the finite element program ANSYS using 3-D truss elements (LINK 180). This type of element is a uniaxial tension-compression element, which can be used to model trusses, sagging cables, links, and springs. As shown in Figure 5-11, the element has two nodes and each node has three degrees of freedom, i.e. translations in the nodal *x*, *y*, and *z* directions. As a pin-connected structure, no bending effect is considered for the element under nodal loading (ANSYS 2011).

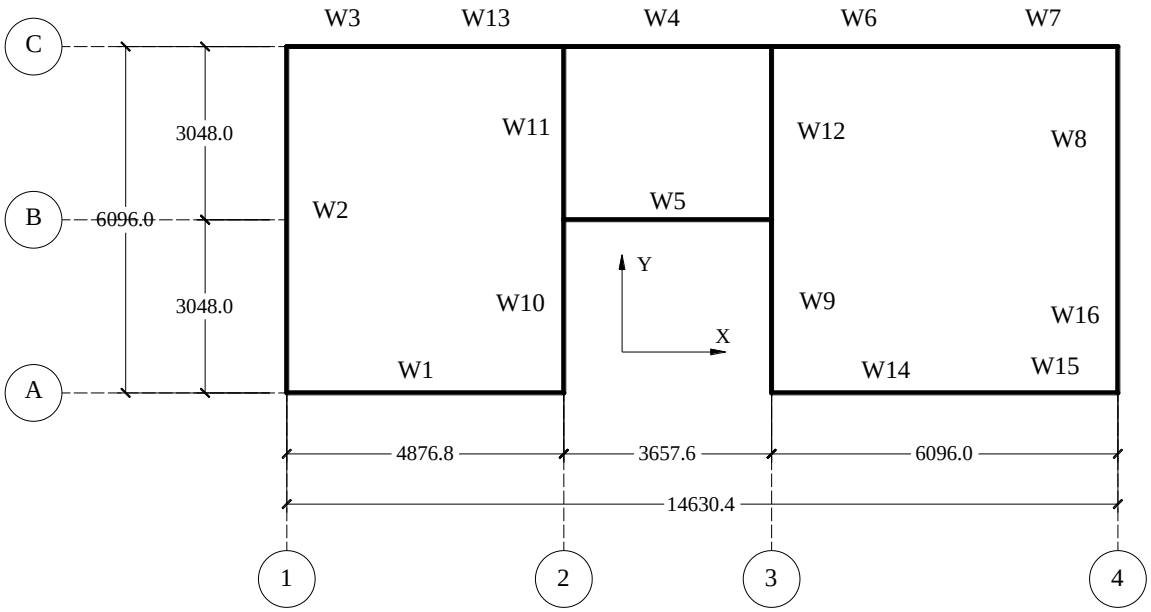

Figure 5-9 Building plan view (mm)

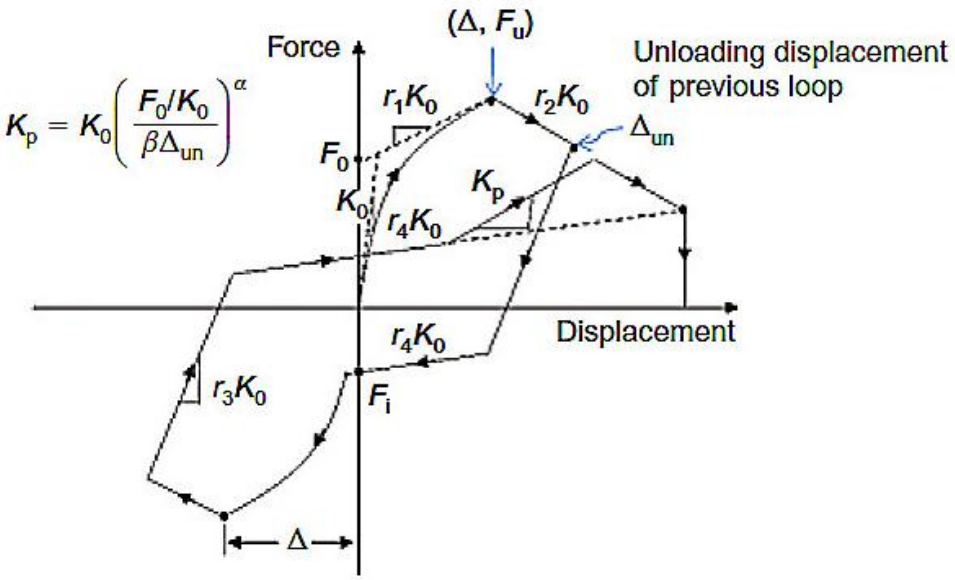

Figure 5-10 Modified hysteresis spring model (Pang and Rosowsky 2010)

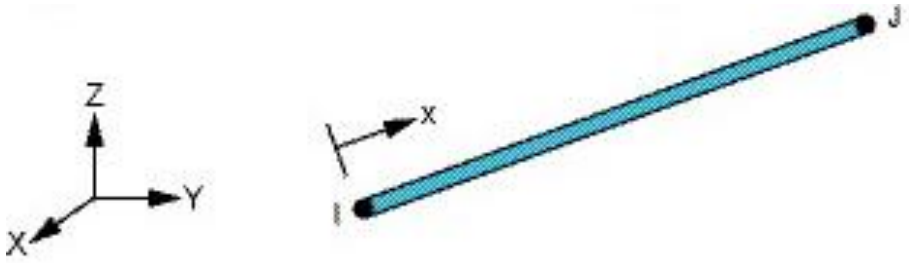

Figure 5-11 Link 180 geometry (ANSYS 2011)

As shown in Figure 5-12, the diaphragm is simplified with three types of truss units. The flexible diaphragm is realized by assigning relatively small cross-sectional areas to the diagonal bracing elements. Similarly, the rigid diaphragm is realized by assigning relatively large cross-sectional areas to the diagonal bracing elements. In the case of semi-rigid diaphragm, the axial stiffness of the diagonal bracing elements is calibrated according to Eq. (5.1.9). The utilized properties of the truss units are listed in Table 5-5.

Table 5-4 Shear wall properties

Shear Wall Number	L_S (mm)	H_S (mm)	K_S (kN/mm)
1	4876.8	2740	4.04
2	6096	2740	1.36
3	2438.4	2740	1.81
4	3657.6	2740	2.88
5	3657.6	2740	0.78
6	3048	2740	2.66
7	3048	2740	2.42
8	3048	2740	2.60
9	3048	2740	1.85
10	3048	2740	2.18
11	3048	2740	2.26
12	3048	2740	1.96
13	2438.4	2740	1.81
14	3048	2740	2.66
15	3048	2740	2.42
16	3048	2740	2.60

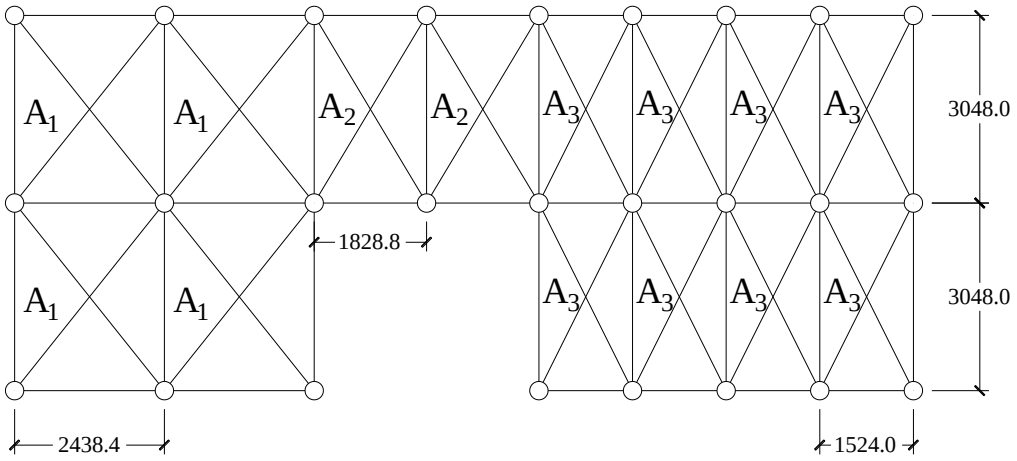

Figure 5-12 Simplified diaphragm model (mm)

Table 5-5 Properties of diaphragm truss units

Truss Unit Number	a (mm)	d (mm)	E (MPa)	A_t (mm^2)
1	2438.40	3048	12000	1067.9
2	1828.8	1828.8	12000	1075.4
3	1524	3048	12000	1136.9

The shear walls are also modelled using truss units, which are calibrated in a similar way as the diaphragm, as explained shortly. As shown in Figure 5-13, when subjected to a point load, *F*, by reference to Eq. (5.1.5), the displacement at the top of the shear wall, Δ, is calculated as:

$$\Delta = \sum_{n=1}^{2n_t} \frac{\overline{N}_n N_n L_t}{EA_t} = (2n_t) \cdot \frac{\left(\frac{1}{2n_t \sin\theta}\right) \cdot \left(\frac{F}{2n_t \sin\theta}\right) \cdot \left(\frac{d}{\cos\theta}\right)}{EA_t} \qquad (5.2.1)$$

where n_t is the number of the truss units that are used to represent the shear wall, and $\sin\theta = a / \sqrt{a^2 + d^2}$.

According to Table 5-4, since the stiffness of the shear wall, K_S, is known, Δ can also be calculated as:

$$\Delta = \frac{F}{K_S} \qquad (5.2.2)$$

By setting the two Δ to equal, i.e. by combining Eq. (5.2.1) and Eq. (5.2.2), EA_t can be expressed in terms of K_S as:

$$EA_t = \frac{K_S (a^2 + d^2)^{\frac{3}{2}}}{2n_t a^2} \qquad (5.2.3)$$

Properties of truss units for each shear wall are listed in Table 5-6.

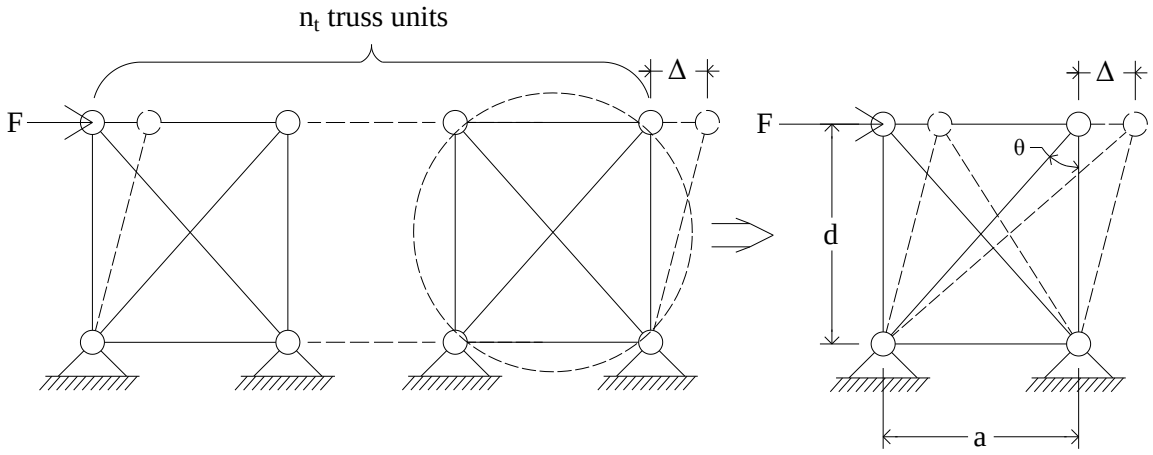

Figure 5-13 Shear wall truss units

Table 5-6 Properties of shear wall truss units

Number	a (mm)	d (mm)	n_t	E (Mpa)	A_t (mm^2)
1	2438.4	2740	2	12000	698.6
2	3048	2740	2	12000	210.0
3	2438.4	2740	1	12000	625.9
4	1828.8	2740	2	12000	641.4
5	1828.8	2740	2	12000	173.7
6	1524	2740	2	12000	735.5
7	1524	2740	2	12000	669.1
8	3048	2740	1	12000	802.9
9	3048	2740	1	12000	571.3
10	3048	2740	1	12000	673.2
11	3048	2740	1	12000	697.9
12	3048	2740	1	12000	605.3
13	2438.4	2740	1	12000	625.9
14	1524	2740	2	12000	735.5
15	1524	2740	2	12000	669.1
16	3048	2740	1	12000	802.9

The boundary condition of the building model is shown in Figure 5-14. For nodes located at the bottom, all displacements are constrained, i.e. $u_x=u_y=u_z=0$.

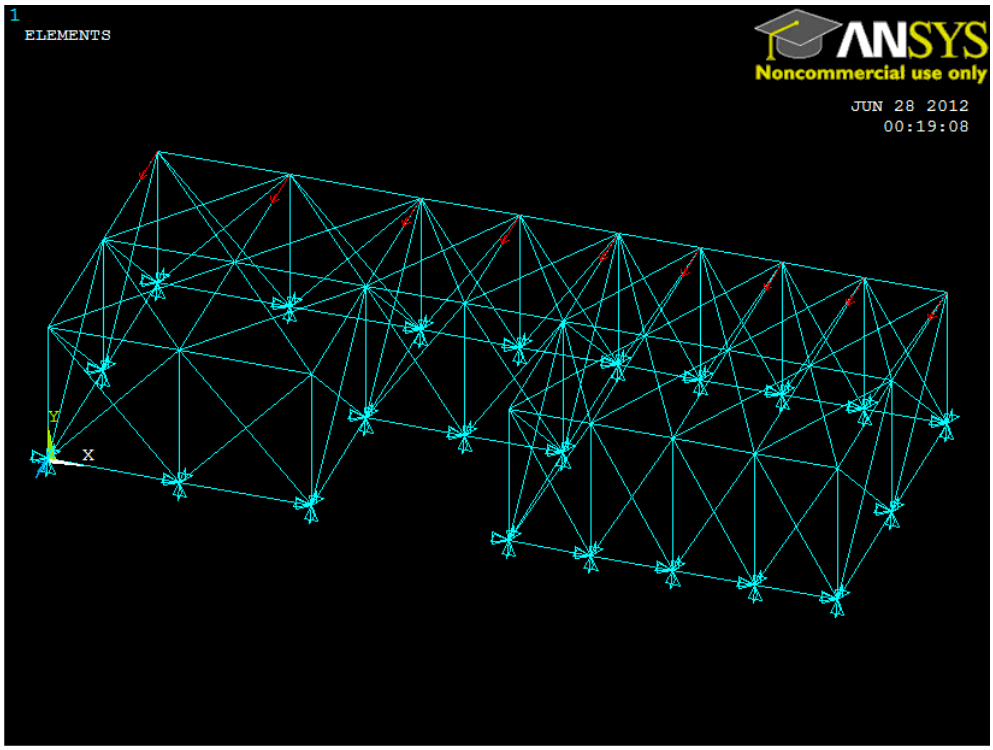

Figure 5-14 Boundary condition for the building model

It is assumed that the building is subjected to lateral loads that are parallel to the direction of the diaphragm joists. The total gravity load carried by the load-bearing shear walls, W, is around 356 kN (Pang and Rosowsky 2010), and the lateral load applied to the building is assumed to be $F=0.03W=10.69$ kN. It is assumed that the lateral load is uniformly distributed on the diaphragm. For the building model, since loads can only be applied at nodes, the lateral load applied at each node is calculated based on the tributary area of the node. As shown in Figure 5-15, in this case study, the lateral load is applied at nodes located along the continuous edge line of the building. Table 5-7 summarizes the load applied on each node.

Table 5-7 Loads on edge line nodes

Node Number	Tributary Area (m^2)	Load (kN)
40	7.43	1.02
41	14.86	2.04
42	10.22	1.40
43	5.57	0.76
44	7.43	1.02
45	9.29	1.27
46	9.29	1.27
47	9.29	1.27
48	4.65	0.64

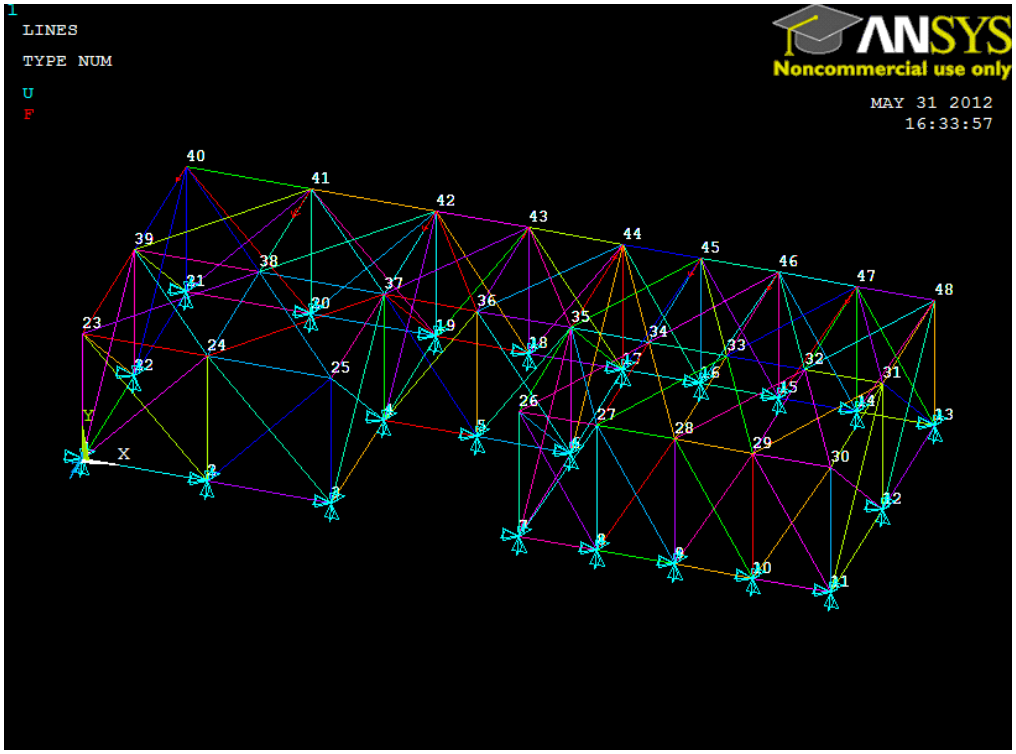

Figure 5-15 Load Condition for the building model

5.2.2 Results and Discussions

In this section, the building model is analyzed under the three diaphragm flexibility assumptions. According to the International Building Code (IBC) (ICC 2003): "a diaphragm is defined as flexible if the maximum in-plane deflection of the diaphragm alone is more than two times the average inter-storey drift of the vertical lateral force resisting elements". Deformation results obtained from the semi-rigid diaphragm case, i.e. the actual wood-frame diaphragm, are shown in Table 5-8. It is observed that since the ratio between the maximum diaphragm deflection and the average shear wall inter-storey drift is 1.06/0.75=1.42< 2, the semi-rigid diaphragm is classified as rigid in accordance with the code.

Table 5-8 Deflections of the building model

Shear wall Number	Inter-storey Drift (mm)	Average Shear Wall Inter-storey Drift $D_{S,avg}$ (mm)	Maximum Diaphragm Deflection D_{dia} (mm)	Ratio of $D_{dia}/D_{S,avg}$
2	1.07	0.75	1.06	1.41
10	0.79			
11	0.79			
9	0.76			
12	0.76			
8	0.55			
16	0.55			

As mentioned in Chapter 1, in the cases of the rigid diaphragm and the flexible diaphragm, the lateral load distribution to shear walls can be computed by hand calculation methods, i.e. the relative stiffness method and the tributary area method, as introduced shortly. In order to demonstrate the methods, the building introduced in Section 5.2.1 is examined here, and the results of the hand calculation methods are compared with the outputs of the building model.

In the relative stiffness method, the lateral load distributed to each shear wall is calculated by the following steps:

1. The starting point of the analysis is to establish the stiffness matrix, $\mathbf{k}_{wn}$, for each shear wall (the subscript *n* represents the number of the shear wall). The degrees of freedom (DOFs) of the shear walls are shown in Figure 5-16. For reference, the stiffness matrices for shear walls in the demonstrated building are listed in the following. Both the out-of-plane moment of inertial and torsion stiffness of the shear wall are assumed to be zero, and the in-plane stiffness of the shear wall is given earlier in Table 5-4.

$$\mathbf{k}_{w1}=\begin{bmatrix}4.4 & 0 & 0\\ 0 & 0 & 0\\ 0 & 0 & 0\end{bmatrix},\qquad \mathbf{k}_{w2}=\begin{bmatrix}0 & 0 & 0\\ 0 & 1.36 & 0\\ 0 & 0 & 0\end{bmatrix},\qquad \mathbf{k}_{w3}=\begin{bmatrix}1.81 & 0 & 0\\ 0 & 0 & 0\\ 0 & 0 & 0\end{bmatrix},$$

$$\mathbf{k}_{w4}=\begin{bmatrix}2.88 & 0 & 0\\ 0 & 0 & 0\\ 0 & 0 & 0\end{bmatrix},\qquad \mathbf{k}_{w5}=\begin{bmatrix}0.78 & 0 & 0\\ 0 & 0 & 0\\ 0 & 0 & 0\end{bmatrix},\qquad \mathbf{k}_{w6}=\begin{bmatrix}2.66 & 0 & 0\\ 0 & 0 & 0\\ 0 & 0 & 0\end{bmatrix},$$

$$\mathbf{k}_{w7}=\begin{bmatrix}2.42 & 0 & 0\\ 0 & 0 & 0\\ 0 & 0 & 0\end{bmatrix},\qquad \mathbf{k}_{w8}=\begin{bmatrix}0 & 0 & 0\\ 0 & 2.60 & 0\\ 0 & 0 & 0\end{bmatrix},\qquad \mathbf{k}_{w9}=\begin{bmatrix}0 & 0 & 0\\ 0 & 1.85 & 0\\ 0 & 0 & 0\end{bmatrix},$$

$$\mathbf{k}_{w10}=\begin{bmatrix}0 & 0 & 0\\ 0 & 2.18 & 0\\ 0 & 0 & 0\end{bmatrix},\qquad \mathbf{k}_{w11}=\begin{bmatrix}0 & 0 & 0\\ 0 & 2.26 & 0\\ 0 & 0 & 0\end{bmatrix},\qquad \mathbf{k}_{w12}=\begin{bmatrix}0 & 0 & 0\\ 0 & 1.96 & 0\\ 0 & 0 & 0\end{bmatrix},$$

$$\mathbf{k}_{w13}=\begin{bmatrix}1.81 & 0 & 0\\ 0 & 0 & 0\\ 0 & 0 & 0\end{bmatrix},\qquad \mathbf{k}_{w14}=\begin{bmatrix}2.66 & 0 & 0\\ 0 & 0 & 0\\ 0 & 0 & 0\end{bmatrix},\qquad \mathbf{k}_{w15}=\begin{bmatrix}2.42 & 0 & 0\\ 0 & 0 & 0\\ 0 & 0 & 0\end{bmatrix},$$

$$\mathbf{k}_{w16}=\begin{bmatrix}0 & 0 & 0\\ 0 & 2.60 & 0\\ 0 & 0 & 0\end{bmatrix}.\qquad \text{(unit: kN/mm)}$$

2. In the second step, the transformation matrices, $\mathbf{T}_w$, which are used to link the DOFs of the shear wall to the DOFs of the diaphragm, are determined. As shown in Figure 5-16, the DOFs of the diaphragm are assumed to originate at the lower left corner of the building. The transformation matrix of the shear wall is determined as:

$$\mathbf{T}_w = \begin{bmatrix} 1 & 0 & b \\ 0 & 1 & -a \\ 0 & 0 & 1 \end{bmatrix}$$

where a and b are the distances from the center of the shear wall to the original point of the diaphragm along x and y directions, respectively. For reference, transformation matrices for all the shear walls are listed in the following:

$$\mathbf{T}_{w1} = \begin{bmatrix} 1 & 0 & 0 \\ 0 & 1 & 2438.4 \\ 0 & 0 & 1 \end{bmatrix}, \quad \mathbf{T}_{w2} = \begin{bmatrix} 1 & 0 & -3048 \\ 0 & 1 & 0 \\ 0 & 0 & 1 \end{bmatrix}, \quad \mathbf{T}_{w3} = \begin{bmatrix} 1 & 0 & -6096 \\ 0 & 1 & 1219.2 \\ 0 & 0 & 1 \end{bmatrix},$$

$$\mathbf{T}_{w4} = \begin{bmatrix} 1 & 0 & -6096 \\ 0 & 1 & 6705.6 \\ 0 & 0 & 1 \end{bmatrix}, \quad \mathbf{T}_{w5} = \begin{bmatrix} 1 & 0 & -3048 \\ 0 & 1 & 6705.6 \\ 0 & 0 & 1 \end{bmatrix}, \quad \mathbf{T}_{w6} = \begin{bmatrix} 1 & 0 & -6096 \\ 0 & 1 & 10058.4 \\ 0 & 0 & 1 \end{bmatrix},$$

$$\mathbf{T}_{w7} = \begin{bmatrix} 1 & 0 & -6096 \\ 0 & 1 & 13106.4 \\ 0 & 0 & 1 \end{bmatrix}, \quad \mathbf{T}_{w8} = \begin{bmatrix} 1 & 0 & -4572 \\ 0 & 1 & 14630.4 \\ 0 & 0 & 1 \end{bmatrix}, \quad \mathbf{T}_{w9} = \begin{bmatrix} 1 & 0 & -1524 \\ 0 & 1 & 8534.4 \\ 0 & 0 & 1 \end{bmatrix},$$

$$\mathbf{T}_{w10} = \begin{bmatrix} 1 & 0 & -1524 \\ 0 & 1 & 4876.8 \\ 0 & 0 & 1 \end{bmatrix}, \quad \mathbf{T}_{w11} = \begin{bmatrix} 1 & 0 & -4572 \\ 0 & 1 & 4876.8 \\ 0 & 0 & 1 \end{bmatrix}, \quad \mathbf{T}_{w12} = \begin{bmatrix} 1 & 0 & -4572 \\ 0 & 1 & 8534.4 \\ 0 & 0 & 1 \end{bmatrix},$$

$$\mathbf{T}_{w13} = \begin{bmatrix} 1 & 0 & -6096 \\ 0 & 1 & 3657.6 \\ 0 & 0 & 1 \end{bmatrix}, \quad \mathbf{T}_{w14} = \begin{bmatrix} 1 & 0 & 0 \\ 0 & 1 & 10058.4 \\ 0 & 0 & 1 \end{bmatrix}, \quad \mathbf{T}_{w15} = \begin{bmatrix} 1 & 0 & 0 \\ 0 & 1 & 13106.4 \\ 0 & 0 & 1 \end{bmatrix},$$

$$\mathbf{T_{w16}} = \begin{bmatrix} 1 & 0 & -1524 \\ 0 & 1 & 14630.4 \\ 0 & 0 & 1 \end{bmatrix}.$$

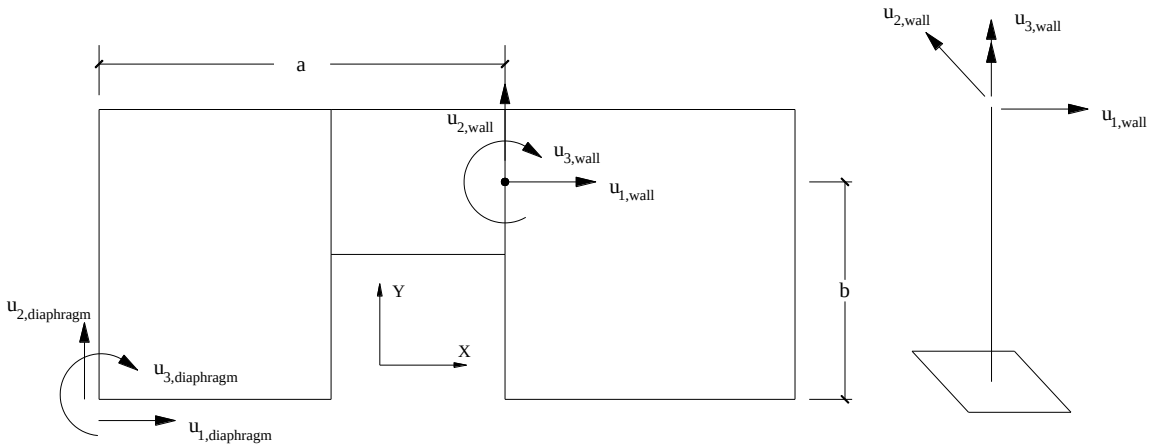

Figure 5-16 Rigid diaphragm coordinate system

3. After obtaining the stiffness matrix and the transformation matrix for each shear wall, the stiffness matrix of the entire diaphragm, $\mathbf{K_d}$, is assembled as:

$$\mathbf{K_d} = \sum_{n=1}^{16} \mathbf{T_{wn}}^{\mathrm{T}} \cdot \mathbf{k_{wn}} \cdot \mathbf{T_{wn}} = \begin{bmatrix} 21.84 & 0 & -7.297\times10^{4} \\ 0 & 14.81 & 1.302\times10^{5} \\ -7.297\times10^{4} & 1.302\times10^{5} & 1.934\times10^{9} \end{bmatrix} (\text{kN/mm})$$

4. The load vector, $\mathbf{F_d}$, for the diaphragm is:

$$\mathbf{F_d} = \begin{bmatrix} 0 \\ -10.69 \\ -7.91\times10^{4} \end{bmatrix} (\text{kN})$$

The displacement vector for the diaphragm, $\mathbf{u_d}$, is obtained by solving the following equations as:

$$\mathbf{u_d} = \mathbf{K_d}^{-1} \cdot \mathbf{F_d} = \begin{bmatrix} 0.092 \\ -0.963 \\ 2.74\times10^{-5} \end{bmatrix} (\text{mm})$$

5. Finally, the load distributed to each shear wall is obtained according to the following equation:

$$\mathbf{F}_{\mathbf{wn}} = \mathbf{k}_{\mathbf{wn}} \cdot \mathbf{T}_{\mathbf{wn}} \cdot \mathbf{u}_{\mathbf{d}} \tag{5.2.4}$$

The distribution of lateral loads on the transverse shear walls, which is obtained from the relative stiffness method, is listed in Table 5-9.

Table 5-9 Load in each shear wall by the relative stiffness method

Shear Wall Number	Load (kN)
2	1.31
10	1.81
11	1.87
9	1.35
12	1.43
8	1.46
16	1.46

In the tributary area method, the lateral load distribution to shear walls is calculated by the following formula:

$$F_i = \frac{A_i}{A} \cdot F, \qquad i=1,2,3,4 \tag{5.2.5}$$

where i is the shear wall line number, as shown in Figure 5-9; F_i is the lateral force in the shear walls line i, and F is the total lateral force; A_i is the tributary area associated with the shear wall line i, and A is the total area of the diaphragm. For each shear wall line, the load is distributed based on the relative stiffness of each shear wall. The distribution of lateral loads on the transverse shear walls of the demonstrated building, which is obtained from the tributary area method, is listed in Table 5-10.

Table 5-10 Load in each shear wall by the tributary area method

Shear Wall Number	Shear Wall Line Number	A_i (m^2)	A_i/A	F_i (kN)	Stiffness Ratio	Load (kN)
2	1	14.86	0.19	2.04	1	2.04
10	2	20.44	0.26	2.80	0.49	1.37
11					0.51	1.43
9	3	24.15	0.31	3.31	0.49	1.61
12					0.51	1.70
8	4	18.58	0.24	2.55	0.50	1.27
16					0.50	1.27

The lateral load distribution to shear walls obtained from the finite element model under the three diaphragm flexibility assumptions are listed in Table 5-11, and are shown in Figure 5-17. When comparing Table 5-11 with Table 5-9 and Table 5-10, it is observed that the results of the hand calculation methods agree well with that of the building model. In Figure 5-17, it is observed that the load distribution results of the semi-rigid diaphragm case always fall in between that of the other two extreme cases. According to the comparisons listed in Table 5-11, the behaviour of the semi-rigid diaphragm in this case study is closer to rigid. This conclusion agrees with the flexibility classification in IBC, while is contrast to the general flexible wood-frame diaphragm assumption. The possible reason is explained as follows: according to FEMA 310 (Federal Emergency Management Agency 1998), in the seismic design, the rigidity of the diaphragm means the rigidity relative to the vertical lateral load resisting elements. The seismic design handbook (Naeim 1989) indicates that: "The absolute size and stiffness of a diaphragm, while important, are not the final determining factors whether or not a diaphragm will behave as a rigid, flexible or semi-rigid. The distribution of horizontal forces by the horizontal diaphragm to the various vertical lateral load resisting elements depends on the relative rigidity of the horizontal diaphragm and the vertical lateral load resisting

elements." The stiffness of the diaphragm in this case study is relatively large when compared with the stiffness of the shear walls. Under lateral loads, the deformation of the diaphragm is insignificant in comparison to that of the shear walls. As such, the diaphragm will move as a rigid body and force the connected shear walls to move together (Naeim 1989).

Table 5-11 Load distribution results

Shear Wall Number	Load Distribution			Comparison	
	F_{Rig}(kN)	F_{Flex} (kN)	F_{Semi}(kN)	Difference between F_{rig} and F_{Semi}	Difference between F_{Flex} and F_{Semi}
2	1.31	2.04	1.45	-9.48%	40.76%
10	1.81	1.37	1.72	5.07%	-20.16%
11	1.88	1.43	1.79	5.07%	-20.16%
9	1.35	1.61	1.41	-4.05%	14.35%
12	1.43	1.70	1.49	-4.06%	14.34%
8	1.46	1.27	1.42	2.70%	-10.17%
16	1.46	1.27	1.42	2.70%	-10.17%

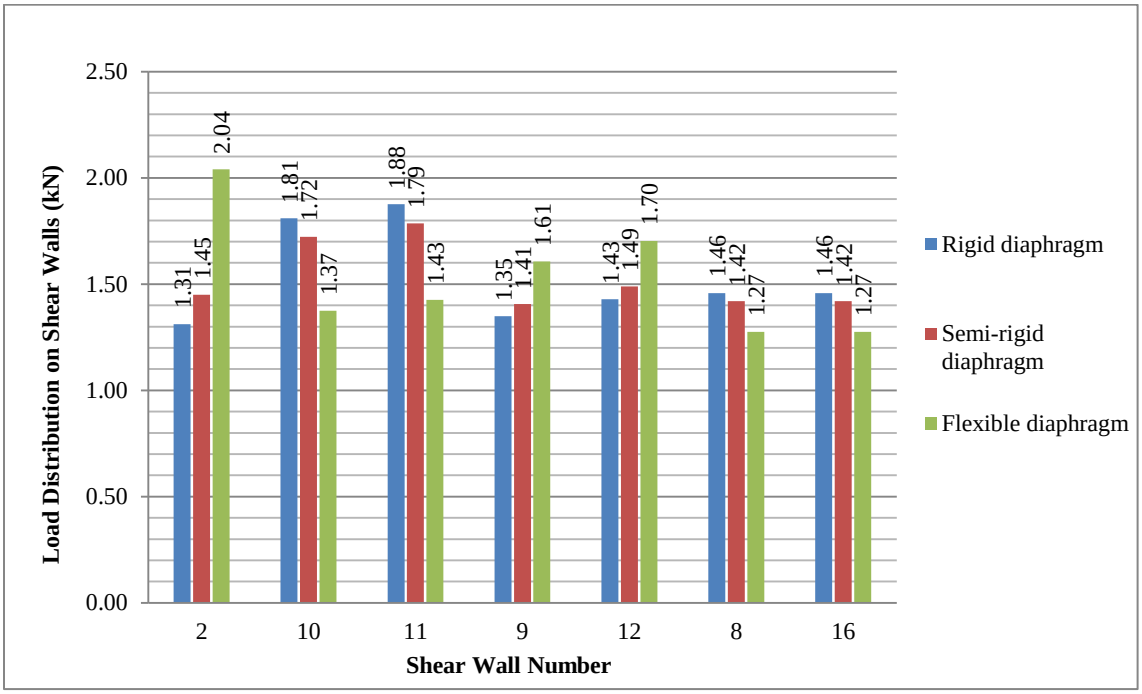

Figure 5-17 Load distribution under three diaphragm flexibility assumptions

In order to verify the viewpoint indicated above, for the semi-rigid diaphragm case, load distribution results under various shear wall stiffness conditions are investigated. The results are listed in Table 5-12, and are shown in Figure 5-18. By comparing the load distribution results with that of the rigid and flexible diaphragm cases, it is observed that as the stiffness of the shear walls increases, the behaviour of the semi-rigid diaphragm becomes closer to flexible than rigid. In particular, according to Table 5-12, when the stiffness of the shear walls is doubled, the load distribution results show bigger differences between the flexible model and semi-rigid model. However, the differences decrease with increasing shear wall stiffness. When the stiffness of the shear walls increases ten-fold, differences between the load distribution results of the rigid model and semi-rigid model become bigger, which indicates that the behaviour of the semi-rigid diaphragm is closer to flexible. The displacement results for the three shear wall stiffness conditions are listed in Table 5-13. It is observed that when the stiffness of the shear walls increases by two, five, and ten times, the ratios between the maximum diaphragm deflection and the average shear wall deflection are 1.60, 2.19, and 3.49, respectively. The semi-rigid diaphragms in the three cases are classified as rigid, flexible, and flexible respectively in accordance with the code, which agree well with the analysis results. In short, this confirms that the load distribution onto shear walls is strongly dependent on the stiffness of the diaphragm relative to the stiffness of the shear walls.

It is also noted that compared with the semi-rigid diaphragm case, the rigid diaphragm model underestimates the load sharing among shear walls 2, 9 and 12. On the contrary, the flexible diaphragm analysis underestimates the load sharing among the other shear walls. This indicates that neither the rigid nor the flexible diaphragm assumption

could assure conservative load demands for all the shear walls. As a result, the two assumptions are suggested to be considered together in the design to avoid underestimate on the design loads for shear walls.

Table 5-12 Load distribution results for various shear wall stiffness conditions

Shear Wall Number		2	10	11	9	12	8	16
$2K_S$	Load Distribution F_{Semi}(kN)	1.54	1.67	1.73	1.44	1.53	1.39	1.39
	Difference between F_{rig} and F_{Semi}	-14.66%	8.46%	8.46%	-6.63%	-6.62%	4.85%	4.85%
	Difference between F_{Flex} and F_{Semi}	32.71%	-17.58%	-17.59%	11.28%	11.28%	-8.30%	-8.30%
$5K_S$	Load Distribution F_{Semi}(kN)	1.69	1.58	1.63	1.50	1.59	1.35	1.35
	Difference between F_{rig} and F_{Semi}	-22.43%	14.78%	14.78%	-10.29%	-10.28%	8.29%	8.29%
	Difference between F_{Flex} and F_{Semi}	20.62%	-12.78%	-12.79%	6.92%	6.92%	-5.29%	-5.29%
$10K_S$	Load Distribution F_{Semi}(kN)	1.81	1.51	1.56	1.54	1.63	1.32	1.32
	Difference between F_{rig} and F_{Semi}	-27.48%	20.01%	20.01%	-12.51%	-12.51%	10.62%	10.62%
	Difference between F_{Flex} and F_{Semi}	12.76%	-8.81%	-8.81%	4.26%	4.27%	-3.25%	-3.25%

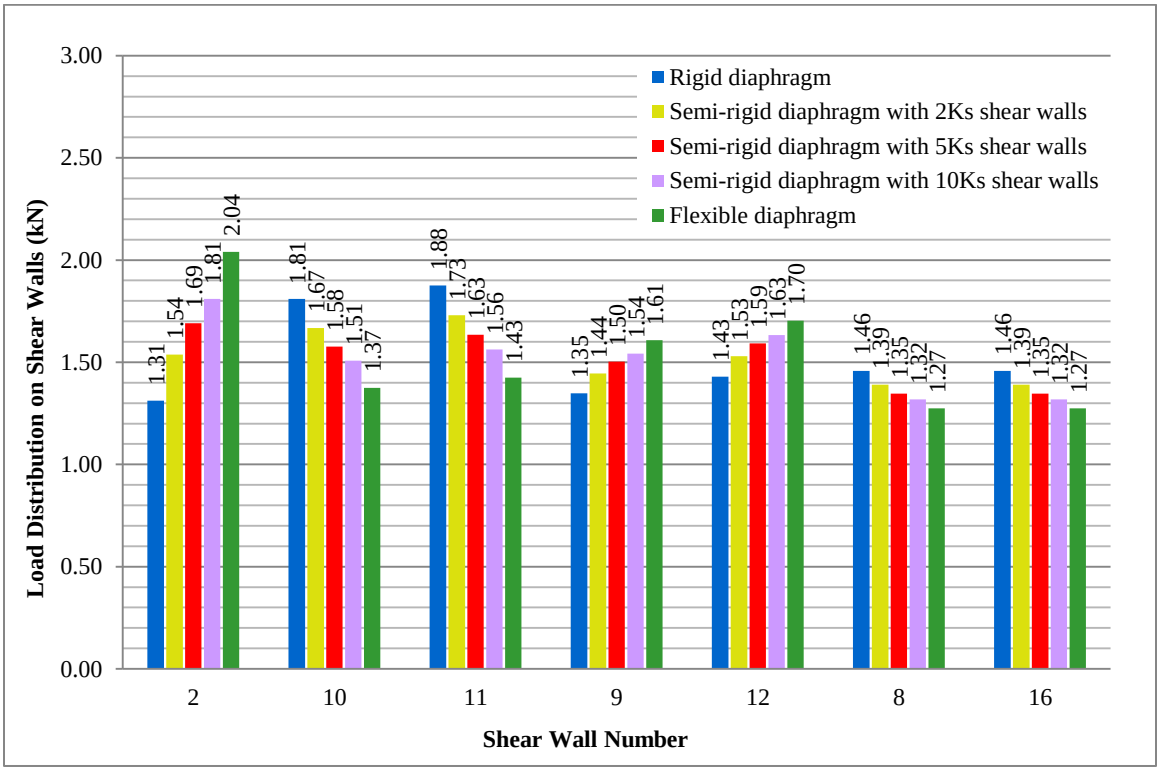

Figure 5-18 Load distribution results for various shear wall stiffness conditions

Table 5-13 Displacement results for various shear wall stiffness conditions

Shear Wall Number		2	10	11	9	12	8-1	8-2	IBC Diaphragm Classification
$2K_S$	**Shear Wall Deflection (mm)**	0.57	0.38	0.38	0.39	0.39	0.27	0.27	Rigid
	Average Shear Wall Deflection $D_{S,avg}$ (mm)	0.38							
	Maximum Diaphragm Deflection D_{dia} (mm)	0.60							
	Ratio of $D_{dia}/D_{S,avg}$	1.60							
$5K_S$	**Shear Wall Deflection (mm)**	0.25	0.14	0.14	0.16	0.16	0.10	0.10	Flexible
	Average Shear Wall Deflection $D_{S,avg}$ (mm)	0.15							
	Maximum Diaphragm Deflection D_{dia} (mm)	0.33							
	Ratio of $D_{dia}/D_{S,avg}$	2.19							
$10K_S$	**Shear Wall Deflection (mm)**	0.13	0.07	0.07	0.08	0.08	0.05	0.05	Flexible
	Average Shear Wall Deflection $D_{S,avg}$ (mm)	0.08							
	Maximum Diaphragm Deflection D_{dia} (mm)	0.27							
	Ratio of $D_{dia}/D_{S,avg}$	3.49							

Chapter 6: Conclusions and Recommendations

This thesis has studied the in-plane behaviour of light wood-frame diaphragms. In particular, the flexibility of the diaphragm, which affects the lateral load distribution to shear walls, has been investigated. A detailed numerical model of the wood-frame diaphragm was developed in the finite element program FLOOR2D (Li and Foschi 2004), and was validated with test data. The model is capable of predicting the in-plane behaviour of diaphragms with various configurations, and can be served as a powerful tool for further studies on wood-frame diaphragms. Based on the detailed diaphragm model, a simplified truss model was developed for the building analysis. The simplified model is capable of representing the main aspects of the in-plane behaviour of the diaphragm, i.e., the maximum deformation and the in-plane stiffness. Compared with the detailed model, it better balances the simulation accuracy with computational efficiency, and can be calibrated using analytical methods. It should be noted that the simplified model is only applicable for wood-frame diaphragms within the aspect ratio of 0.8 to 3.

The lateral load distribution to shear walls was investigated under three diaphragm flexibility conditions: rigid, semi-rigid, and flexible. The semi-rigid condition represents the actual flexibility of the wood-frame diaphragm, while the rigid and flexible conditions are considered in modern design codes for design purposes. By comparing the distribution of lateral loads to shear walls for all the three conditions, the general flexible wood-frame diaphragm assumption and the accuracy of the provisions in the IBC code (ICC 2003) for determining the diaphragm flexibility were examined. It was found that for the purpose of distributing the lateral loads to shear walls, the rigidity of the wood-frame diaphragm should be defined as the relative rigidity of the diaphragm to shear

walls. Moreover, it was found that neither the rigid nor the flexible diaphragm assumption could assure conservative load demands for the design of shear walls. For all the cases studied in this thesis, the classification results of the code agreed well with that of the analyses.

The context of this work can be extended in the future in several ways. First, as concluded in the thesis, the distribution of lateral loads to shear walls depends on the relative rigidity of the diaphragm to the shear walls. This relative rigidity is affected by several factors: 1) the aspect ratio of the diaphragm; 2) the position and size of openings or offsets in the building plan or elevations; and 3) the layout of shear walls, etc. Therefore, for further studies, it is recommended to involve more building configurations in the analysis. As such, design guidelines can be developed to help determine the rigidity of the diaphragm for a specific building configuration.

Due to the simplifying assumptions made in the building analysis, this study involved several limitations: 1) only static load condition was considered; 2) the building was modelled as a truss system, thus was not capable of representing the connections between the diaphragm and the shear wall; 3) both the diaphragm and the shear wall in the building model were assumed to behave linearly. The linear shear wall assumption was not able to represent the nonlinear behaviour of the shear walls under seismic loads, thus the application of the building model was limited to analyses at the early stage of loading only. Moreover, the linear diaphragm assumption may not be applicable under the increasing loads. The nonlinear behaviour of the diaphragm may lead to a change of the diaphragm rigidity, therefore a change of the lateral load distribution to shear walls; 4) the effect of diaphragm openings on the distribution of lateral loads was not considered.

The presence of openings will weaken the diaphragm and may change the distribution of lateral loads to shear walls. It was found in the previous study (Bott 2005) that the stiffness of the diaphragm decreases proportionally with the percentage of sheathing removed. For diaphragms with corner openings, the distribution of lateral loads to shear walls is also affected by torsional effects; and 5) the load was applied only on one edge of the building. In reality, when subjected to seismic loads, the loads are uniformly distributed on the diaphragm. This may result in a different distribution of lateral loads to shear walls.

Considering the limitations indicated above, further studies are recommended to account the nonlinear behaviour of the shear wall and incorporate more realistic representations of the connections between the diaphragm and the shear wall in the building model. It is recommended to conduct more diaphragm tests, in which the diaphragm would be pushed further to capture the nonlinear behaviour of the diaphragm under lateral loads. It is also recommended to include irregular diaphragm configurations in the building analysis, e.g. diaphragms with large corner openings, to introduce the torsional effect and the potential local damage mechanism. In the context of seismic design, dynamic analyses are suggested to help understand the in-plane behaviour of the wood-frame diaphragm and the load shearing among shear walls under time-varying loads.

References

Al Harash, M. T., Panahshahi, N., and Rathore, A. (2010). "Inelastic Seismic Response of Rectangular RC Buildings with Plan Aspect Ratio of 3:1 with Floor Diaphragm Openings." American Society of Civil Engineers, 1971-1980.

ANSYS (2011). *ANSYS Mechanical Release 14.0 User's Manual.* ANSYS Inc., Canonsburg, PA.

ASCE7 (2005). *Minimum Design Loads for Buildings and Other Structures.* American Society of Civil, Reston, VA.

ASTM (2011). *Standard Test Methods for Cyclic (Reversed) Load Test for Shear Resistance of Vertical Elements of the Lateral Force Resisting Systems for Buildings.* ASTM E2126 – 11, ASTM, West Conshohoken, PA.

I. P. Boeraeve. (2010). "Introduction to the Finite Element Method." http://www.gramme.be/unite9/beton/Documents/manuel_calcul_beton_arme.pdf (Oct.10, 2012).

Bott, J. W. (2005). "Horizontal Stiffness of Wood Diaphragms". Master Degree. Virginia Polytechnic Institute and State University, Virginia, United States.

Brignola, A., Podestà, S., and Pampanin, S. (2008). "In-Plane Stiffness of Wooden Floor." *NZSEE Conference,* Wairakei, New Zealand.

Building and Housing Research Center (2005). *Iranian Code of Practice for Seismic Resistant Design of Buildings.* 2800, Tehran, Iran.

Chui, Y. H., Ni, C., and Jiang, L. (1998). "Finite-element model for nailed wood joints under reversed cyclic load." *Journal of Structural Engineering New York, N.Y.,* 124(1), 96-102.

Countryman, D. (1952). "Lateral Tests on Plywood Sheathed Diaphragms." *Rep. No. Laboratory Report No. 63,* Douglas Fir Plywood Association, Tacoma, Washington.

Dolan, J. D., and Madsen, B. (1992). "Monotonic and Cyclic Nail Connection Tests." *Canadian Journal of Civil Engineering,* 19(1), 97-104.

Dolce, M., Lorusso, V. D., and Masi, A. (1992). "Inelastic Seismic Response of Building Structures with Flexible Diaphragm." *10 vols,* Publ by A.A. Balkema, Madrid, Spain, 3967.

Earl, C. (2009). "Deflection of Light Frame Wood Diaphragms". Washington State University, Pullman, Washington.

Earthquake Planning and Protection Organization (2000). *Earthquake Resistant Design of Structures.* Greek Seismic Code, Athens, Greece.

European Committee for Standardization (CEN) (1994). *Earthquake Resistant Design of Structures. Part 1: General Rules and Rules for Buildings.* Eurocode 8, ENV 1988-1-1, Brussels, Belgium.

Federal Emergency Management Agency (1998). *Handbook for the Seismic Evaluation of Buildings—A Prestandard.* FEMA 310, Washington, D.C.

Federalc Emergency Management Agency (1998). *National Earthquake Hazard Reduction Progran Guidelines for Seismic Rehabilitation of Buildings.* FEMA-273, Washington, D.C.

Filiatrault, A., Fischer, D., Folz, B., and Uang, C. M. (2002). "Experimental Parametric Study on the In-Plane Stiffness of Wood Diaphragms." *Canadian Journal of Civil Engineering,* 29(4), 554-566.

Foschi, R. O. (2000). "Modeling the Hysteretic Response of Mechanical Connections for Wood Structures." *Proceedings, 6th Word Conference on Timber Engineering,* Whistler, Canada.

Foschi, R. O., and Yao, F. (2000). "Determining Embedment Response Parameters from Connector Tests." *Proceedings, 6th World Conference on Timber Engineering,* Whistler, Canada.

He, M. (2002). "Numerical Modeling of Three-Dimensional Light Wood-Framed Buildings". Doctor of Philosophy. University of British Columbia, Vancouver, British Columbia, Canada.

He, M., Li, S., Guo, S., and Ni, C. (2011). "The Seismic Performance in Diaphragm Plane of Multi-Storey Timber and Concrete Hybrid Structure." *12th East Asia-Pacific Conference on Structural Engineering and Construction, EASEC12, January 26, 2011 - January 28,* Elsevier Ltd, Hong Kong, Hong kong, 1606-1612.

Hibbeler, R. C. (2005). *Mechanics of Materials.* Pearson Prentice Hall, Upper Saddle River, New Jersey.

ICBO (1997). *Uniform Building Code.* International Conference of Building Officials, Whittier, Calif.

ICC (2003). *International Building Code.* CA: International Code Concil, Whittier.

Li, M. H., and Foschi, R. O. (2004). "FLOOR2D User's Manual." .

Li, M. H., Foschi, R. O., and Lam, F. (2011). "Modeling Hysteretic Behavior of Wood Shear Walls with A Protocol-Independent Nail Connection Algorithm." *ASCE,* 138(1), 99-108.

Li, S., He, M. J., Guo, S. Y., and Ni, C. (2010). "Lateral Load-Beariing Capacity of Wood Diaphragm in Hybrid Structure with Concrete Frame and Timber Floor." *11th World Conference On Timber Engineering,* WCTE 2010, Riva del Garda, Italy.

Moeini, M., and Rafezy, B. (2011). "Investigation into the Floor Diaphragms Flexibility in Reinforced Concrete Structures and Code Provision." *Global Journal of Researches in Engineering,* 11(1).

Naeim, F. (1989). *The Seismic Design Handbook.* Springer.

Panahshahi, N., Kunnath, S. K., and Reinhorn, A. M. (1988). "Modelling of RC Building Structures with Flexible Floor Diaphragms (IDARC2)." *Rep. No. NCEER Technical Report 88-0035,* State University of New York at Buffalo, Buffalo, NY.

Pang, W. C., and Rosowsky, D. V. (2010). "Beam–Spring Model for Timber Diaphragm and Shear Walls." *Structures and Buildings 163,* (SB4), 227–244.

Pathak, R., and Charney, F. A. (2008). "The Effects of Diaphragm Flexibility on the Seismic Performance of Light Frame Wood Structures." *The 14th World Conference on Earthquake Engineering,* Beijing, China.

Rammer, D. R., and Winistorfer, S. G. (2001). "Effect of Moisture Content on Dowel-bearing Strength." *Wood Fiber Sci.,* 33(1), 126-139.

Sadashiva, V. K., MacRae, G. A., and Deam, B. L. (2011). "A Mechanics Based Approach to Quantify Diaphragm Flexibility Effects." *Proceedings of the Ninth Pacific Conference on Earthquake Engineering 2011,* Auckland, New Zealand.

Standards Assiciation of New Zealand (1992). *Code of Practice for General Design and Design Loading for Buildings.* Standards Assiciation of New Zealand NZS 4203, Wellington, New Zealand.

Structural Engineers Association of California (SEAOC) (1990). *Recommended Lateral Force Requirements and Commentary.* Seismology Committee, SEAOC, Sacramento, California.

Tena-Colunga, A., and Abrams, D. P. (1996). "Seismic Behavior of Structures with Flexible Diaphragms." *Journal of Structural Engineering New York, N.Y.,* 122(4), 439-445.

Winistorfer, S. G., and Soltis, L. A. (1994). "Lateral and Withdrawal Strength of Nail Connections for Manufactured Housing." *J.Struct.Eng.,* 120(12), 3577-3594.